Chemical and Nuclear Properties of Rutherfordium (Element 104)

Christian D. Kacher

Ph. D. Thesis

October 30, 1995

Department of Chemistry
University of California, Berkeley

and

Nuclear Science Division
Lawrence Berkeley National Laboratory
University of California
Berkeley, CA 94720

DISCLAIMER

Portions of this document may be illegible
in electronic image products. Images are
produced from the best available original
document.

Abstract

Chemical and Nuclear Properties of Rutherfordium (Element 104)

by

Christian D. Kacher

Doctor of Philosophy in Chemistry

University of California at Berkeley

Professor Darleane C. Hoffman, Chair

The chemical properties of rutherfordium (Rf) and its group 4 homologs were studied by sorption on glass support surfaces coated with cobalt(II)ferrocyanide and by solvent extraction with tributylphosphate (TBP) and triisooctylamine (TIOA). The surface studies showed that the hydrolysis trend in the group 4 elements and the pseudogroup 4 element, Th, decreases in the order Rf>Zr≈Hf>Th. This trend was attributed to relativistic effects which predicted that Rf would be more prone to having a coordination number of 6 than 8 in most aqueous solutions due to a destabilization of the $6d_{5/2}$ shell and a stabilization of the $7p_{1/2}$ shell. This hydrolysis trend was confirmed in the TBP/HBr solvent extraction studies which showed that the extraction trend decreased in the order Zr>Hf>Rf?Ti for HBr, showing that Rf and Ti did not extract as well because they hydrolyzed more easily than Zr and Hf. The TIOA/HF solvent extraction studies showed that the extraction trend for the group 4 elements decreased in the order Ti>Zr≈Hf>Rf, in inverse order from the trend of ionic radii Rf>Zr≈Hf>Ti. An attempt was made to produce ^{263}Rf a) via the ^{248}Cm(^{22}Ne, α3n) reaction employing thenoyltrifluoroacetone (TTA) solvent extraction chemistry and b) via the ^{249}Bk(^{18}O,4n) reaction employing the Automated Rapid Chemistry Apparatus (ARCA). In the TTA

studies, 16 fissions were observed but were all attributed to ^{256}Fm. No alpha events were observed in the Rf chemical fraction. A 0.2 nb upper limit production cross section for the ^{248}Cm(^{22}Ne, α3n)^{263}Rf reaction was calculated assuming the 500-sec half-life reported previously by Czerwinski et al. [CZE92A]. In the ARCA studies, 13 fissions were attributed to ^{263}Rf and had a half-life of 600 $^{+300}_{-200}$ seconds. Based on the 10-nb production cross section for ^{263}Ha by Kratz et al. [KRA92], a 5% EC branch for ^{263}Ha was calculated.

Dedication

This thesis is dedicated to Obachan Otani, a most wonderful teacher, philanthropist, and human being.

Acknowledgements

I would first like to express my greatest appreciation to my thesis advisor, Dr. Darleane Hoffman, for all of her support and guidance. Nuclear chemistry is but just one of the many things I have learned from you.

I would also especially like to thank Dr. Aleksander Bilewicz for all of his excellent contributions to this work. You are an exemplary scientist.

I would also like to acknowledge the members of the Hoffman group who made all of those cyclotron runs bearable and even, dare I say, enjoyable:

Diana- Supportive, helpful, insightful. You've been just great.

Ken- You have been a tremendous source of help. I cant imagine what it would have been like to get through all of those cyclotron runs without you.

Al- I really enjoyed our lunchtime talks. When I think of the few who have been able to achieve so much throughout their life from intelligence, hard work, and dedication, your name comes to mind. Give my regards to MN when you think of him.

Bobby- So much to say but not enough room to say it here, so I'll just fall back on scintillating, rapier wit. Butthead.

Mike- Weird and wacky. Dont give it up for anybody.

Eric- Today's letter is brought to you by the letter Zzzzzzzzz.

Laurance- Your skills will be needed when Armageddon comes. Until then, dont blow up Bobby's lab.

Dawn- The new Hoffman Group chemist.

Melissa- Hey, aren't you supposed to be studying for your orals right about now?

Nancy- Someday, your kids can play with Steve's kids.

Alan- Best dressed, clean cut. Are you trying to corrupt us all?

Birgit- Someday, I will own a Steinway. I might even let you come over and practice. But hopefully by then, you will no longer be addicted to Solitaire.

Steve- Sure, it might be fun for now, but just wait until Josh gets older and starts doing the things you used to do when you were a kid. Poor Tammy.

Flipper, John, Mary, Andy, Yas, and Jerry- Best to all.

I would also like to thank my immediate family and close friends not involved in science but who somehow managed to contribute in their own special way:

Mom, Dad, Mrs. Yonekura, Greg, Glenn, Mike, Kerry, Parvaneh, Nigel, Ferdi, Darisse, Rob, Gene, Craig, and Otto.

Table of Contents

Figure Captions

x

Tables

Chapter 1

Introduction

The area of transactinide element research poses many challenges to the contemporary chemist. Transactinide isotopes must be studied an atom at a time due to production cross sections that are only a few nanobarns ($\approx 10^{-33}$ cm^2) and half-lives which are minutes or less, many having half-lives of seconds or milliseconds. Figure 1.1 shows some nuclear properties of known transuranium isotopes. Undiscovered neutron rich isotopes and isotopes with added stability due to shell effects could have longer half-lives. However, there is the general tendency for the half-life of each element's longest-lived isotope to decrease with increasing atomic number, which makes study of the transactinide elements even more challenging.

The longest-lived known isotopes of rutherfordium (Rf, Z=104) and hahnium (Ha, Z=105) are 78-sec ^{261}Rf [KAD93A] and 34-sec ^{262}Ha [GOB92], [GHI71]. Fast chemical procedures must therefore be devised so the chemical and nuclear properties of the isotopes in question can be studied. These experiments must be performed in a time comparable to the half-life of the isotope and must be repeated many times until statistically significant results are obtained.

In addition, any activity that is produced along with the isotope of interest that has an interfering alpha decay group must be removed so a positive identification of the isotope can be made. Positive identifications are frequently made by measuring and time-correlating the parent's alpha decay energy with the daughter's alpha decay energy;

1

therefore, any daughter formed initially during the bombardment must be removed before a positive identification can be made. Furthermore, alpha spectroscopy requires thin samples to minimize alpha energy degradation. Solvent extraction, surface sorption, and column separation techniques were used in this study to meet these requirements.

Even with these technical problems met, other complexities arise from the chemical nature of the transactinide elements. Extrapolating characteristics down groups in the periodic table has been a powerful and accurate way to determine shared chemical and physical properties within a group. However, such simple extrapolations are not possible down to the transactinide element region because of increasing relativistic effects which alter the chemical and physical properties of the heavier elements.

Relativistic effects become more important with increasing atomic number because electrons become more tightly bound to the nucleus. The innermost $s_{1/2}$ and $p_{1/2}$ electrons experience an increase in velocity. At Z=90, the innermost electrons are already travelling with velocities near c/2. Einstein's relativistic mass equation shows that electrons will gain mass as their velocities approach c:

Equation 1.1
$$m = \frac{m_0}{\sqrt{1 - \frac{v^2}{c^2}}}$$

Hence an electron travelling at 0.5c will experience a 15% gain in mass over its rest mass. Consequently, the innermost electrons which travel at high velocities will contract and spend even more of their time near the nucleus. This contraction of the innermost $s_{1/2}$ and $p_{1/2}$ orbitals causes the higher lying $s_{1/2}$ and $p_{1/2}$ orbitals to contract as well because of orthogonality requirements. The radially contracted s and p orbitals screen more of the nuclear charge from the more extended d and f orbitals causing their orbits to expand radially. The net effects are a change in the element's predicted ionic radius, different energies for the valence orbitals, and possibly a change in the electron configuration of

the element if the change in the valence orbital energies is great enough. These effects can also change the complexing ability of the element.

Table 1.1 [BAG75], [PIT79] shows nonrelativistic and relativistic radii for the series from Hf to Bi. The pseudoatom nonrelativistic calculations were made to measure the 4f shell effect for these elements immediately following the lanthanides by removing the 4f orbitals while reducing the nuclear charge by 14 units. The 6s orbital nonrelativistic calculations between pseudoatom and real atom show that the contraction caused by the 4f shell decreases from 0.33 Å for Hf to 0.22 Å for Hg to 0.13 Å for Bi while the 6s orbital real atom calculations between the nonrelativistic and relativistic scenarios show that the difference remains roughly constant at 0.2 Å. Therefore, relativistic effects become more important than the 4f orbital lanthanide contraction effect for the heavier elements. Notice that for the 5d shell, the relativistic effect is in the opposite direction and increases the average radii of these orbitals.

Table 1.1 Nonrelativistic and Relativistic Average Ionic Radii (Å) for 5d and 6s Orbitals

	Ground State Electronic Structure	Pseudoatom Nonrelativistic[a]		Real Atom Nonrelativistic[b]		Real Atom Relativistic[c]	
		5d	6s	5d	6s	5d	6s
Hf	$[Xe]4f^{14}5d^26s^2$	1.325	2.484	1.179	2.153	1.263	1.955
Re	$[Xe]4f^{14}5d^56s^2$	1.076	2.231	0.952	1.955	0.992	1.734
Au	$[Xe]4f^{14}5d^96s^2$	0.912	2.235	0.817	1.958	0.839	1.620
Hg	$[Xe]4f^{14}5d^{10}6s^2$	0.849	1.984	0.758	1.761	0.779	1.515
Tl	$[Xe]4f^{14}5d^{10}6s^26p$		1.762		1.570		1.365
Pb	$[Xe]4f^{14}5d^26s^26p^2$		1.613		1.442		1.266
Bi	$[Xe]4f^{14}5d^26s^26p^3$		1.499		1.373		1.187

[a] To measure the effect that the 4f shell has on ionic radius, the nuclear charge was reduced by 14 units and the 4f orbitals were removed.
[b] Calculated nonrelativistic ionic radii.
[c] Calculated ionic radii with relativistic effects taken into account.

Relativistic effects are also observed for the heavier members of groups 13 through 16 in the periodic table (Figure 1.2). The heavier members often have oxidation states that are two less than their lighter homologs. This phenomenom has been called the inert pair effect and is due to an increased stability of the $6s^2$ electron pair down a group. Relativistic effects stabilize the 6s shell more so than the 5s shell; therefore, a larger energy is required to remove the 6s electrons from Tl, Pb, and Bi than is required to remove the 5s electrons from In, Sn, and Sb. The most common oxidation state of Tl in aqueous solution is 1+ instead of 3+ and the most common state of Pb is 2+ instead of 4+. Indeed, the stability of the 1+ oxidation state for group 13 elements increases in the order Al<Ga<In<Tl. This inert pair effect is also observed in the $6p_{1/2}$ pair in both Bi and Po giving Bi its univalent oxidation state and Po its divalent oxidation state. Similarly, the actinide Lr, while favoring a trivalent state, could possibly be reduced to a univalent state if the relativistic stabilization of its 7s orbital is large enough. However, previous attempts [SCH88], [HEN90] to reduce Lr have been unsuccessful.

Groups 1 and 2 also exhibit relativistic effects in the heaviest members. The ionization energy for the group 1 elements decreases steadily down the group to an energy of 375.6 kJ/mol for Cs but then stabilizes at 375 kJ/mol for Fr. This is also seen in the group 2 elements where the energy decreases down the group to a first ionization energy of 502.7 kJ/mol for Ba but then actually increases to 509.1 kJ/mol for Ra. In both cases, the ionization energies for Fr and Ra are due to the relativistic stabilization of the 7s orbital.

Gold is a particularly interesting element because its color is a result of relativistic effects. In one previous study, experimental optical reflectivities were measured for both gold and silver [SAE77]. The absorption for gold at hv=2.4 eV occurred in the visible region and was assigned the transition from 5d to 6s [CHR71]. The absorption for silver at hv=3.7 eV (assigned the transition from 4d to 5s), on the other hand, was high enough to place it in the ultraviolet region. The transition energy for gold was much lower

because of the relativistic stabilization of the 6s orbital and the destabilization of the 5d orbital bringing their orbital energies closer together. Therefore, nonrelativistic gold would be white, like silver.

Figure 1.3 [SEA90] shows the nonrelativistic and relativistic orbital energy ordering for uranium. The relativistic orbitals are no longer degenerate and now take into account spin-orbit splitting. The $6s_{1/2}$, $7s_{1/2}$, and $6p_{1/2}$ orbitals are lower in energy than the nonrelativistic 6s and 6p orbitals while the $5f_{5/2,7/2}$ and the $6d_{3/2,5/2}$ orbitals are higher in energy than the 5f and 6d orbitals, respectively. The $6p_{3/2}$ orbital is slightly more destabilized than the nonrelativistic 6p orbital because the effect of contraction is counteracted by spin-orbit effects.

It has been suggested that the great stability of the uranyl ion is largely due to the 5f, 6d, 7s, and 7p orbitals, each being able to contribute to the bonding to create very short and strong U-O bonds [CON52], [YAN78]. Relativistic arguments validate this hypothesis. Table 1.2 [PIT79] shows the nonrelativistic and relativistic valence orbital energies and the radii for the 5f, 6d, and 7s orbitals of uranium. Even though the average radius of the nonrelativistic 5f orbital is much smaller than that of the 7s orbital, largely due to the imperfect screening of 5f electrons from each other, a phenomenon known as the actinide contraction, relativistic effects destabilize the 5f orbitals and increase their radii while they stabilize the 7s orbital and decrease its radius. Thus, relativistic effects narrow the ranges of orbital energies and radii and allow the 5f orbitals to participate in bonding along with the 6d and 7s orbitals.

Table 1.2 Valence Orbital Energies (eV) and Radii (Å) for Uranium

	Relativistic	Nonrelativistic
ε, 5f	9.01	17.26
ε, 6d	5.09	7.25
ε, 7s	5.51	4.54
$<r>$, 5f	0.76	0.67
$<r>$, 6d	1.71	1.52
$<r>$, 7s	2.30	2.67

Table 1.3 shows the valence electron configurations of the lanthanides and actinides. The 6d and 5f orbital energies of the actinide elements protactinium, uranium, and neptunium are close enough that mixing can occur. One electron occupies the 6d orbital for these three elements, a configuration not observed in the complementary lanthanides.

Table 1.3 Ground State Electron Configurations For Neutrally Charged Atoms

Lanthanide		**Actinide**	
La	[Xe] $5d6s^2$	Ac	[Rn] $6d7s^2$
Ce	[Xe] $4f5d6s^2$	Th	[Rn] $6d^27s^2$
Pr	[Xe] $4f^36s^2$	Pa	[Rn] $5f^26d7s^2$
Nd	[Xe] $4f^46s^2$	U	[Rn] $5f^36d7s^2$
Pm	[Xe] $4f^56s^2$	Np	[Rn] $5f^46d7s^2$
Sm	[Xe] $4f^66s^2$	Pu	[Rn] $5f^67s^2$
Eu	[Xe] $4f^76s^2$	Am	[Rn] $5f^77s^2$
Gd	[Xe] $4f^75d6s^2$	Cm	[Rn] $5f^76d7s^2$
Tb	[Xe] $4f^96s^2$	Bk	[Rn] $5f^97s^2$
Dy	[Xe] $4f^{10}6s^2$	Cf	[Rn] $5f^{10}7s^2$
Ho	[Xe] $4f^{11}6s^2$	Es	[Rn] $5f^{11}7s^2$
Er	[Xe] $4f^{12}6s^2$	Fm	[Rn] $5f^{12}7s^2$
Tm	[Xe] $4f^{13}6s^2$	Md	[Rn] $5f^{13}7s^2$ (pred.)
Yb	[Xe] $4f^{14}6s^2$	No	[Rn] $5f^{14}7s^2$ (pred.)
Lu	[Xe] $4f^{14}5d6s^2$	Lr	[Rn] $5f^{14}6d7s^2$ or $5f^{14}7s^27p$ (pred.)

If the contraction and expansion effects become large enough, a change in the energy ordering of the outermost valence orbitals can occur. Table 1.3 shows how lawrencium (Lr, Z=103) could have the $5f^{14}6d7s^2$ electron configuration, analogous to lutetium's configuration, or it could have the $5f^{14}7s^27p$ configuration if the amount of destabilization in the $6d_{3/2}$ orbital and stabilization in the $7p_{1/2}$ orbital is large enough to switch the energy ordering of these two orbitals. Multiconfiguration Dirac-Fock (MCDF) calculations predict that the configuration is more likely to be $5f^{14}7s^27p$ [DES80], [ZHU90].

Figure 1.4 [GLE89] shows the relativistic orbital energies for the group 4 elements. Since relativistic effects become more important with Z, the 7s and $7p_{1/2}$ levels of Rf are lower in energy than those of either Zr or Hf, and the energy of the s orbital decreases from Zr to Hf to Rf due to stabilization effects. Meanwhile, the energy of the 6d orbital increases down the group due to destabilization effects.

The exact ordering of the 6d and 7p orbitals for Rf is unclear and some mixing of these orbitals may be present. Rutherfordium was first predicted to have the $5f^{14}6d^27s^2$ electron configuration [DES73], [FRI75], similar to the configurations of the other group 4 elements. This prediction was based on relativistic calculations using only one jj-configuration. A more accurate MCDF calculation done on various electron configurations of Rf were made using 468 jj-configurations [GLE89]. The $5f^{14}6d7s^27p$ electron configuration was found to have the lowest energy with the $6d^27s^2$ level slightly higher. The $5f^{14}7s^27p^2$ electron configuration predicted to be the ground state by Keller et al [KEL83] by analogy to Lr was found to be 2.9 eV higher than the ground state.

Regardless of the actual electronic configuration of Rf, which is most likely a mixture of configurations due to the close orbital energy level spacing for the first few levels with the greatest contribution coming from the $5f^{14}6d7s^27p$ configuration, it is clear that relativistic effects influence the ordering of its valence orbitals and thus should also affect its ionic radius, its bonding and complexing properties, and possibly its

coordination number. A recent study [CZE94] examined the complexing behavior of Rf in tributylphosphate (TBP) extractions from various concentrations of chloride while keeping the hydrogen ion concentration constant. It showed that Rf behaved differently compared to its lighter group 4 homologs Zr and Hf as the chloride concentration increased, forming unextractable anionic complexes such as $RfCl_6^{2-}$. This was the first time Rf was shown to chemically deviate from a smoothly extrapolated trend from the group 4 elements, zirconium and hafnium.

Previously, aqueous studies of rutherfordium had shown that it behaved like a group 4 element. In an early experiment [SIL70], zirconium, hafnium, and rutherfordium along with various trivalent actinides were sorbed on a cation exchange column. Zr, Hf, and Rf eluted with 0.1 M ammonium α-hydroxyisobutyrate at pH=4 while the trivalent actinides remained on the column.

A more recent study compared the behavior of hafnium and rutherfordium along with the trivalent actinides, curium and fermium [HUL80]. The isotopes were sorbed on an anion exchange column containing quaternary amines held on inert supports. At 12 M HCl, Hf and Rf sorbed on the column indicating formation of similar anionic chloride complexes while Cm and Fm did not.

The similarities and differences found in the behavior of Rf compared to its lighter homologs Zr and Hf are illustrative of the problems involved in simply extrapolating a chemical trend down to the heaviest members of a given group. Relativistic effects which become more pronounced in this heavy region of the periodic table make theoretical predictions about chemical behavior much more difficult and challenging. Indeed, unexpected deviations in the behavior of rutherfordium continue to be observed and are reported in this work.

Chart of the nuclides for elements 101–109 (mass number / half-life / decay mode)

Element	N=145	146	147	148	149	150	151	152	153	154	155	156	157	158	159	160	161
109 Mt													266 3.4ms α				
108 Hs											263 ? α	264 0.08ms α, SF?	265 2ms α				
107 Ns										261 12ms α, SF?	262 8ms|0.1s α|α						
106 Sg									259 0.5s α,SF	260 4ms α,SF	261 0.3s α,SF?		263 0.9s SF,α		265 2–30 s α ?	266 20–30 s α ?	
105 Ha				253 1.5s SF,α?		255 1.5s SF		257 1.3s α,SF	258 4.4s EC,α		260 1.5s α,SF	261 1.8s α,SF	262 34s EC,α	263 27s SF,α			
104 Rf					253 ?	254 ? 0.5ms SF	255 1.4s SF,α?	256 7ms α,SF	257 4.8s α,SF	258 13ms SF,α?	259 3.0s α,SF	260 20ms SF	261 78s α,SF?	262 47 ms|2 s SF	263 ? SF		
103 Lr						253 ?	254 13 s α	255 22 s α,EC	256 ~6 m / 30m|10m EC	257 0.65 s α,EC	258 3.9 s α	259 6.1 s α,SF	260 3 m α,EC	261 39 m SF	262 216m EC		
102 No	247 3 s α	248 7 s EC,α		250 0.3ms SF	251 0.6s α	252 2.3 s α,SF	253 1.7m α	254 55s / 0.3s α / IT	255 3.1m α,EC	256 2.9 s α,SF	257 25 s α	258 1.2ms SF	259 58 m α,EC	260 106ms SF			
101 Md				249 24 s α,EC	250 50 s EC,α	251 4 m EC,α	252 2 m EC,α			255 27 m EC	256 1.3h EC,α	257 5.5h EC,α	258 57m|52d α	259 1.6h SF	260 27.8d SF		262 5 ms SF ?

N

Fig. 1.1

Periodic Table of the Elements

GROUP

1	2	3	4	5	6	7	8	9	10	11	12	13	14	15	16	17	18
1 H																	2 He
3 Li	4 Be											5 B	6 C	7 N	8 O	9 F	10 Ne
11 Na	12 Mg											13 Al	14 Si	15 P	16 S	17 Cl	18 Ar
19 K	20 Ca	21 Sc	22 Ti	23 V	24 Cr	25 Mn	26 Fe	27 Co	28 Ni	29 Cu	30 Zn	31 Ga	32 Ge	33 As	34 Se	35 Br	36 Kr
37 Rb	38 Sr	39 Y	40 Zr	41 Nb	42 Mo	43 Tc	44 Ru	45 Rh	46 Pd	47 Ag	48 Cd	49 In	50 Sn	51 Sb	52 Te	53 I	54 Xe
55 Cs	56 Ba	57 La	72 Hf	73 Ta	74 W	75 Re	76 Os	77 Ir	78 Pt	79 Au	80 Hg	81 Tl	82 Pb	83 Bi	84 Po	85 At	86 Rn
87 Fr	88 Ra	89 Ac	104 Rf	105 Ha	106 Sg	107 Ns	108 Hs	109 Mt	110	111	(112)	(113)	(114)	(115)	(116)	(117)	(118)

Lanthanides

58 Ce	59 Pr	60 Nd	61 Pm	62 Sm	63 Eu	64 Gd	65 Tb	66 Dy	67 Ho	68 Er	69 Tm	70 Yb	71 Lu

Actinides

90 Th	91 Pa	92 U	93 Np	94 Pu	95 Am	96 Cm	97 Bk	98 Cf	99 Es	100 Fm	101 Md	102 No	103 Lr

Fig. 1.2

10
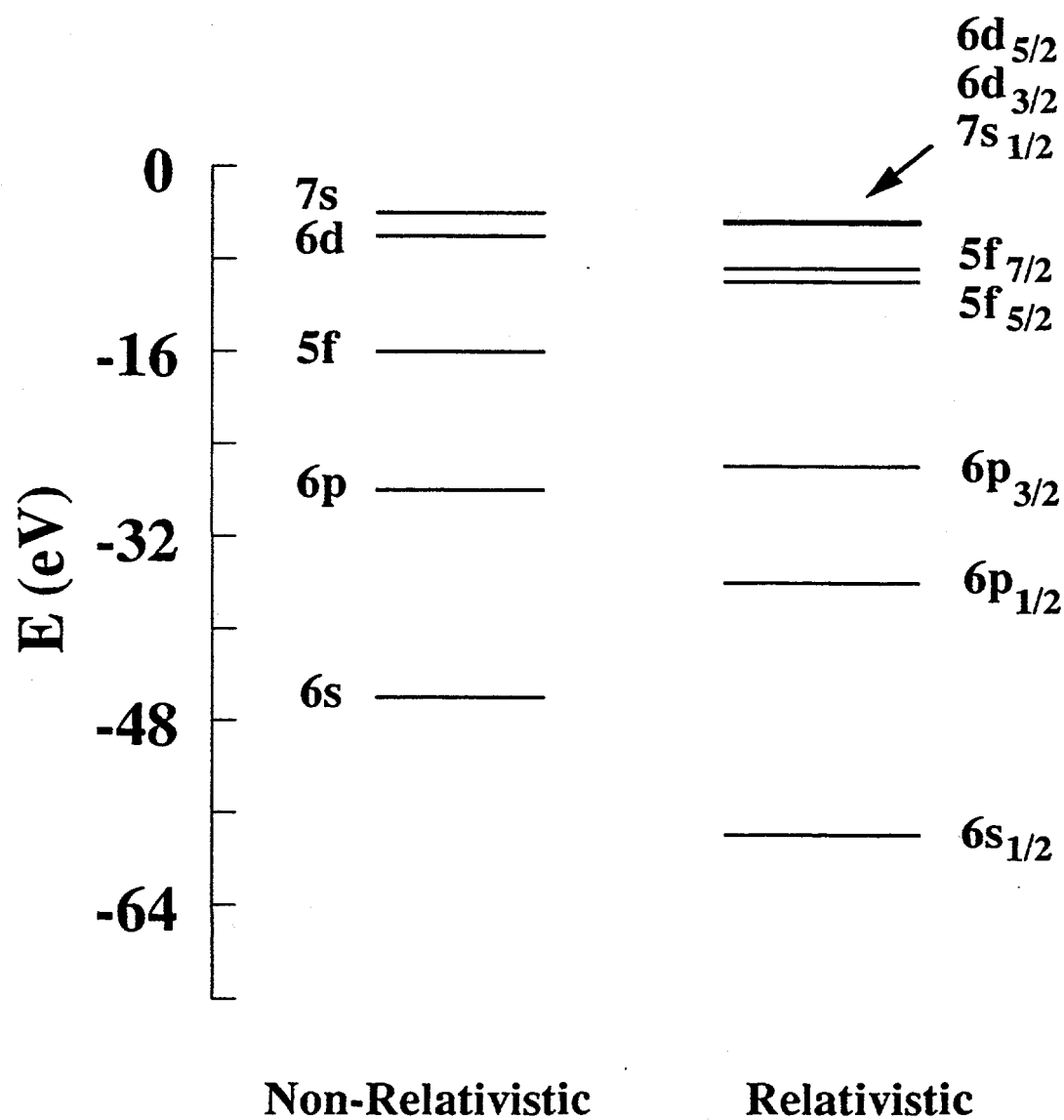
Figure 1.3 Energy level diagram showing non-relativistic and relativistic orbital energies for uranium [SEA90].
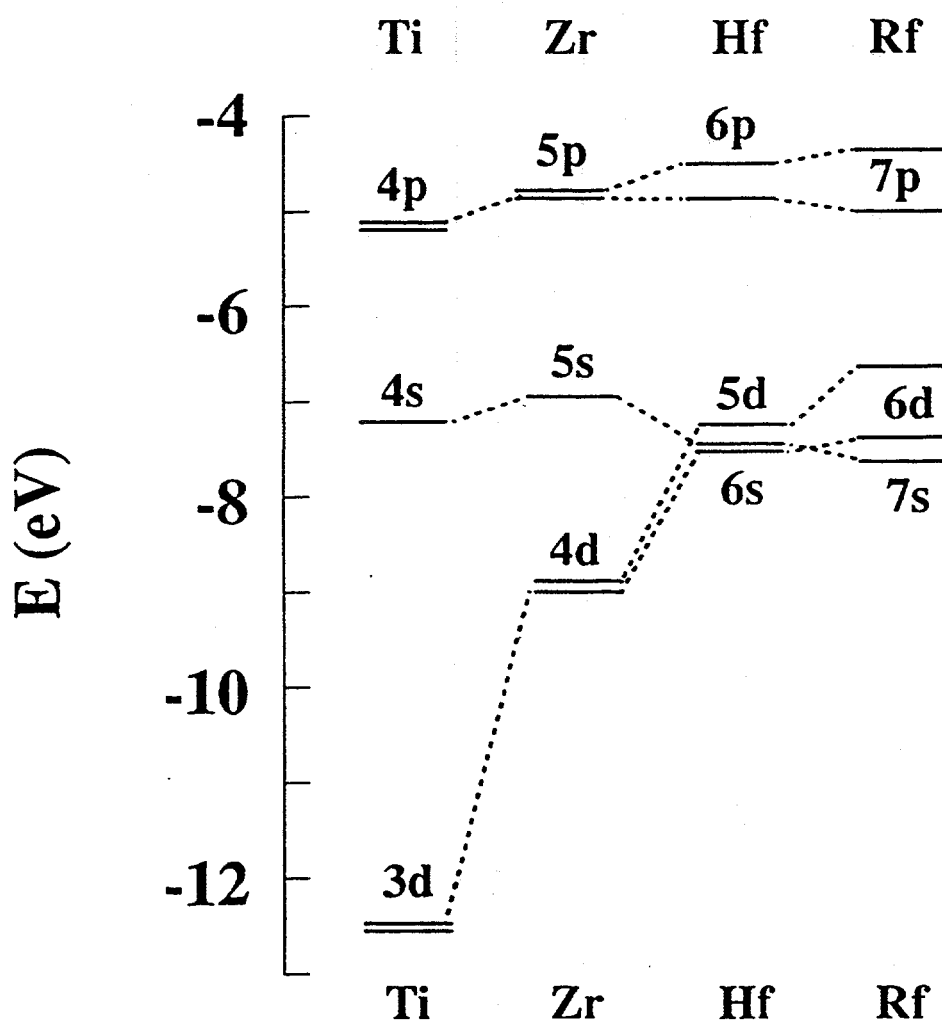
Figure 1.4 Energy level diagram showing relativistic orbital energies for group 4 elements Ti, Zr, Hf, and Rf [GLE89].

Chapter 2

Experimental Procedures

2.1 Target System

Targets composed of either $^{248}Cm_2O_3$ or $^{249}BkO_x$ were prepared by high voltage electrodeposition of the nitrates from isopropanol solution onto beryllium backings. These targets were used to produce various transactinide isotopes of interest at the Lawrence Berkeley Laboratory 88-Inch Cyclotron by bombarding either $^{248}Cm_2O_3$ or $^{249}Bk_2O_3$ targets with an appropriate heavy-ion beam. ^{248}Cm and ^{249}Bk are neutron-rich isotopes with relatively long half-lives making them useful as target materials for transactinide isotope production. Since the targets are bombarded at beam intensities as high as one particle microampere, temperatures at the target can be high. Targets produced using this high voltage molecular plating technique [EVA72], [AUM74], [MUL75], [MOO83] with beryllium as a target backing can withstand temperatures up to several hundred °C and are able to withstand extreme ionizing conditions without losing any significant amount of target material.

The first step in target production is the dissolution of the actinide in dilute nitric acid and then in isopropanol. Once dissolved, the actinide can then be electroplated onto a Be foil which has a typical thickness of a few mg/cm^2. A cross-sectional view of the plating cell is shown in Figure 2.1. A beryllium foil is placed at the bottom of the plating

cell, held in place by a clamped plate on an aluminum base which serves as the cathode. A Pt foil, positioned on the mid ring, serves as the anode. A teflon chimney holds the target-salt-isopropanol solution and is placed on the Be foil. The 6-mm diameter of the chimney defines the diameter of the material plated onto the Be foil. During plating, several hundred volts are applied between the positive and negative electrodes and a glass rod is used to stir the solution. After about 30 minutes, the Be foil which now contains some plated target material is placed in a furnace at 550°C to convert the hydrated deposit into the oxide. This procedure is repeated until the desired target thickness is reached. The target thickness is determined by counting the alpha emissions in a low geometry alpha- spectrometer system. The target can then be mounted in the target system.

A schematic of the target system is shown in Figure 2.2. An ^{18}O or ^{22}Ne positive ion beam first enters the target system through a water-cooled graphite collimator. The 6-mm i.d. of the collimator defines the diameter of the beam which is the same diameter as that of the target. The beam then passes through a 2.58 mg/cm^2 Be window which serves to separate the target system from the cyclotron vacuum. 0.3 mg/cm^2 of nitrogen gas flows between the vacuum window and the 2.4 mg/cm^2 Be target backing to keep the target cool during irradiations. The beam passes through the Be target backing and then into the target where it produces many recoil products. The ^{248}Cm target thickness was 491 µg/cm^2. The ^{249}Bk target thickness used in the attempts to produce ^{263}Rf with the Automated Rapid Chemistry Apparatus (ARCA) was 790 µg/cm^2 and for its confirmation experiment, the target thickness was 390 µg/cm^2. Beam current was 0.5 particle microamperes. A beam stop located 15 cm from the target is used to stop the beam and a Faraday cup records the beam intensity.

2.2 Gas-Jet Transport System

The reaction products recoiling from the target must be transported in an efficient manner to a collection site where their chemical and nuclear properties can be studied. This is accomplished by an aerosol-seeded gas-jet system.

To begin with, KCl aerosols are produced when a crystalline form of KCl situated in a quartz tube is heated to 640°C in a tube furnace. Helium gas flows through the quartz tube and sweeps out the KCl aerosols which experience a large temperature drop upon leaving the furnace. This sudden drop in temperature produces a super-saturated KCl vapor which condenses into relatively large aerosol particles. The aerosols exit into a polyvinyl chloride presorter capillary which is 5 meters in length and 2.2 mm in diameter and is wound into several coils that are about 15 cm in diameter. The presorter capillary serves to remove the largest of the KCl clusters. The clusters are then transported to the target chamber via a capillary tube. The reaction products attach themselves to the clusters which recoil out of the thin target and are stopped in 1 atm of He. A vacuum pump located at the collection site creates a pressure differential that directs the active clusters through a 1.4-mm i.d. capillary and deposits them on a collection plate inside a hood some 7 meters away. The clusters make little contact with the capillary walls due to laminar flow which produces Bernoulli forces that focus the clusters toward the center of the capillary. This results in very efficient transport of the KCl aerosols and activities.

The collection plate (see Figure 2.2) is situated inside a lucite box in the corner of the chemistry hood which is located above Cave 0 in the upper mezzanine area. The brass collection plate measures 30 cm in diameter and contains four collection sites on its periphery. Platinum or mylar foils are placed in the collection sites to collect the active KCl clusters coming through the capillary under vacuum. An electric solenoid valve is used to disengage the vacuum each time the collection plate has to be turned.

15

Sudden or extreme changes in the target system pressure or beam intensities can damage the target. Therefore, an alpha/SF detector was positioned above the exit of the capillary at the collection site and connected to an alarm which would sound if any target activities were detected, indicating possible rupture of the target.

2.2.1 Gas-Jet Transport Efficiency Studies

Low gas-jet yields prompted a series of experiments to understand and improve gas-jet transport efficiencies. Several parameters influence gas-jet yield including capillary diameter, gas-jet flow rate, recoil chamber diameter, position of the capillary in the recoil chamber, KCl oven temperature, and gas pressure.

In the first series of studies, the gas-jet yield was measured by detecting the alpha particles from 3-minute ^{211}Fr with the Merry-Go-Round (MG) rotating wheel system [HOF80] and comparing the ^{211}Fr yield to the yield obtained with a Au catcher foil which was positioned so as to catch all of the target recoil products. The catcher foil yield, therefore, represented 100% yield.

^{211}Fr was produced from the ^{197}Au(^{18}O, 4n) reaction at the 88-Inch Cyclotron. The ^{197}Au target was 22 μg/cm^2 thick electroplated on a 2.75 mg/cm^2 Be backing. Recoil activities from the target, after transport through the gas-jet, were collected on a foil on the MG wheel for 2 minutes. After a 2-minute waiting period to let the shorter activities decay away, the foil was moved in front of one of the MG detectors and counted to detect ^{211}Fr.

The first study investigated the effect of capillary diameter on gas-jet yield. Teflon capillaries with inner diameters measuring 0.8 mm, 1.4 mm, and 1.6 mm were used in the study. The 1.4-mm i.d. capillary gave the best yield of close to 100%. The 0.8 mm i.d. capillary gave the worst yield because of a poor He flow rate of 0.5 L/min

16

even when pressure was set at a maximum of 5.5 psi. The He flow rates for the 1.4-mm and 1.6-mm i.d. capillaries were 2.2 L/min and 3.5 L/min, respectively. Both flow rates were above a certain threshold above which flow rate had little effect on the yield.

Different recoil chamber insert diameters were studied next. Recoil chamber inserts were constructed with 0.75-, 1.00-, and 1.25-inch diameters. Each chamber had four positions into which the capillary could fit (Figure 2.3). The four positions were 1.5, 2.0, 2.5, and 3.0 cm downstream from the target. The tip of the capillary came into one of the positions of the recoil chamber at a 90° angle to the tip of the insert and protruded inward 2 mm from the inner wall. The gas-jet yield was not affected by changing the position of the capillary except with the 0.75 inch diameter recoil chamber where lower jet yields were measured for the capillary positions closest to the target.

In the second series of studies, experiments were performed to measure the gas-jet yield dependence on temperature of the KCl oven. A four-zone tube furnace [KAD93] was used to find the temperature profile resulting in the highest transport efficiency. KCl-aerosol clusters were generated from within a quartz tube positioned inside the four-zone tube furnace.

First, a ^{225}Ac recoil source was produced from a ^{229}Th source. A potential difference of 300 V was applied between a ^{229}Th source and a brass pin (Figure 2.4). The brass pin was placed 1 cm away from the ^{229}Th source and used to collect ^{225}Ra, ^{225}Ac, ^{221}Fr, ^{217}At, and other members of the decay chain (Figure 2.5). After removing the ^{229}Th source, the brass pin had ^{225}Ra, ^{225}Ac and shorter-lived daughter activities in equilibrium. This brass pin was then placed in a recoil chamber (Figure 2.6). The 5.83 MeV alpha decay energy of ^{225}Ac imparts a recoil energy to the ^{221}Fr which is large enough to cause the ^{221}Fr atoms to recoil out of the source. A constant bias voltage of 50 V/cm was applied to move the ^{221}Fr atoms away from the source while KCl clusters were passed over the source to capture the ^{221}Fr recoils and transport them to the collection site at the far end of the capillary. The recoils were collected for a predetermined time

17

and the decay rate of the 5-minute ^{221}Fr atoms (E_α=6.341 MeV) was then measured to determine the gas-jet yield.

The effects of oven temperature on gas-jet yield illustrated in Figure 2.7 show that the yield peaked at 640°C. Temperatures above 650°C cause over-sublimation of the KCl (melting point=650°C) resulting in too much KCl depositing at the collection plate. The best gas-jet yields were achieved with an oven temperature of 640°C, provided the newly formed KCl clusters experienced a sharp drop in temperature after the 640°C section of the oven. This sharp temperature drop caused the smaller KCl clusters to condense into larger, more optimally sized aerosol particles, of which the largest were removed in the presorter capillary.

2.3 Isotopes Used

The transactinide elements do not occur naturally in nature and must, therefore, be produced in heavy ion reactions. Production rates typically are on the order of a few atoms per minute or less. Once the isotopes are produced, their chemical properties may be studied using a variety of experimental techniques.

Elements belonging to the same group in the periodic table are expected to share similar chemical and physical properties. Therefore, studies of the chemical behavior of various homolog tracers usually precede the studies of the transactinides themselves. In this work, the chemical behaviors of the group 4 homologs, zirconium and hafnium, and the pseudogroup 4 homolog thorium were studied and the results were used to predict and model the chemical behavior of rutherfordium.

Even though thorium does not belong to the group 4 elements, thorium is considered a pseudogroup 4 element because its 4+ oxidation state contains no f-electrons in its outermost shell, just like the group 4 elements. Tetravalent plutonium, however,

has less in common with the group 4 elements because of its outermost 5f valence electrons resulting in different complexing abilities. Still, plutonium studies were also carried out to see how the chemical behavior of plutonium(IV) compared with that of rutherfordium.

The tracers were stored in 6 M HCl or stronger solutions to prevent them from hydrolyzing. Tetravalent tracers in particular are prone to hydrolyze in acidic solutions of low concentration. Sufficient HCl solution was added to the alpha emitting tracers to typically give a specific activity 0.5 nCi/30 μL. Typical specific activities of gamma emitting tracers were on the order of 10 nCi/30μL. See Chapter 4, Section 4.3, for detailed information on the solvent extraction procedure as well as potential problems to avoid and Chapter 3, Section 3.2 for information on the surface adsorption procedure.

Decay information on these and related isotopes is listed in Tables 2.1 and 2.2, respectively. A brief discussion of the main isotopes studied follows.

Table 2.1 Nuclear Properties of Isotopes Studied

Isotope	$t_{1/2}$	Decay Modes (Primary)	Prominent Energies (MeV)	Relates To	Ref
95Zr	64.02 d	β-, γ	.7567, .7242	TBP, surface studies, 263Rf search	[REU83]
95Nb	34.97 d	β-, γ	.7658	TBP, surface studies, 263Rf search	[REU83]
152Eu	13.3 y	EC, β+, β-	.1218, .3443	TBP, surface studies, 263Rf search	[REU83]
172Hf	1.87 y	EC, γ	.024, .1259	TBP, surface studies	[REU83]
175Hf	70 d	EC, γ	.3434	TBP	[WAL84]
181Hf	42.4 d	β-, γ	.408	TBP	[WAL84]
229Th	7300 y	α	4.845	TBP, surface studies	[WAL84]
239Pu	2.411e4 y	α	5.155	TBP	[WAL84]
249Cf	351 y	α	5.813	263Rf search	[WAL84]
261Rf	78 s	α	8.29	TBP, surface studies	[KAD93A], [WAL84]
263Rf	500 s ? 600 s ?	SF? SF?		263Rf search	[CZE92a] This work
	800-8000 s	α?	7.74–8.00		[SAT88], [MOL88]
	> 8000 s	α?	<7.74		[SAT88], [MOL88]
263Ha		α EC (5%) ?	8.3–8.4	263Rf search	[GOB92] This work

Table 2.2 Nuclear Properties of Related Isotopes [CHA87], [REU83], [WAL84]

Isotope	t$_{1/2}$	Decay Modes (Primary)	Prominent Energies (MeV)	Origin
211Bi	2.14 m	α	6.623	Transfer reaction with Pb impurity in target
211mPo	25.2 s	α	7.275, 8.885	"
212Po	0.298 μs	α	8.7844	Transfer reaction with Pb impurity in target
214Po	163.7 μs	α	7.6871	"
221Fr	4.8 m	α	6.341	Used to measure gas-jet efficiency
225Ac	10 d	α	5.83	Recoil source
241Am	432 y	α	5.4857	Catcher foil chemical yield tracer
248Cm	3.4e5 y	α	5.078	Target material
249Bk	320 d	β⁻, γ	.3270, .3080	Target material
249Cf	351 y	α	5.813	Recoiled from 249Bk target
250Fm	30 m	α	7.43	Used as a yield tracer
251Fm	0.22 d	α	6.83	"
252Fm	1.1 d	α	6.26	"
253Fm	3 d	α	6.63	"
254Fm	0.14 d	α	7.06-7.19	"
256Fm	0.11 d	SF		"
257No	26 s	α	8.22, 8.27, 8.32	261Rf daughter
259No	58 m	α	7.50, 7.53	263Rf(?) daughter
259Lr	5.4 s	α	8.46	263Ha daughter

2.3.1 Trivalent Tracers ^{152}Eu / ^{241}Am / ^{249}Cf

Contaminant transplutonium activities such as the actinide fermium appear in trivalent form. Europium, americium, and californium were, therefore, used to model its behavior. Europium is a member of the lanthanide series and americium and californium are members of the actinide series. Because of their trivalency, they were used in separation experiments (see Table 2.1) to insure that trivalent species would be held back while tetravalent species such as rutherfordium had high chemical yields.

Among the candidates of trivalent species available for comparison, europium was chosen because of its favorable gamma-decay energies. It was purchased from Isotope Products in Burbank, CA in 4 M HCl solution.

In the ^{263}Rf experiment (Chapter 6), fermium would interfere with the detection of ^{263}Rf. Therefore, the alpha-emitting, carrier-free, long-lived isotope ^{249}Cf was chosen to model fermium behavior. In addition, ^{249}Cf progeny have alpha-decay energies that do not overlap with the primary ^{249}Cf alpha decay energy of 5.812 MeV making alpha-spectroscopic detection of ^{249}Cf clean and simple.

Carrier-free ^{241}Am was chosen as a trivalent tracer because it could be effectively used as both an alpha and a gamma emitter (E_α=5.4857 MeV, E_γ=59.5 keV). It was used as a yield tracer in the gold catcher foil experiments (Section 6.4.2).

2.3.2 Tetravalent Tracers

2.3.2.1 ^{95}Zr / $^{172,175,181}Hf$

Zirconium and hafnium are both group 4 elements. Their chemical behavior was compared to that of the heaviest group 4 element, rutherfordium as discussed previously.

^{95}Zr was purchased from Isotope Products in Burbank, CA is an isotopically pure form. It is typically produced as a fission product and therefore must be made isotopically pure by chemically separating it from the other fission products. It arrived carrier free in an oxalic acid form and therefore had to be converted to a chloride form. The conversion procedure was based on a well-known lanthanum co-precipitation technique that has been used in many studies [KLE90]. 10 μCi of the ^{95}Zr were taken from the stock solution and placed into a 15 ml glass centrifuge cone. 0.125 mg of lanthanum nitrate ($La(NO_3)_3$) powder were added to the cone to give a concentration of 10 mg/ml $La(NO_3)_3$. Just enough 2 M HCl was added to dissolve the $La(NO_3)_3$ to keep the solution volume small. Once dissolved, a few drops of ammonium hydroxide ($NH_4(OH)$) were then added to precipitate out the $La(OH)_3$. The lanthanum served as a carrier, carrying zirconium with it as it precipitated out leaving the oxalate behind in the solution. The supernate was discarded and the white precipitate was washed twice with water. The precipitate was then dissolved in 12 M HCl and added to a 2 mm i.d. column packed 2 cm with AG X 10 anion exchange resin. The column was washed with 3 free column volumes (FCV=volume of liquid in a resin packed column external to the resin itself) of 12M HCl to remove the lanthanum. 2.5 M HCl was then added to remove and collect the zirconium. These HCl concentrations were based on data from a previous study [HOF] which showed that zirconium stayed on the column above 5 M HCl, started to elute at 4 M HCl with some tailing, and eluted below 3 M HCl. The study was conducted using Dowex 1 anion exchange resin and HCl as the eluting agent. In

23

retrospect, zirconium would be best eluted using an even lower HCl concentration since some mixing in the column with 12 M HCl occurred raising the effective HCl concentration close to 4M which caused tailing. However, care should be taken not to go too low (<0.25M HCl) such that the zirconium hydrolyzes.

^{172}Hf was also purchased from Isotope Products in Burbank, CA but in a chloride form in 6 M HCl. It was produced as a spallation product by bombarding a bismuth target with high energy protons. ^{175,181}Hf was produced from neutron irradiation of its oxide.

2.3.2.2 ^{229}Th / ^{239}Pu

Thorium and plutonium are both members of the actinide series. Solvent extraction studies were performed with carrier free thorium and plutonium tracers because of their tetravalent oxidation states. Their chemical behaviors were compared to the behaviors of tetravalent group 4 elements zirconium, hafnium, and rutherfordium. The comparison of elements with same oxidation states is not new. Previous studies [GRE88], [ZVA74], [ZVA76] compared the behavior of some pentavalent tracers such as group 5 elements niobium and tantalum to that of hahnium and showed that similarities existed within the group as expected. More recent studies [GOB92] compared the behavior of pseudo group 5 pentavalent tracers such as protactinium and neptunium to that of group 5 hahnium and showed that chemical differences were present even though the elements shared the same oxidation state.

2.3.3 Pentavalent Tracer ^{95}Nb

Niobium is a group 5 homolog of hahnium. Since it is pentavalent, its chemical behavior can be used to model the behavior of hahnium. ^{95}Nb is the β^- decay daughter of ^{95}Zr.

2.3.4 Production of Transactinides ^{261}Rf / ^{263}Rf / ^{263}Ha

The chemical properties of ^{261}Rf were studied using surface sorption (Chapter 3) and solvent extraction (Chapter 4) techniques. A ^{248}Cm target was used to produce 78-s [KAD93A] ^{261}Rf from the ^{248}Cm(^{18}O,5n) reaction. The reaction cross section was 5 nb using an ^{18}O^{5+} beam with an incident energy into the target of 98 MeV in the laboratory system [GHI70]. Typical average beam intensities were 2.5 electrical microamps (eμA).

Experiments were performed to search for ^{263}Rf (Chapter 6). The ^{248}Cm (^{18}O, 3n) and ^{248}Cm (^{22}Ne, α3n) reactions with incident energies of 98 MeV and 116 MeV, respectively, were used to attempt the direct production of ^{263}Rf. Additionally, an attempt to indirectly produce ^{263}Rf using a ^{249}Bk target to first produce ^{263}Ha in the ^{249}Bk (^{18}O,4n) reaction, then search for its electron-capture decay daughter ^{263}Rf was performed. The ^{263}Ha reaction cross section is about 10 nb using an ^{18}O^{5+} beam with an on-target energy of 93 MeV [SCH92].

2.3.5 Production of ^{18}O Gas

^{18}O was produced prior to each experiment by electrolyzing a solution of $H_2^{18}O$. After evacuating a rubber inner tube, its valve was closed and the inner tube was attached to the positive side of a glass U-tube using a jacket screw and flex connector. The positive and negative electrode terminals on the U-tube were connected by wire leads to the respective positive and negative terminals on a power supply. 4 mL of $H_2^{18}O$ was added to the U-tube. Small amounts of Na metal were also added which reacted with the $H_2^{18}O$ to produce electrolyte.

An ice bath was prepared and the U-tube was placed into the ice bath so that the water level of the ice bath was just above the level of the U-tube's electrodes to prevent overheating. After warming up the power supply at 10 V for 5 minutes, the voltage was increased to 22 V for an additional five minutes and the inner tube valve was kept closed while the jacket screw connecting the inner tube to the U-tube was kept open. This served to remove any ^{16}O in the U-tube and in the connecting attachments by pushing the ^{18}O out through the open jacket screw. The jacket screw was then tightened and the inner tube valve was opened slightly such that water levels on both sides of the U-tube remained above the electrode levels. Since the inner tube had been evacuated earlier, care had to be taken not to open the inner tube valve too far or negative pressure would result causing the $H_2^{18}O$ to shoot up into the inner tube. Consequently, the valve was opened slowly over a period of about 1 hour before the pressure in the inner tube came to equilibrium with the evolving ^{18}O at the positive electrode in the U-tube.

Additional Na metal had to be added after about 2 hours to maintain sufficient conductivity. After several hours, the ^{18}O was transferred from the inner tube by freezing it into a small metal cylinder with liquid nitrogen. The metal cylinder could be used for injection of ^{18}O into the ECR source at the LBL 88-Inch Cyclotron or for long term storage.

26

2.4 Radiation Detection and Data Acquisition Systems

All gamma-emitting isotopes were assayed for gamma activity using a high-purity 50-mm Ge gamma-ray spectrometer system. The system included Canberra System 100 and Ortec ACE 4K hardware and software for data acquisition and analysis.

Alpha-emitting isotopes ^{229}Th, ^{237}Np, ^{239}Pu, ^{241}Am, and ^{249}Cf were assayed with Ortec or Tennelec silicon surface barrier detectors. Ortec ADCAM spectrometer and Ortec 676A ALPHA-KING spectrometer systems were used for data acquisition and analysis.

Alpha emitting and spontaneously fissioning isotopes of rutherfordium were assayed with passivated ion-implanted planar silicon (PIPS) detectors. Prior to each experiment, the PIPS detectors were pre-calibrated with a ^{212}Pb source, produced from ^{224}Rn daughter activities emanating from a ^{228}Th source. Fission energies were pre-calibrated with a ^{252}Cf source, and the fission threshold energy was set at 20 MeV to prevent interference from alpha energies. At the end of each experiment, the detectors were recalibrated and any shift in gain was corrected for in the post-run data analysis.

Our Realtime Data Acquisition and Graphics System (RAGS) [LER87] was initially used for data acquisition and storage. However, a change was made to an improved data acquisition system that was list processor-based. The new system employed a HyTec LP1341 list processor that read and buffered data from the Hytec buffer and sent the data to an on-line display and stored the data on a host computer hard drive in list mode. The time, channel number, and detector number of each incoming event was stored in the hard drive. Both the RAGS and the list processor based data acquisition systems employed Ortec AD811 analog-to-digital-converters (ADC). Signals initiated at PIPS detectors from alpha or spontaneous fission (SF) events were fed into

27

preamplifiers then into the appropriate amplifiers. The ADC's which were controlled by a CAMAC crate controller then digitized the amplified output sigals.

The Hytec list processor and a Jorway 73A-1 CAMAC crate controller were driven with Chaos data acquisition and analysis software [RAT91], [RAT93]. An instruction list of CAMAC commands was stored inside the list processor which was used to execute the commands and buffer the incoming data.

2.5 Data Analysis

Alpha and SF event listings were produced using the histogramming program CHEMHIST [GRE]. CHEMHIST histogrammed the events by channel number and sorted the events into appropriate time intervals specified by the user. The histograms were graphically displayed using the alpha integration program (AINT) [GRE]. Regions of interest (ROI) were set by the user and ROI integrals were saved in decay-curve files. The event listings included any or all of the following information: sample number, detector number, total number of alpha events such as from bismith, fermium, and rutherfordium, total number of SF events, beam dumps, gas-jet collection time, time between end of collection and beginning of chemical separation, time between end of collection and beginning of count, time the event took place, and total count time for each sample. CHEMHIST also produced a separate listing of sample number, detector number, channel number, energy, lifetime, and time the event took place for each sample. This listing was tailored to list only the events that fell within a specified energy range.

The decay-curve files were fed into the Maximum Likelihood Decay by the Simplex Method program (MLDS) [GRE90] to generate a decay curve and calculate half-lives, error limits, and initial activities for each component of the curve. Half-life fits based on the data served to verify the production of various isotopes of interest and to

verify that the experimental half-life was similar to the half-life given by MLDS. Initial activities were used along with corrections for gas-jet efficiency, detector geometry, chemical yield, beam integral, time of separation, counting interval, and decay branch to calculate production cross sections or chemical yields for various isotopes of interest. The production cross section equation is shown below.

Equation 2.1

$$N\lambda = (N_T)(\sigma)(\varphi)(1 - e^{-\lambda t_{irr}})(e^{-\lambda t_{sep}})(1 - e^{-\lambda t_{count}})(jet)(det)(chem)$$

where N=number of events

λ=decay constant

N_T=number of target atoms (typically $\approx 10^{18}$)

σ=production cross section

φ=flux (typically 3×10^{12} / s cm^2)

t_{irr}=gas-jet collection time

t_{sep}=time between end of collection and beginning of count

t_{count}=time on detector

jet=gas-jet efficiency (typically 0.6)

det=detector geometry (typically 0.35 for alphas and 0.7 for fissions)

chem=chemical yield

2.6 Column Procedure for Attempted Production of ^{263}Rf

The following procedure was used to confirm the production of ^{263}Rf (Chapter 6). To separate pentavalent cations from tetravalent cations, low (α-HiB)$^-$ concentrations were required. Trivalent, tetravalent, and pentavalent tracers were run through columns packed with AG50 x 12 (-400 mesh) and an AG50 X 4 (-400 mesh) cation exchange resin. The resins were mixed with H$_2$O then centrifuged to remove any very small resin particles. This was repeated until the distilled H$_2$O above the resin took on a clear appearance indicating a substantial removal of the fines. Various lower concentrations of

α-HiB were used to identify optimal elution conditions for separating pentavalent cations from tetravalent cations. 0.075 M α-HiB and 0.5 M α-HiB, both unbuffered, were found to be optimal for eluting pentavalent and tetravalent cations, respectively, while keeping the trivalent cations on the column. It was important that the separation between tetravalent and trivalent cations be better than 1000:1 because of the interfering trivalent actinides such as Fm that were produced during a bombardment. To insure the accuracy of the α-HiB solution concentrations and the integrity of the original α-HiB solid from which the solutions were made, the pH of each α-HiB solution was measured. Unbuffered 0.075 M α-HiB had a pH of 2.52 and unbuffered 0.5 M α-HiB had a pH of 2.11, both as expected, based on its K_a of 1×10^{-4}.

The glass column used was platinum tipped for smaller drops, had a 2 mm inner diameter and was 2.5 cm in length. The column was first prepared with H_2O, then the free column volume (FCV=volume of liquid in a resin packed column external to the resin itself) was measured using a 1 M HCl solution which was pushed through the column using N_2 pressure and collected into sodium bicarbonate powder which reacted with the HCl and produced gas. The FCV was found to be just over 2 drops (>80 μl).

^{95}Zr, ^{95}Nb, ^{152}Eu, and ^{249}Cf tracers were picked up with 20 μl of 0.075 M α-HiB/0.013 M KCl solution and loaded onto an AG50 x 12 (-400 mesh) cation exchange column and an AG50 x 4 (-400 mesh) cation exchange column both already pretreated with 0.075 M α-HiB. The KCl was added to simulate experimental conditions at the cyclotron where approximately 0.013 M KCl comes through the gas jet during a ten minute collection. The active solution was pushed through to just the top of the resin level then a few drops of 0.075 M α-HiB were added onto the column to elute the pentavalent ^{95}Nb. Any excess 0.075 M α-HiB was pushed through to just the top of the resin level then a few drops of 0.5 M α-HiB was added onto the column to elute the tetravalent ^{95}Zr. Because of the low cross linkage, resin-solution equilibrium was achieved with an elution performed at a flow rate of 5 seconds per drop. Each drop was

30

collected in separate plastic centrifuge cones. The cones were then capped and placed in the appropriate detector for either alpha or gamma spectroscopic analysis.

Plating Cell

Teflon
Chimney

Glass Stirrer

HV Connector

Top Section

Pt Foil (+)

Mid Ring

Clamp Ring

Be Foil (-)

Al Base Plate
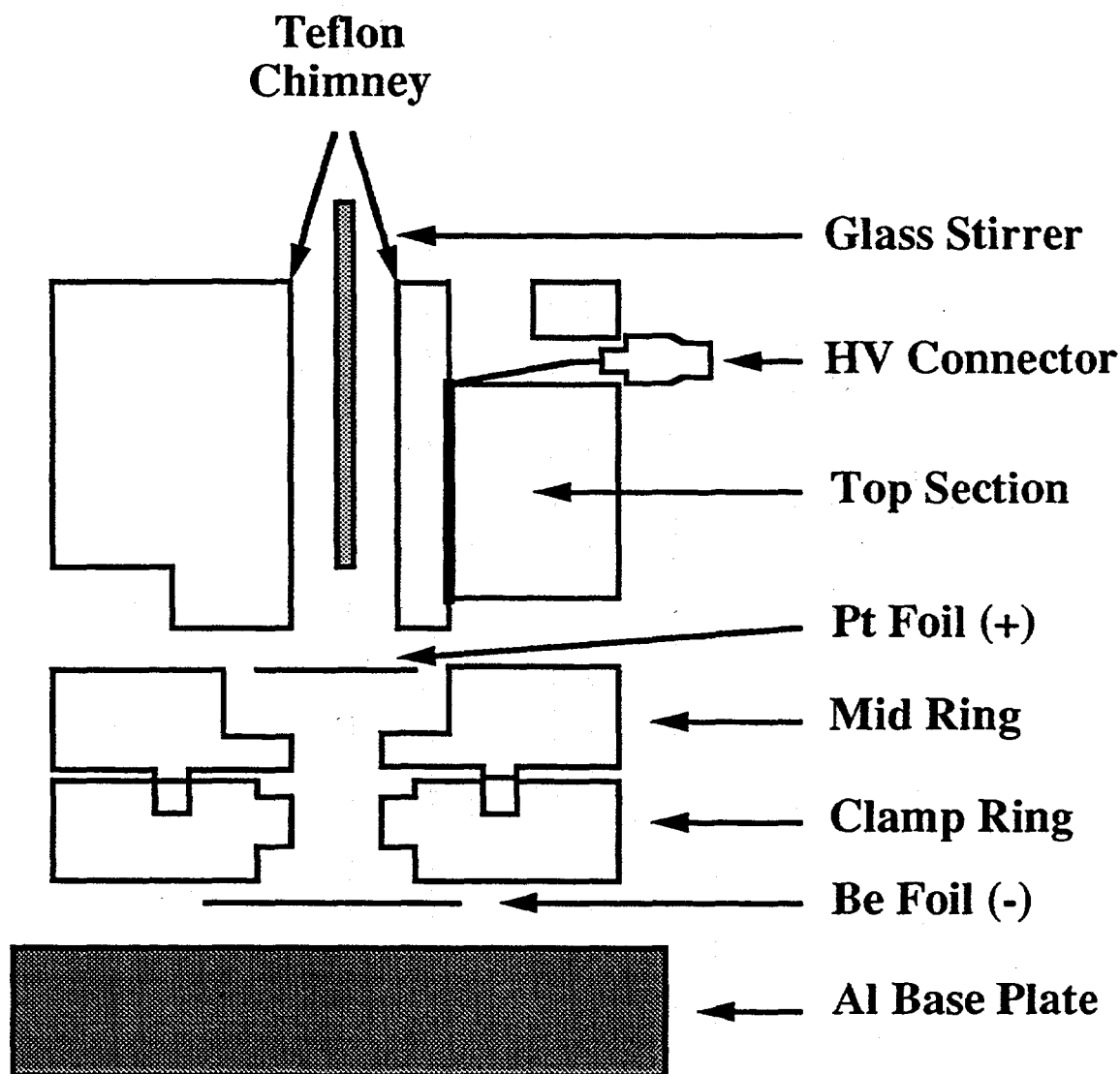
Figure 2.1 Cross sectional view of the electroplating cell.
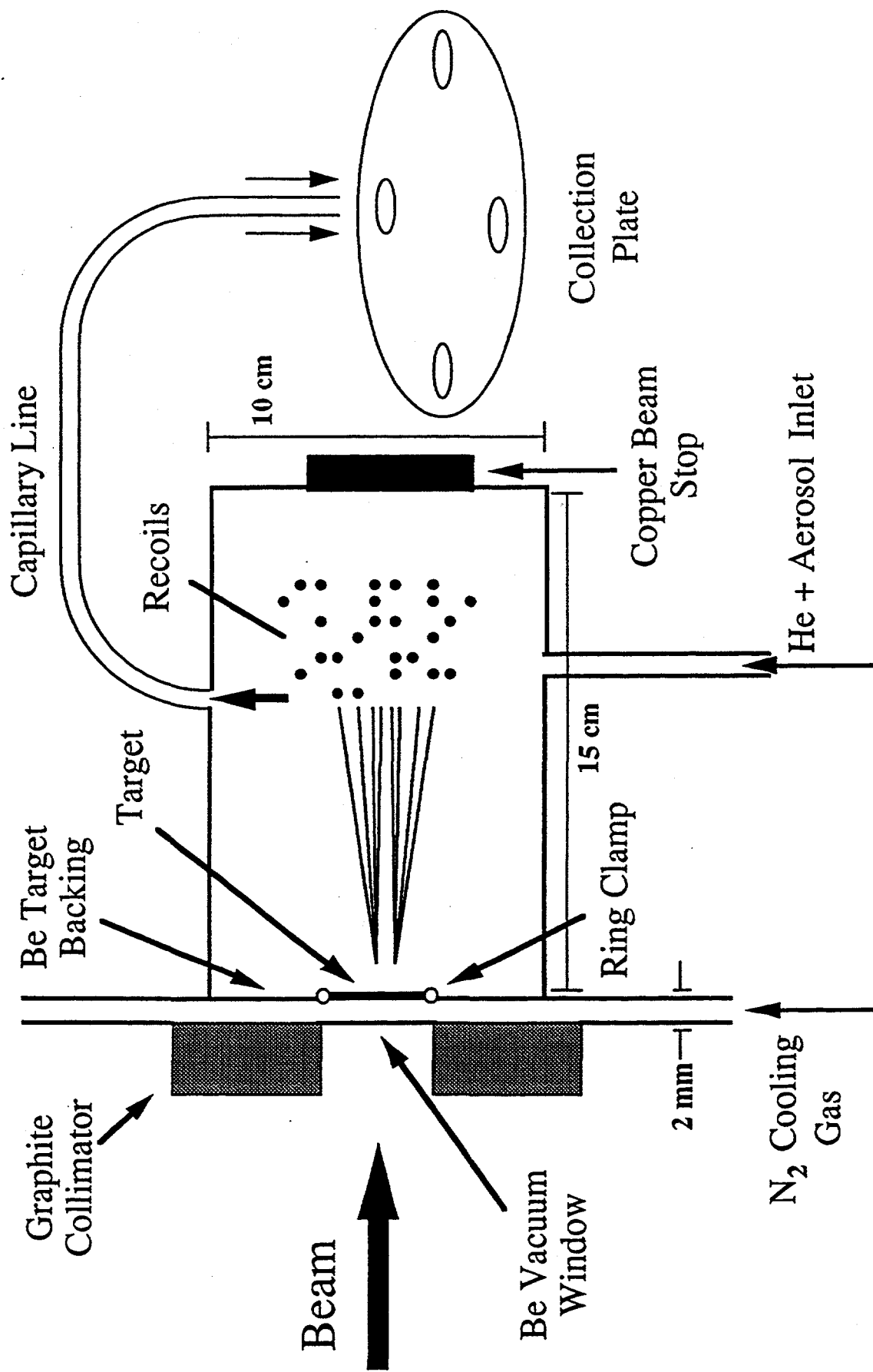
Figure 2.2 Target system schematic in Cave 0 at the LBL 88" Cyclotron.

Capillary Line

Recoils

Collection Plate

10 cm

Copper Beam Stop

He + Aerosol Inlet

15 cm

Target

Be Target Backing

Ring Clamp

Graphite Collimator

Be Vacuum Window

N₂ Cooling Gas

2 mm

Beam

33

Recoil Chamber Schematic

Teflon
Capillary To
Collection
Site

i.d. 0.8,
1.4, or
1.6 mm

Beam

Target

0.75"
1.0"
or
1.25"

He/KCl
Aerosol Inlet
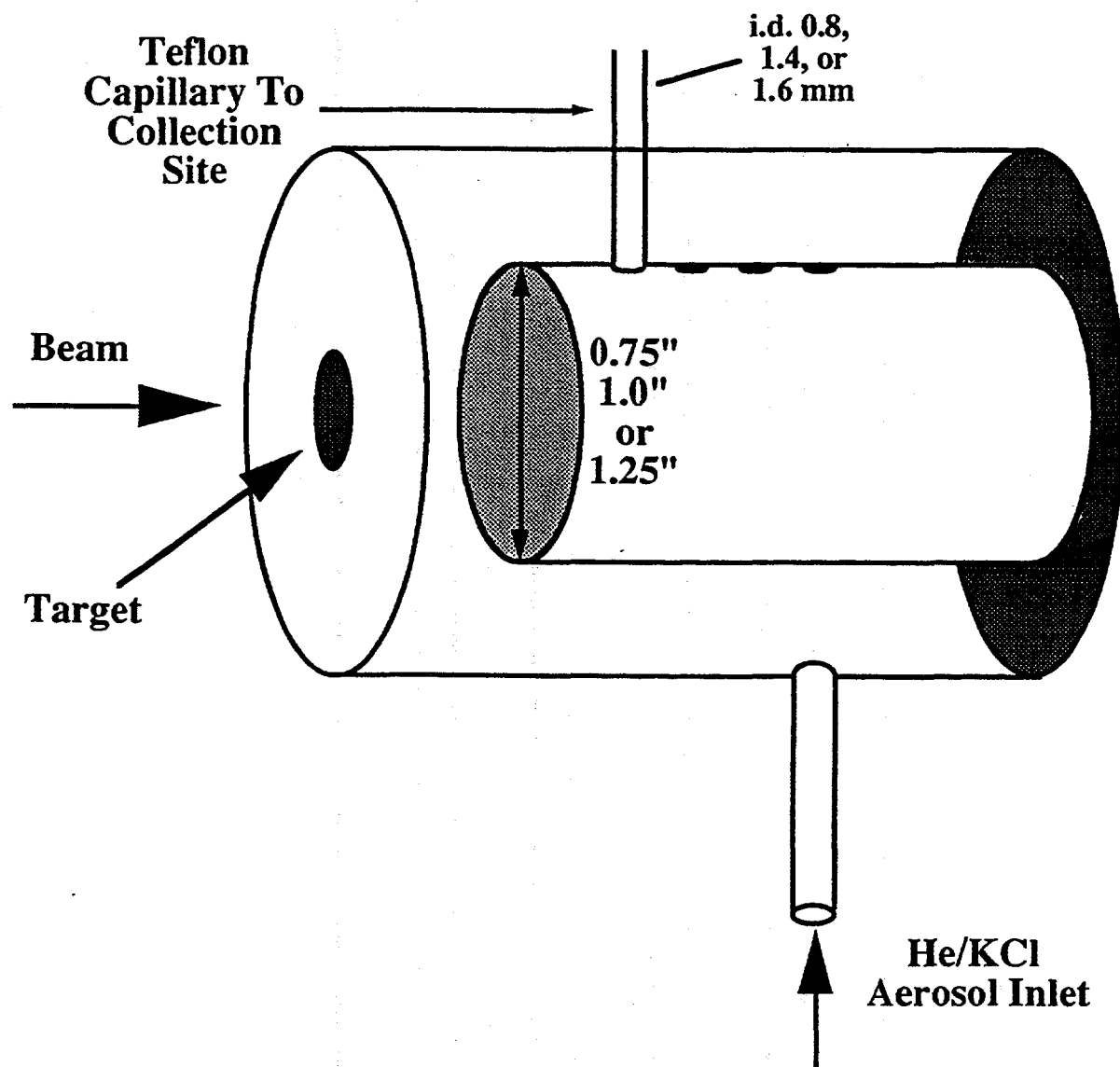
Figure 2.3 Schematic of recoil chamber used in Cave 0 target system at the 88-Inch Cyclotron.

Recoil Source

Ra-225 collected on flat brass pin

300 V Battery

+

-

-

1 atm He

+

Th-229 source

Figure 2.4 Schematic of the Th-229 recoil source. Th-229 alpha decays to Ra-225 which recoils out of the source as positively charged ions and is collected on the negatively charged brass pin.
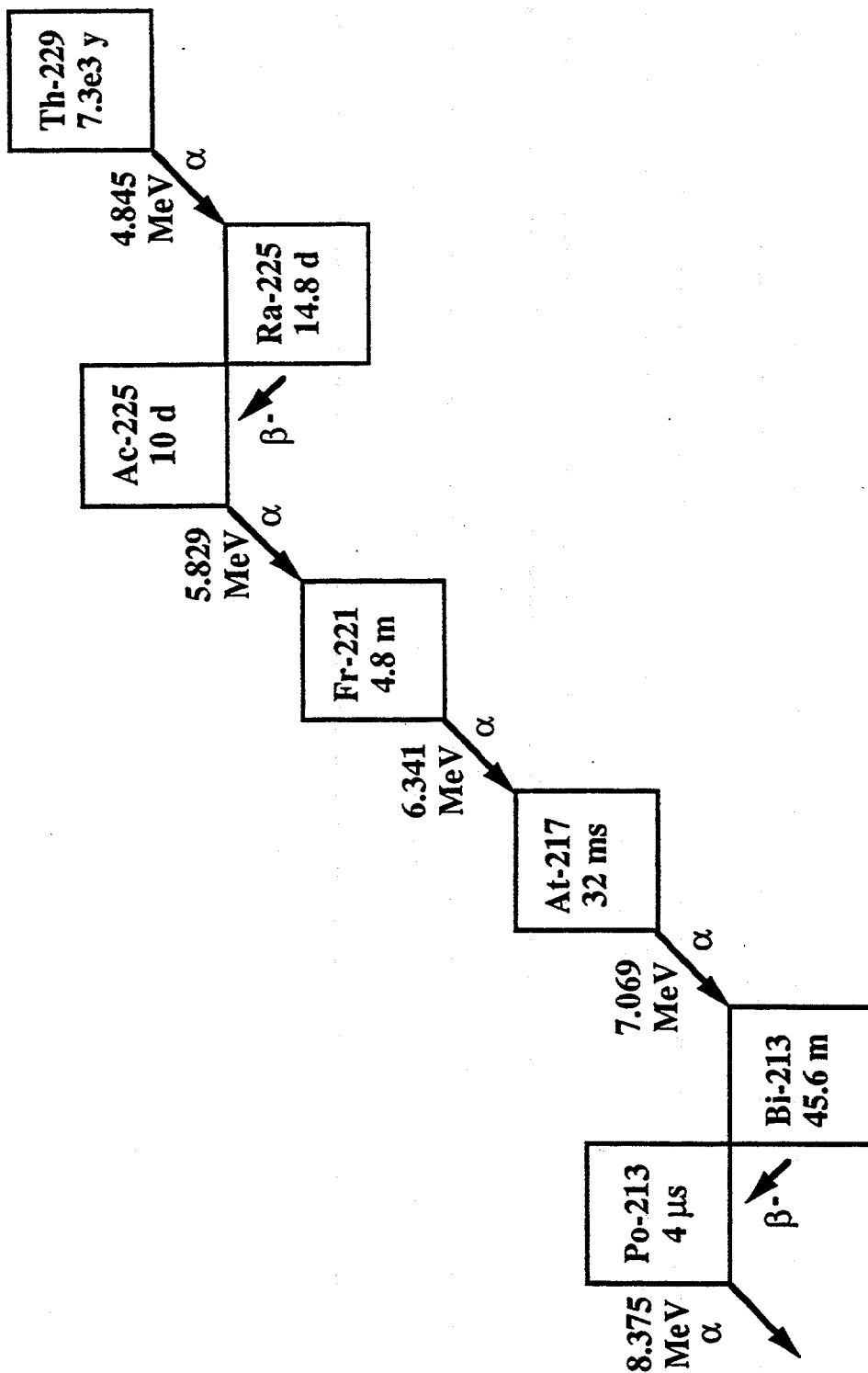
Figure 2.5 Decay Chain of Th-229

Th-229
7.3e3 y

α
4.845
MeV

Ra-225
14.8 d

β-

Ac-225
10 d

α
5.829
MeV

Fr-221
4.8 m

α
6.341
MeV

At-217
32 ms

α
7.069
MeV

Bi-213
45.6 m

β-

Po-213
4 μs

α
8.375
MeV

Ac Recoil Chamber

Positive
End

Brass
Pin

Metal
Pin

Negative
End

225 Ac Recoil
Source

He/KCl
Aerosols In

He/KCl
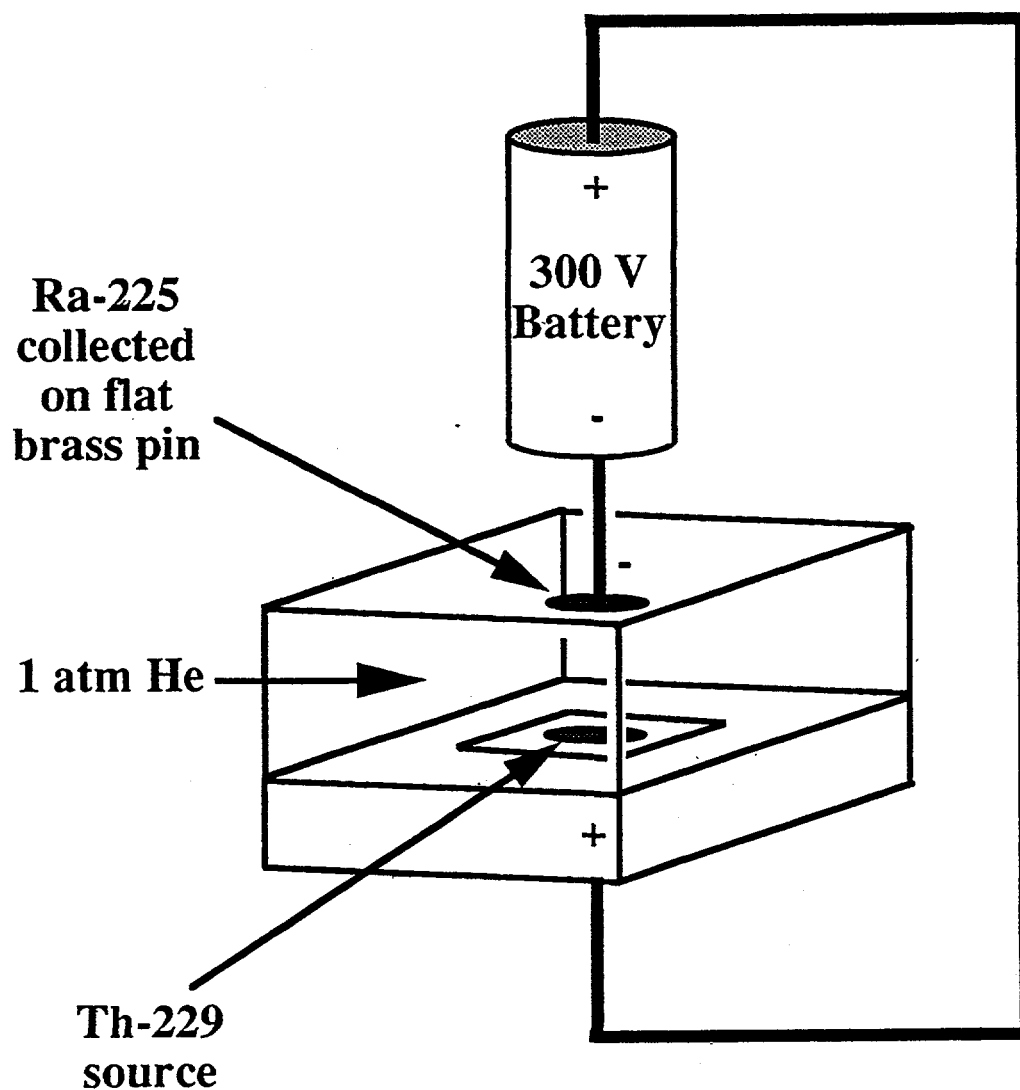Radioactive
Aerosols
Out To Detection
System
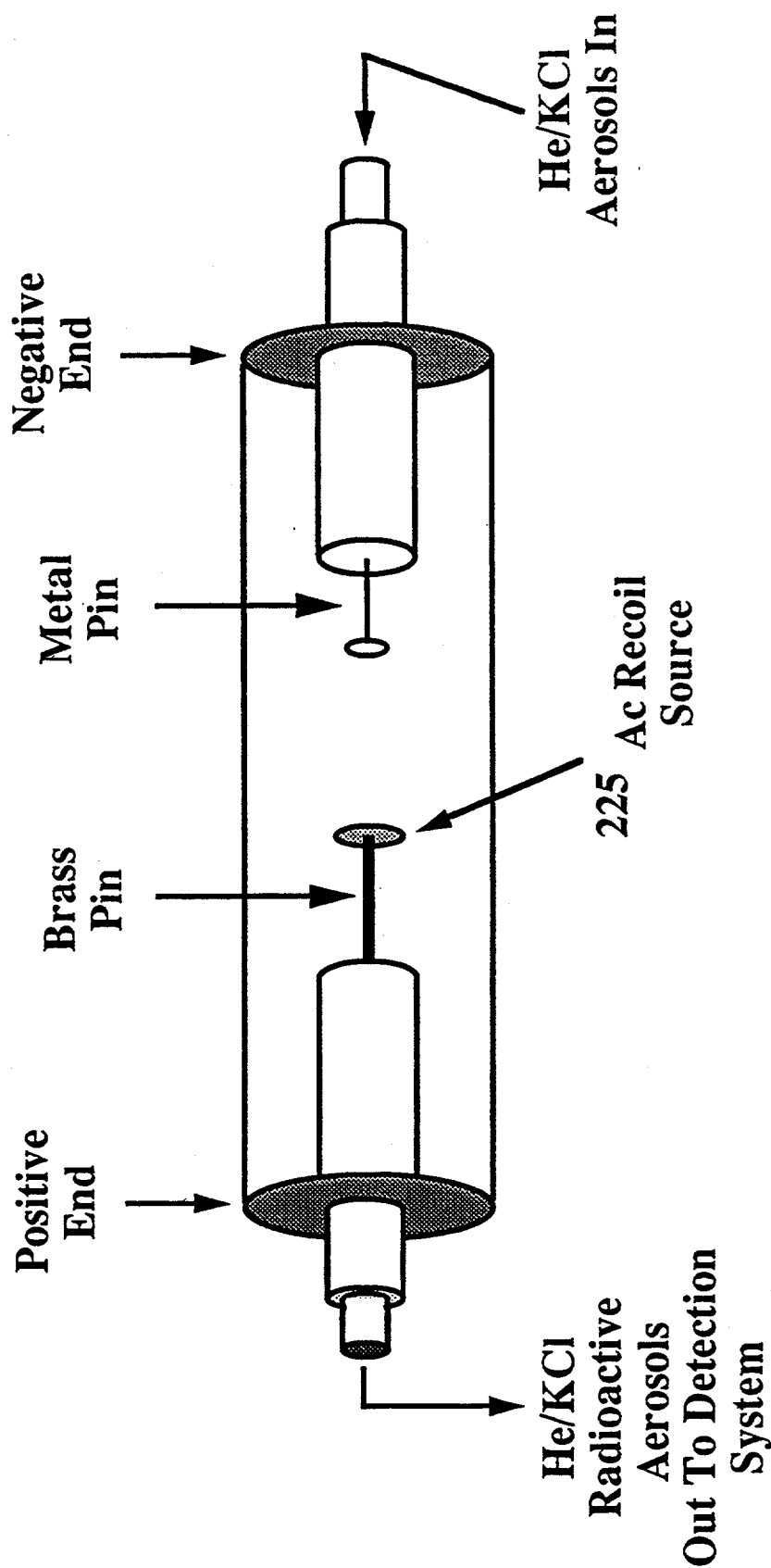
Figure 2.6 Ac-225 recoil chamber used to generate Fr-221 recoil products for gas-jet yield measurements. A bias voltage of 50 V/cm was used to help move the 5-minute Fr-221 recoils away from the source. The Fr-221 atoms then attached to the He driven KCl aerosols and were transported to the collection site at the other end of the capillary.

37

Effect of Oven Temperature on Gas-Jet Yield

Figure 2.7 He/KCl gas-jet yield as a function of temperature. ^{221}Fr recoils were transported to the collection site and counted in ten minute intervals.

Chapter 3

Surface Sorption Chemistry

3.1 Introduction

The ferrocyanides of the transition metal cations are known to be good selective sorbents for heavy alkali metal cations like Rb^+, Cs^+, and Fr^+ [HAA93]. In general, the affinity series for these ferrocyanide sorbents is as follows [LIE67]:
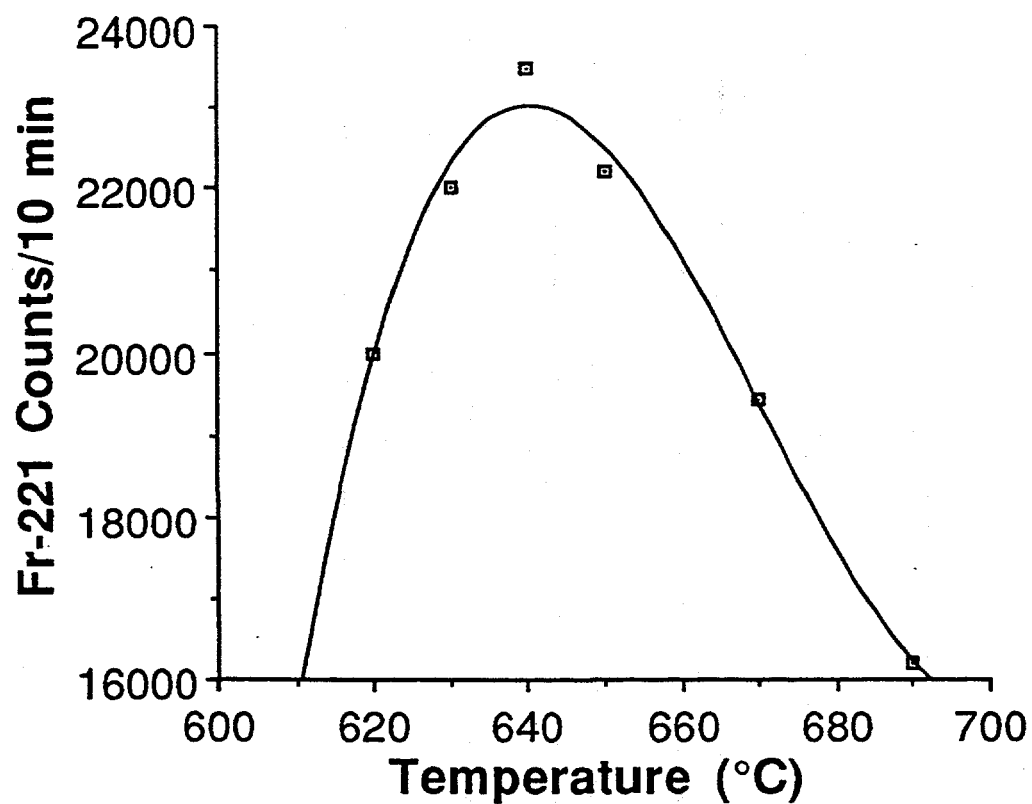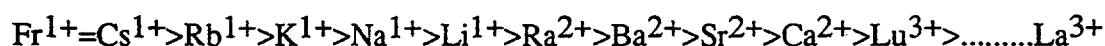
$$Fr^{1+}=Cs^{1+}>Rb^{1+}>K^{1+}>Na^{1+}>Li^{1+}>Ra^{2+}>Ba^{2+}>Sr^{2+}>Ca^{2+}>Lu^{3+}>.........La^{3+}$$

Therefore, the affinity of the ferrocyanides for metal cations increases with decreasing oxidation state and increasing radii. Sorption occurs by way of ion exchange, but the exact ion exchange mechanism for the ferrocyanides is rather complex and has not yet been completely elucidated [QUR91]. However, their ion exchange selectivity does depend largely on the steric effect, such as, in extractions where crown ethers are used to extract various cations [VES72]. Those cations with ionic radii more closely matched to the accomodative radius of the crown ether will be more easily extracted.

The unit cell structure of cobalt(II)ferrocyanide is shown in Figure 3.1. Iron has a low spin configuration; therefore, it bonds with the carbon from the cyanide group while cobalt has a high spin configuration, so it bonds with nitrogen. Spin refers to the number of unpaired electrons in the e_g-t_{2g} electronic orbitals created by an octahedral

arrangement of anions around a central metal ion. The cobalt in the center of the lattice is present in alternate unit cells and is surrounded by four water molecules in a tetrahedral array.

Crystalline and composite adsorbent ferrocyanides have found various applications in analytical chemistry for the preconcentration and separation of ^{137}Cs in environmental samples [VES72], in nuclear and radiochemistry for the separation and identification of [223]Fr [ABD90], and in technological practices for the extraction of [134,137]Cs from various kinds of liquid radioactive wastes [NAR86], [NAR88], [HAA93].

Chemical separation by surface sorption has been found to be a fast and efficient method for separating tetravalent cations such as Rf from trivalent actinide contaminants. The Co and Ni ferrocyanide sorbents have been found to exhibit particularly high affinities for tetravalent elements [LIE67], [BIL84]. The other ferrocyanide sorbents were chosen for study based on their well-known properties and on availability.
Studies of the sorbents were carried out a) in batch powder experiments to determine which sorbent would be best suited to study the group 4 elements and b) in thin film surface experiments to study the sorption characteristics of the group 4 elements.

3.2 Experimental Procedures

## 3.2.1 Preparation of Sorbents

Transition metal salt solutions were mixed with $K_4Fe(CN)_6$. The acidity, the order of mixing, and the initial ratio of the reacting components determined the compositions of the precipitates that formed. The sorbents that were studied are listed in Table 3.1. All of the metals were divalent with the exception of Ti which was tetravalent.

Table 3.1 Sorbents Studied

Sorbent Sample	Sorbent Produced	Metal/Fe Mole Ratio
1	$(TiO)_2Fe(CN)_6$	2
2	$(TiO)_8(OH)_{12}Fe(CN)_6$	8
3	$Ni_2Fe(CN)_6$	2
4	$K_2ZnFe(CN)_6$	1
5	$K_2CoFe(CN)_6$	1
6	$Co_2Fe(CN)_6$	2

The sorbents were prepared by mixing the metal salt with potassium ferrocyanide solution. A solution of 0.1 M $K_4Fe(CN)_6$ was added slowly to a metal salt solution over a period of minutes. The concentration of the titanium tetrachloride metal salt was 0.1 M in sample 1, 0.01 M in sample 2, and the metal salt concentrations for samples 3 through 6 were 0.1 M. After the initial precipitate formed, the solutions were placed in a mixing bath for 8 hours, then the transition metal ferrocyanides were separated from the solutions and air dried. The general precipitation reaction is shown in the following equation:

Equation 3.1 $\qquad Fe(CN)_6^{4-} + 2M^{2+} + xH_2O \rightarrow M_2Fe(CN)_6 \cdot xH_2O$
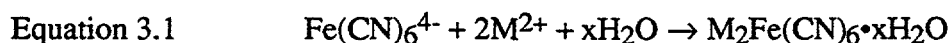
Small variations do occur, however, and such precipitation products can be represented by the general formula $A_{2n}M_{2-n}Fe(CN)_6 \cdot xH_2O$ where A is K^+ and M is the divalent transition metal or divalent cation such as TiO^{2+}.

3.2.2 Batch Powder Procedure

50 mg dry weight of each ferrocyanide sorbent along with 10 mL of 1 M HCl solution and [181]Hf tracer were placed in glass bottles and shaken in a heat bath for 10 hours. The distribution coefficients were calculated from the following equation:

Equation 3.2
$$K_d = \frac{(a_i - a_{eq})V}{(a_{eq})m}$$

where

a_i=initial activity of the radionuclide in solution

a_{eq}=activity of the solution at equilibrium

V=volume of the solution

m=mass of the sorbent

Batch experiments were performed to find which transition metal ferrocyanide sorbents would be best suited to study the group 4 elements.

3.2.3 Preparation of Surfaces

For incorporation of cobalt(II)ferrocyanide onto glass supports, many resins were tested as binding materials. The resin had to be hydrophilic so that an aqueous medium could be easily sorbed, it had to be resistant to acid, and swelling of the resin had to be minimal. Polyvinyl alcohol - formaldehyde polymer met all of these conditions. Polyvinyl alcohol was found to be hydrophilic and resistant to acid with minimal swelling while formaldehybe was used for polymerization.

5 g of polyvinyl alcohol was dissolved in 10 mL of water and added to 20 g of freshly precipitated cobalt(II)ferrocyanide, 0.2 mL of 9.7 M HCl, and 2 mL of 40%

formaldehyde. All substrates were intensively mixed, then the composite paste was spread onto a 2.5 cm^2 glass support disc and air dried at room temperature. The paste, once applied to the glass support disc, typically measured about 0.1 mm in thickness. The surfaces were preequilibrated with an appropriate concentration of HCl for 10 minutes then washed with acetone and dried. Transition metal ferrocyanides typically are stable in HCl up to 2 M, but the ferrocyanides of Co and Ni have been found to be resistant up to 8 M HCl [PRO65]. The surfaces could be stored for up to 6 months for later use.

In a typical experiment, a 2 cm^2 area of each surface was covered with 10 μL of an appropriate concentration of HCl solution containing either ^{95}Zr, ^{172}Hf, or ^{229}Th radiotracer which were used to model the behavior of Rf. After an appropriate equilibration time, determined in experiments that studied the sorption kinetics of each radiotracer (see Section 3.3.2), the surface was washed with 10 mL of the studied HCl solution to remove any activities that did not sorb. The surface was then dried with acetone and an air jet and counted in a germanium or alpha spectrometer system as described in Chapter 2. The % adsorption was calculated for each radiotracer by the following equation:

Equation 3.3 $\qquad$ $\%Ads = \dfrac{a_f}{a_i}$

$\qquad$ where

$\qquad$ a_f=activity on the surface after adsorption and separation

$\qquad$ a_i=initial activity on the surface

For the Rf experiments, ^{261}Rf and other activities were produced and transported to the collection site as described in Section 2.1 and 2.2. They were collected on a cobalt(II)ferrocyanide surface, 10 μL of HCl at the concentration to be studied was spread on the surface in a 2 cm^2 area, then after 10 seconds, the surface was washed with

10 mL of the same HCl solution, dried with acetone and an air jet, and counted in a PIPS detector. The procedure took roughly 60 seconds to complete.

3.3 Tracer and Rutherfordium Surface Sorption Results

3.3.1 Batch Powder Experiments

The sorption of ^{181}Hf with various transition metal ferrocyanide samples was tested to see which would be best suited to study the group 4 elements. Table 3.2 lists the ferrocyanide sorbent and the distribution coefficients obtained for each.

Table 3.2 Distribution Coefficients of ^{181}Hf for Various Ferrocyanide Sorbents

Ferrocyanide Sorbent	Distribution Coefficient
$(TiO)_2Fe(CN)_6$	730
$(TiO)_8(OH)_{12}Fe(CN)_6$	25
$Ni_2Fe(CN)_6$	2300
$K_2ZnFe(CN)_6$	40
$K_2CoFe(CN)_6$	650
$Co_2Fe(CN)_6$	11400

Cobalt(II)ferrocyanide was found to work best as a sorbent. Only samples of $Ni_2Fe(CN)_6$ and $Co_2Fe(CN)_6$ with a mole ratio of nickel and cobalt to iron of 2:1 had a high affinity for Hf^{4+} ions. The samples of mixed ferrocyanides such as $K_2ZnFe(CN)_6$ and

$K_2CoFe(CN)_6$ had lower affinities for Hf^{4+}. Consequently, cobalt(II)ferrocyanide was used in further surface sorption experiments to study the group 4 elements.

3.3.2 Sorption Studies of Alpha-Emitting Isotopes

An experiment was conducted to show that the cobalt(II)ferrocyanide surface could be used as an alpha source. Figure 3.2 shows the alpha spectrum of the surface after sorption of ^{229}Th from 1 M HCl. The equilibration time was 120 seconds. The separation factor between tetravalent ^{229}Th and trivalent ^{225}Ac was greater than 10^3, confirming that cobalt(II)ferrocyanide is a suitable material to separate tetravalent cations from trivalent cations. The resolution of the ^{229}Th peak was poor primarily because the sorption kinetics of ^{229}Th was slower than its diffusion time. A kinetics experiment (Figure 3.3) was performed that showed nearly 100% of the ^{221}Fr sorbed within the first five seconds of surface contact, while ^{229}Th required more than 90 seconds to achieve nearly complete sorption. Diffusion caused the thorium atoms to sorb throughout the layers of the surface material. The kinetics of ^{95}Zr and ^{172}Hf was also studied. Most of the ^{95}Zr sorbed within 20 seconds while ^{172}Hf required about 40 seconds. The tracers were sorbed from 1 M HCl which was chosen because 100% sorption was achievable for all tracers studied at this concentration.

Another but less significant reason contributing to the energy degradation of ^{229}Th was also observed. Since ^{229}Th was kinetically slower at sorbing than the univalent ions, species such as ^{221}Fr were first to occupy the top layer surface sites, forcing the slower sorbing ^{229}Th into sites below the top layer. In addition to being slower sorbing, the large number of ^{229}Th atoms in each experiment was close to the total number of top layer surface sites available (see calculation below). Thus, the resolution of ^{221}Fr was excellent (FWHM$\approx$25 keV) because it sorbed more quickly and was the first

to occupy top layer surface sites as observed from its sharp peak while the large number of ^{229}Th atoms exceeded the remaining number of top layer surface sites available and were therefore forced to sorb below the top layer. Had the diffusion rate for ^{229}Th been slower than its sorption rate, the alpha energy degradation from this effect would have been small and quite tolerable. However, since the diffusion rate for ^{229}Th was faster than its sorption rate, the ^{229}Th atoms sorbed throughout all the layers of the surface material resulting in significant alpha degradation.

The number of atoms in a typically studied 10 nCi sample of ^{229}Th is large because of its long half-life, but when using shorter lived tracers such as ^{95}Zr or ^{172}Hf, there are fewer atoms to sorb; therefore, enough top layer surface sites are present to accomodate a complete sorption assuming that the kinetics of sorption is faster than the diffusion rate. The number of potential top layer surface sites was calculated to be 3.5 x 10^{14} based on an estimated 5.3 Å x 5.3 Å surface area per unit cell over a total area of 2 cm^2. Based on the distribution of the centrally located Co within the cobalt(II)ferrocyanide lattice, it was assumed that there would be one potential site for every two unit cells.

The total number of atoms for each tracer was calculated from Equation 3.4 based on using 10 nCi of each tracer per experiment with no carrier atoms.

Equation 3.4 $$N = \frac{A}{\lambda} \cdot$$

The total number of ^{229}Th atoms was calculated to be 1.2 x 10^{14}, not including the ^{229}Th daughters present, and was close to the potential number of top layer surface sites available. The total ^{95}Zr and ^{172}Hf atoms was 3 x 10^9 and 3 x 10^{10}, respectively, both many orders of magnitude less than that of ^{229}Th.

The poor resolution of ^{229}Th was cause for concern regarding the alpha resolution from ^{261}Rf. In addition, since the activity at the cyclotron is transported to the collection

site via KCl, K^+ may interfere with the sorption of Rf^{4+}. The results from one of the first chemistry experiments are shown in Figure 3.4. The spectrum above 7 MeV shows the events from ^{211}Fm, ^{214}Po, and ^{261}Rf. This experiment was run for less than 8 hours, therefore, few events for these isotopes were observed, but it showed that the surfaces might be used to sorb and detect ^{261}Rf without significant alpha energy degradation. Indeed, subsequent cyclotron experiments showed definitive, high resolution alpha peaks for all three isotopes. Evidently, the sorption kinetics of ^{261}Rf was faster than its diffusion rate and the number of K^+ atoms ($\approx 10^{18}$ atoms), though large, was still small enough such that the small amount of energy degradation due to K^+ taking up the top-most layers could be tolerated. It is also possible that Rf^{4+} easily displaced any K^+ present on the top-most layers.

3.3.3 Surface Sorption Studies of Chloride Complex Formation and Hydrolysis

The cobalt(II)ferrocyanide surfaces were used to study chloride complex formation and hydrolysis for the tetravalent group 4 elements Zr, Hf, and Rf and the tetravalent pseudo-group 4 element Th. Figure 3.5 shows the sorption dependence as a function of HCl concentration. The sorption of Th sharply decreased with increasing [HCl] because Th started to form chloride complexes such as $ThCl^{3+}$ and $ThCl_2^{2+}$ (at 25° C, Th-Cl log K_1 = 1.3838 while Zr-Cl log K_1 = 0.9 [SMI76] indicating that Th forms stronger complexes than Zr with Cl). Such chloride complexes do not sorb because the surfaces tend to preferentially sorb univalent species over divalent and trivalent ones [LIE67]. Indeed, a short experiment done on trivalent Eu, using the tracer procedure discussed in Section 3.2.3, showed that Eu did not sorb at all. It is also possible that such chloride complexes are not sorbed because they are not able to fit inside the lattice

structure of cobalt(II)ferrocyanide. Zr and Hf sorption decreased only slightly from 1 to 5 M HCl because they were less likely than Th to form chloride complexes in this [HCl] range as shown in Figure 3.5.

Below 1 M HCl, sorption sharply decreased for both Zr and Hf because of the formation of hydroxy complexes such as MOH^{3+} and $M(OH)_2^{2+}$. The reaction for hydrolysis of a tetravalent metal is:

Equation 3.5 $\quad xM^{4+} + yH_2O \leftrightarrow M_x(OH)_y^{(4x-y)} + yH^+$
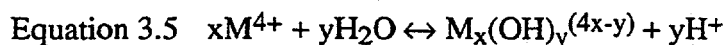
From this equation, the K_{1y} values are defined:

Equation 3.6 $\quad K_{1y} = \dfrac{[M(OH)_y^{(4-y)+}][H^+]^y}{[M^{4+}]}$

Based on the sorption curves in Figure 3.5, Zr hydrolyzed more strongly than Hf. Th sorption stayed high below 1 M HCl, indicating that it did not hydrolyze. This is in agreement with the Zr, Hf, and Th species distribution curves (Figures 3.6-3.8) which show similar concentrations of hydroxy complexes for Zr and Hf than Th at low pH. These distributions were calculated from the hydrolysis constants of the tetravalent tracers shown in Table 3.3 using the program SPCONC [HAR79], [HAR81].

Table 3.3 Tetravalent Tracer Hydrolysis Constants [BAE76]

Element	$\log K_{11}$	$\log K_{12}$	$\log K_{13}$	$\log K_{14}$
Zr	0.3	-1.7	-5.1	-9.7
Hf	-0.25	-2.4	-6.0	-10.7
Th	-3.2	-6.93	-11.7	-15.9

The results for Rf in Figure 3.5 show that Rf behaves more like Zr and Hf than Th. The sorption of Rf increases between 0.5 M and 4 M HCl indicating that it, too, forms hydrolyzed species such as $Rf(OH)^{3+}$ and $Rf(OH)_2^{2+}$ at lower HCl concentrations. Yet, Rf is more sensitive to hydrolysis throughout a wider range of HCl concentrations than are Zr and Hf. Therefore, the hydrolysis trend decreases in the order Rf>Zr≈Hf>Th, in agreement with the hydrolysis data listed in Tables 3.3 and 3.4.

3.4 Discussion

The greater tendency observed for Rf to hydrolyze is largely due to the influence of relativistic effects. To begin with, the first hydrolysis constants listed in Table 3.4 for the group 4 d-block elements, Zr^{4+} and Hf^{4+}, are lower than the group 14 p-block elements Ge^{4+}, Sn^{4+}, and Pb^{4+}. Their hydrolysis constants are lower because their coordination number in water is 8 (oxygen ligand field sp^3d^4 hybridized), and they form the aqueous complexes $Zr(H_2O)_8^{4+}$ and $Hf(H_2O)_8^{4+}$ compared to the group 14 elements, which have a coordination number of 6 in water and form $Ge(H_2O)_6^{4+}$, $Sn(H_2O)_6^{4+}$, and $Pb(H_2O)_6^{4+}$. The group 14 elements form such CN=6 complexes because the energy of the $5d_{5/2}$ orbitals in Sn and the $6d_{5/2}$ orbitals in Pb are too high to form the CN=8 hybridization sp^3d^4. This higher coordination number observed in Zr and Hf results in a lower charge density on the metal cations; therefore, the length of the M^{4+}-O bond is longer, and the proton from the water ligand is not as easily released:

Equation 3.7 $\qquad M(H_2O)_8^{4+} \longrightarrow M(H_2O)_7(OH)^{3+} + H^+$
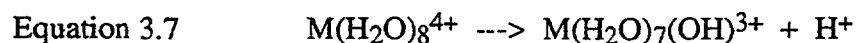
The metal-oxygen bond in CN 6 aqueous complexes for the group 14 elements is stronger because of a higher charge density on the metal cations and, therefore, the tendency for these elements to hydrolyze is greater.

In an attempt to keep the methodology consistent, the values listed in Table 3.4 were measured using similar experimental techniques and ionic strengths [NAZ68A], [NAZ71A], [ANT77] and their values are in good agreement with each other.

Table 3.4 Values of First Hydrolysis Constants For Group 4 and 14 Cations

Cation	Coord # (H$_2$O)	Ionic Radii (pm)	log K$_{11}$	Ref.
Ti^{4+}	6	60.5	1.25	[NAZ71B]
Zr^{4+}	8	79	0.295	[NAZ68]
Hf^{4+}	8	78	0.146	[NAZ71]
Ge^{4+}	6	53	0.807	[NAZ68A]
Sn^{4+}	6	71	0.570	[NAZ71A]
Pb^{4+}	6	84	0.50	[ANT77]

The coordination number of 6 predicted for Rf is largely due to relativistic effects which greatly destabilize the 6d$_{5/2}$ shell while stabilizing the 7p$_{1/2}$ shell making the electron configuration [Rn]6d$_{3/2}$7s^{2}7p$_{1/2}$ for Rf most likely (see Chapter 1 discussion). Therefore, more p character is present in Rf than there would be without relativistic effects. Consequently, Rf may share some characteristics with the group 14 elements, possibly giving it a coordination number of 6 (hybridization of 6d$_{3/2}$, 7s, and 7p$_{1/2}$ orbitals) and a larger first hydrolysis constant than otherwise expected. A coordination

number of 6 would indeed be more likely if the $6d_{5/2}$ orbital was energetically too high to participate in bonding.
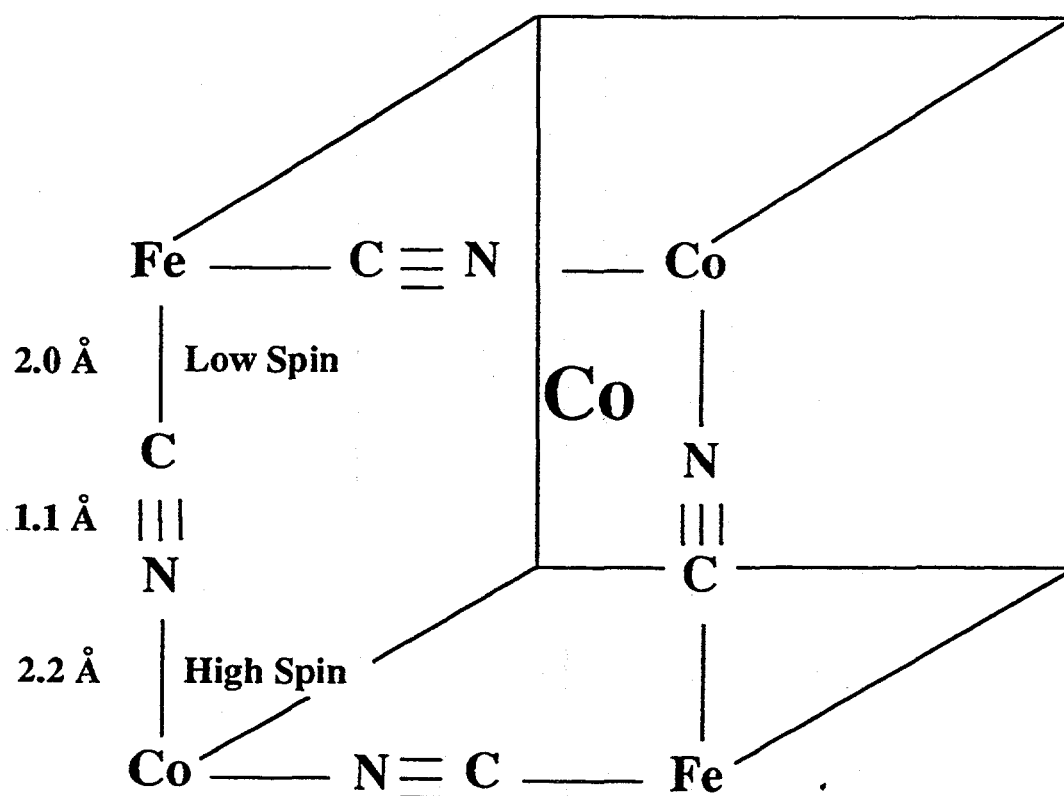
Structure of $Co_2Fe(CN)_6$

Figure 3.1 Unit cell of cobalt(II)ferrocyanide. Iron has a low spin configuration; therefore, it bonds with the carbon from the cyanide group. Cobalt has a high spin configuration so it bonds with the nitrogen from the cyanide group. The cobalt in the center of the lattice is surrounded by four water molecules in a tetrahedral array.
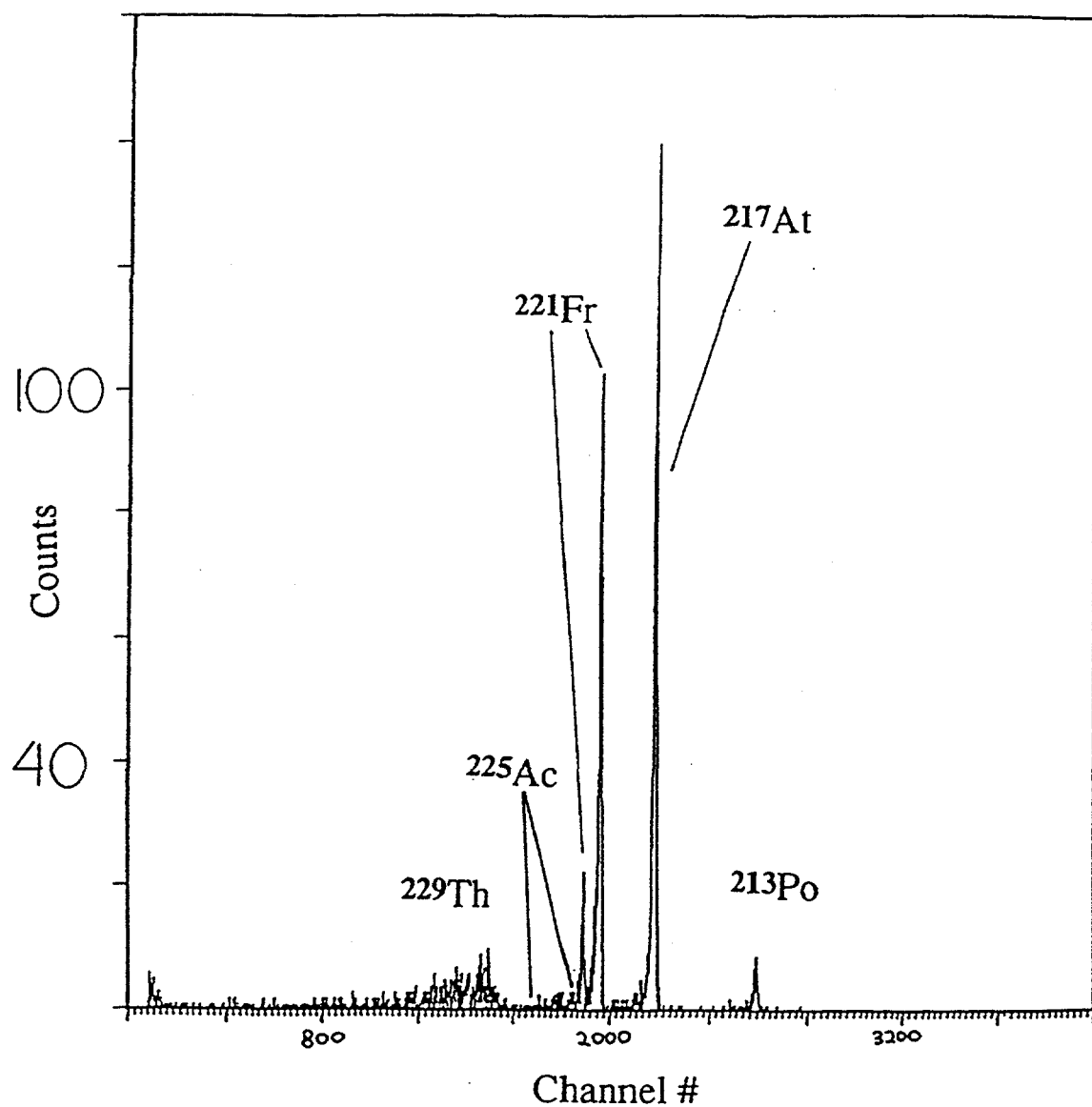
Fig.3.2 α-particle spectrum of cobalt(II)ferrocyanide surface. The equilibration time was 120 seconds. The resolution of the ^{229}Th peak is poor compared to the ^{221}Fr and ^{217}At peaks. Most of trivalent ^{225}Ac did not sorb as is evident from the low number of counts in its region of interest.
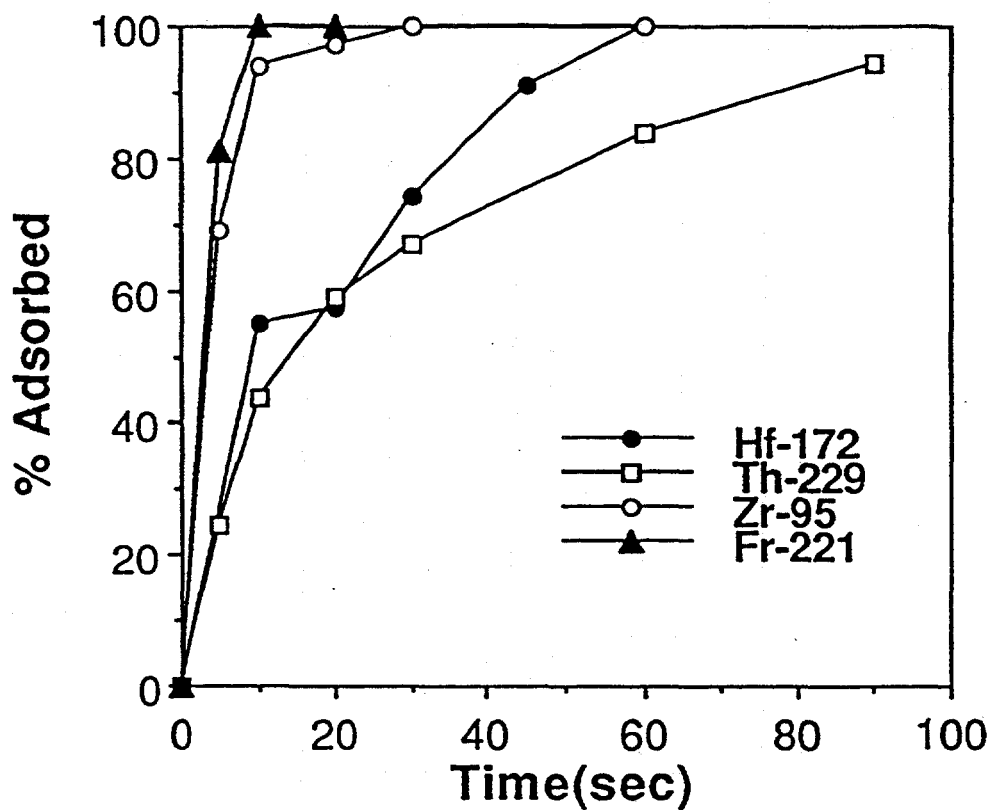
Figure 3.3 % sorbed vs. time obtained in sorption kinetics study of cobalt(II)ferrocyanide surfaces. Univalent francium came to equilibrium the quickest; hafnium took about 60 seconds; and thorium more than 90 seconds to come to equilibrium.
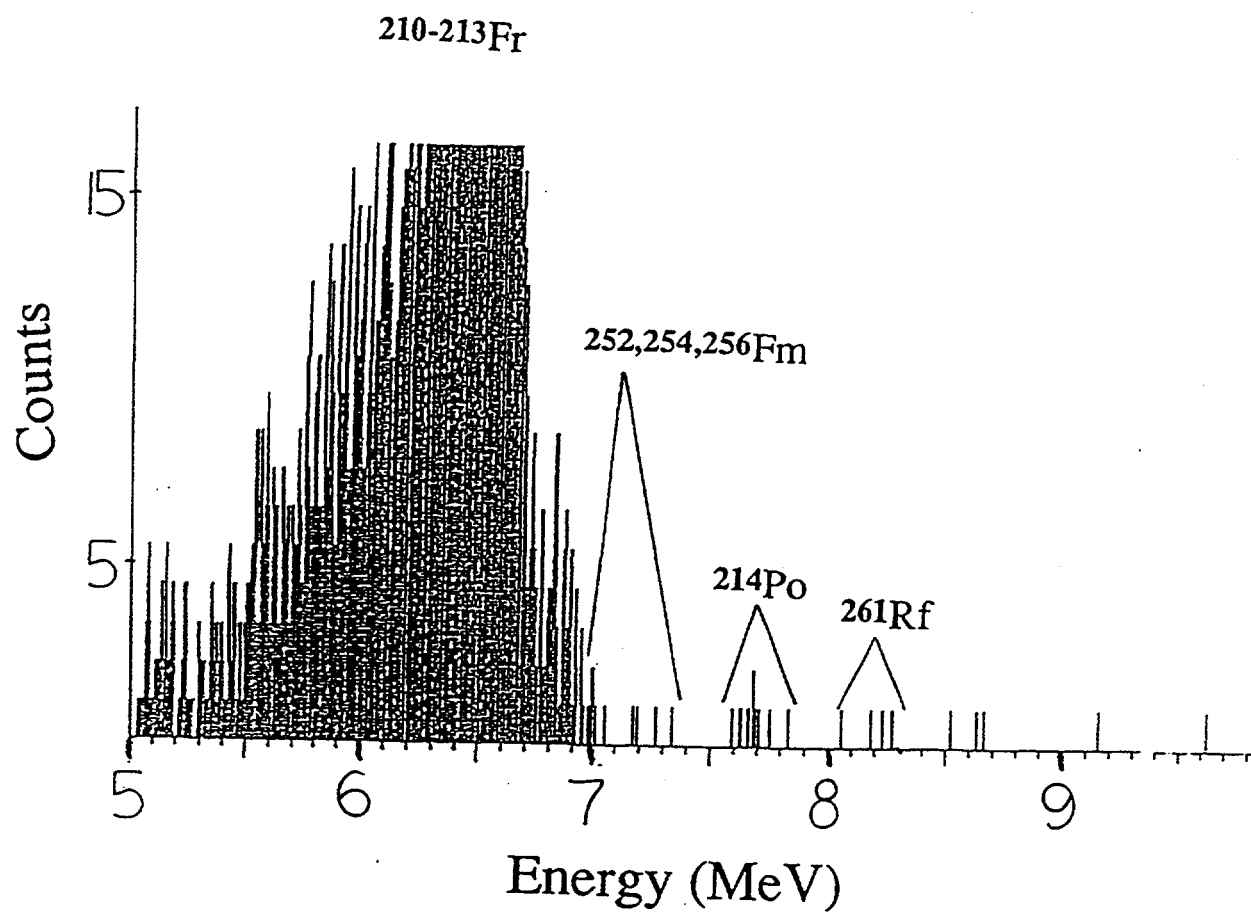
Figure 3.4 Summed α-particle spectrum from ^{261}Rf separations using cobalt(II)ferrocyanide surfaces and 1 M HCl.
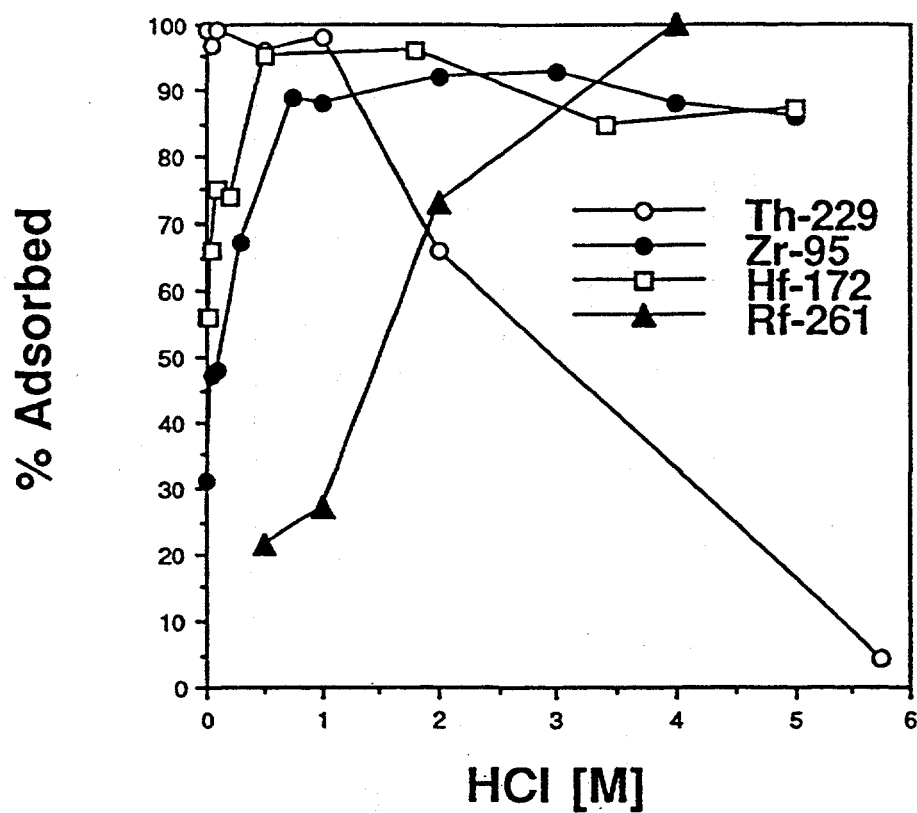
Figure 3.5 Sorption study on cobalt(II)ferrocyanide surfaces using various [HCl].
Zr and Hf behave much the same while the % adsorption of Th drops after 1 M
HCl. The % adsorption of Rf is less than that of Zr or Hf because Rf has a greater
tendency to hydrolyze below 4 M HCl.
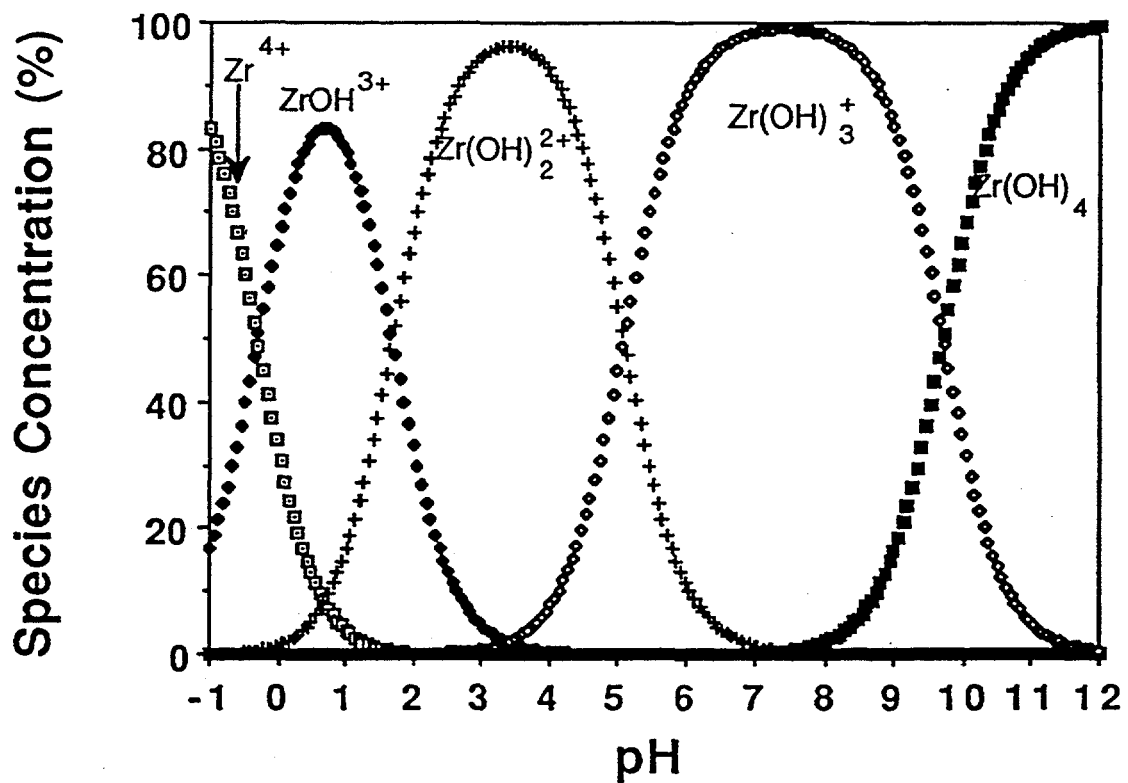
Figure 3.6 Concentration of zirconium hydrolysis species plotted as a function of pH. Zr easily hydrolyzes over the range of pH values examined and has already started to hydrolyze at pH = -1 (H^+ = 10 M). [BAE76]
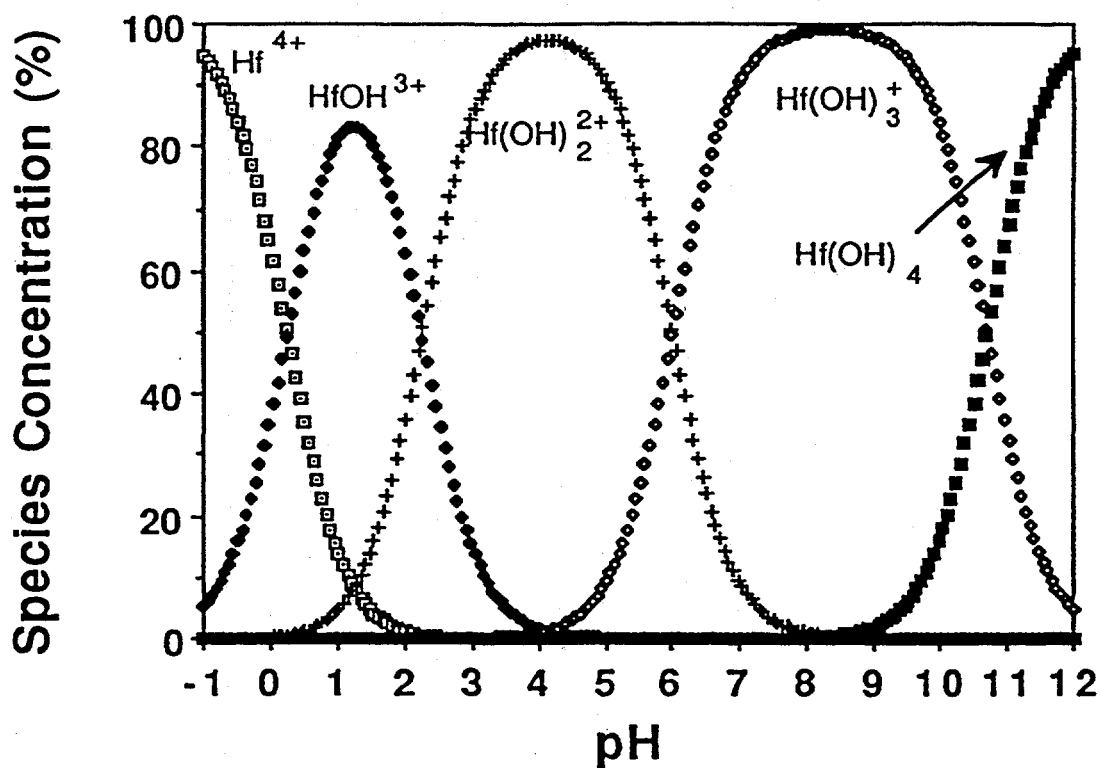
Figure 3.7 Concentration of hafnium hydrolysis species plotted as a function of pH.
Hf easily hydrolyzes over the range of pH values examined though Hf is slightly less
prone to hydrolyzing than Zr (Figure 4.6). [BAE76]

Figure 3.8 Concentration of thorium hydrolysis species plotted as a function of pH. Th is much less prone to hydrolyzing than either Zr (Figure 4.6) or Hf (Figure 4.7). Th mostly remains in its free, unhydrolyzed state below pH = 1.5. [BAE76]
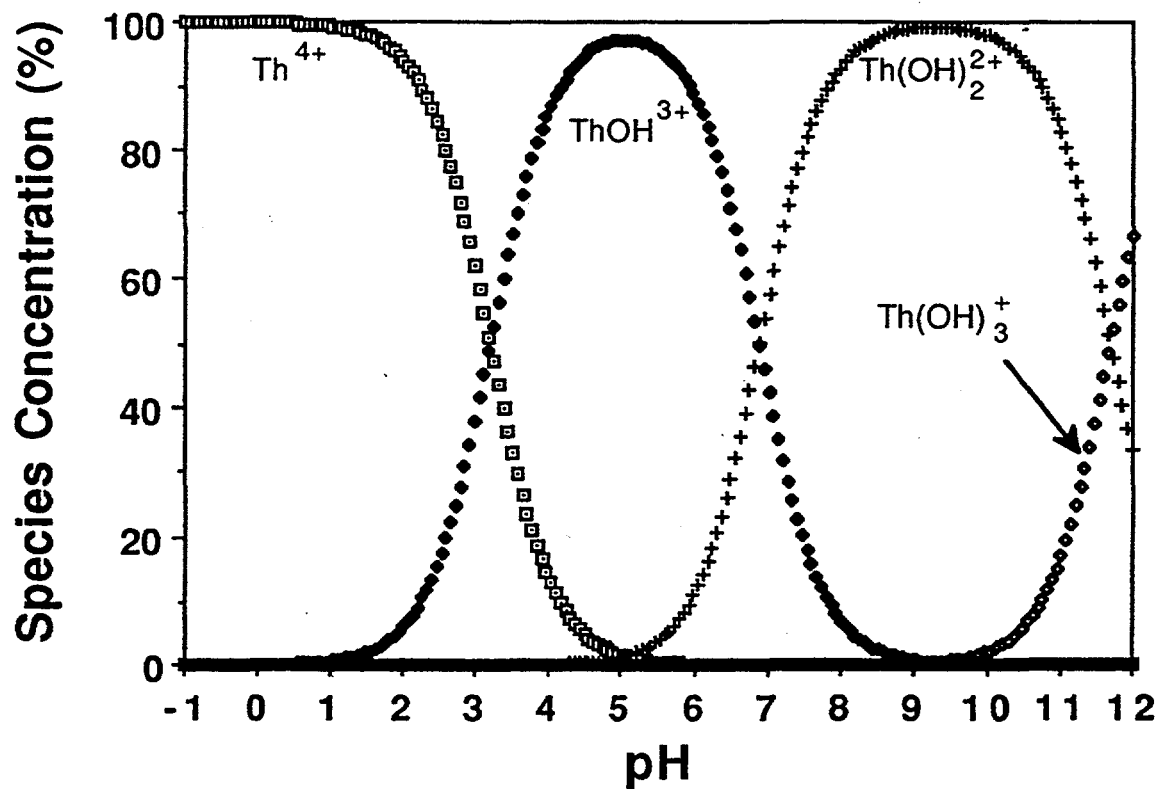
Chapter 4

Solvent Extraction With Tributylphosphate

4.1 Introduction

The technique of solvent extraction has commonly been used to separate metal ions from each other. In organic solvent extraction, a metal ion in some aqueous medium is selectively complexed to an organic ligand and extracted into an organic solvent. The aqueous and organic phases are nearly immiscible in each other.

To extract the metal, it must be more soluble in the organic phase than in the aqueous phase. But before the metal can be extracted, the inner hydration sphere that surrounds the metal ion must be broken. The sphere is broken when the metal ion complexes to an organic ligand. But if the metal stays hydrated, it will remain in the aqueous phase due to the hydrogen bonding that takes place in this phase.

There are three main types of organometallic complexing agents. The first type extracts neutral metal complexes by forming adducts with the complex. The second type extracts negatively charged metal complexes by forming ion pairs with the complex. The third type extracts the metal by forming chelates with the metal cation. This chapter focuses on the first type of extractant. Chapter 5 focuses on the second type of extractant.

The method of solvent extraction is frequently used in the heavy chemicals industry and in the subset of nuclear chemistry known as radiochemistry. Solvent extraction was developed and widely used during the Manhattan Project to extract uranyl

nitrate into diethyl ether. The purified uranium was used in the first nuclear reactors. Uranium and plutonium were then recovered from the spent nuclear fuel using a similar extraction technique with methyl isobutyl ketone, a neutral extractant [SEA90A]. This method was one of the first large scale industrial processes and was known as the Redox process.

There are many neutral extractants that vary widely in their selectivity and all are water insoluble. Their selectivity is influenced by the concentration of the anions in the aqueous phase, the concentration of the acid, the type of diluent used, and the concentration of the extractant itself. A high concentration of anions in the aqueous phase will affect the concentration of the neutral metal species in the aqueous phase. A high acid concentration will decrease the extraction of the metal into the organic phase because the undissociated acid competes with the metal for the organic extracting ligands. The type of diluent affects the degree to which the metal is extracted [NAK69], [NAK70], [MAE61], [WIL62] since the organometallic complex's organophilicity varies depending on the diluent used. The characteristics of diluent polarity and diluent molecular weight are also important factors[SCH84]. Finally, if the concentration of the organic extractant is too high, aggregation can occur. Aggregation is the tendency for some of the organic molecules to cluster together, reducing their ability to extract the metal. Selectivity can, therefore, be controlled by changing one or all of these variables.

4.2 Tributylphosphate

Tributylphosphate (TBP) is one of the most widely used neutral extractants. Many reprocessing plants use TBP to separate uranium and plutonium from spent nuclear fuel [MAR69] and to further purify uranium and plutonium [MCK75]. TBP has also

been used to purify uranium from "yellow cake" [HAR59] and to separate various actinides and lanthanides from reprocessing plant wastes [MCK77].

During the Manhattan Project, scientists noticed that TBP could extract a variety of metals such as thorium and plutonium [COL78], [KAT86]. But undiluted TBP was difficult to work with because of its high viscosity and the belief that it would hydrolyze greatly in acid. Furthermore, the idea of diluting TBP with organic solvents had not yet been considered. TBP was therefore considered inappropriate for the Manhattan Project.

Diluents were introduced in the late 1940's. Diluents have the advantage of increasing the extracting power of TBP by reducing aggregation effects. Also, dilution decreases the solubility of TBP in water and acids, and the solubility of water and acids in TBP. A research group [COL78] used hexane to dilute TBP and the positive results of their extraction prompted scientists at the Oak Ridge National Laboratory (ORNL) [COL78] to employ their procedure, using a less volatile diluent than hexane, to separate uranium from reprocessing plant wastes generated during World War II. This separation procedure was refined and used at Hanford in the early 1950's in uranium separations. In addition to uranium, plutonium also had to be separated from nuclear reactor waste products, and researchers found TBP could be used for this purpose. The process whereby plutonium and uranium are refined by extraction into TBP was thus developed and came to be known as the PUREX process [LAN49].

TBP has the molecular form $(C_4H_9O)_3P=O$. The phosphoryl oxygen in TBP coordinates with the metal forming an adduct (Equation 4.1):

Equation 4.1 $\qquad M^{n+}_{aq} + nA^-_{aq} + xTBP \leftrightarrow MA_n \bullet xTBP_{org}$
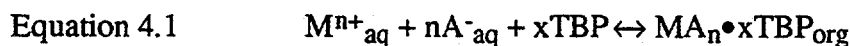
where M is a metal and A^- is the deprotonated form of the acid.

TBP most easily extracts tetravalent and higher charged metals. The anion that bonds with the metal is typically nitrate, chloride, or perchlorate. The resulting complex that forms from TBP coordinating to the metal can have several charge states, but only the neutral one extracts. TBP always extracts the metal in the form of a neutral species. The equilibrium constant for Equation 4.1 is

Equation 4.2
$$K_1 = \frac{[MA_n \bullet xTBP]_{org}}{[M^{n+}]_{aq}[A^-]^n[TBP]^x}$$

The distribution coefficient, K_d, is defined as the ratio of the concentration of metal in the organic phase to the concentration of the metal in the aqueous phase at equilibrium and is represented by the equation:

Equation 4.3
$$K_d = \frac{[MA_n \bullet xTBP]_{org}}{[M^{n+}]_{aq}} = K_1[TBP]^x[A^-]^n$$

Some of the physical properties of TBP are listed in Table 4.1. It is important that the aqueous and organic phases be relatively immiscible with respect to each other. Tables 4.2-4.4 show solubilities of TBP in various aqueous media and Table 4.5 shows the solubility of water in TBP. From these tables, it is apparent that TBP is nearly immiscible with aqueous media, while water is somewhat miscible in TBP. Tables 4.2, 4.4 [BEL75], and 4.5 show that temperature also affects miscibility. Because of this, it is important to preequilibrate the phases before any experimental work is performed and to perform all experimental work at roughly the same temperature.

Table 4.1 Physical Properties of TBP

Molecular Weight	Density (g/ml)	Boiling Point (°C)	Viscosity (mP)
266.32	0.9727	284	39.9
[MAR69A]	[MAR69A]	[MAR69A]	[BUR50]

Table 4.2 Solubility of TBP in Water

Temp (°C)	Solubility (g/l)	Ref.
3.4	1.075	[HIG59]
4.0	1.012	[HIG59]
5.0	0.957	[HIG59]
13.0	0.64	[HIG59]
16.0	0.42	[ALC56]
19.0	0.397	[ALC56]
22.0	0.38	[ALC56]
25.0	0.422	[HIG59]
35.0	0.35	[BEL75]
45.0	0.29	[BEL75]

Table 4.3   Solubility of TBP in Aqueous Nitric Acid Solutions at 25 °C

Conc. HNO$_3$ (M)	Solubility in H$_2$O/ Solubility in acid	Ref.
0.05	1.00	[ALC56]
0.125	0.88	[ALC56]
0.25	0.93	[ALC56]
0.5	0.95	[ALC56]
0.79	1.08	[BUR51]
0.994	0.997	[HIG59]
1.00	1.00	[ALC56]
1.50	1.09	[ALC56]
1.98	1.2	[HIG56]
2.15	1.2	[ALC56]
3.09	1.4	[HIG59]
5.26	2.1	[ALC56]
6.41	2.4	[BUR51]
7.00	3.2	[ALC56]
9.92	2.9	[ALC56]
11.0	2.5	[ALC56]
12.0	1.3	[ALC56]
13.1	1.3	[BUR51]
13.8	0.64	[BUR51]
15.6	0.25	[BUR51]
15.9	0.35	[ALC56]

Table 4.4 Solubility of TBP in HCl Solutions

Conc. HCl (M)	5°C	15°C	Temperature 25°C (Solubility in mM)	35°C	45°C
0	3.6	2.4	1.68	1.3	1.1
1	3.2	2.2	1.67	1.3	1.2
2	2.7	2.0	1.66	1.4	1.3
3	2.0	1.9	1.68	1.5	1.5
4	2.4	2.0	1.88	1.8	1.7
5	2.5	2.2	2.17	2.2	2.1
6	2.6	2.5	2.56	2.5	2.5
7	2.9	2.9	2.93	2.9	2.9
8	---	---	3.26	---	---
9	---	---	3.56	---	---

Table 4.5 Solubility of Water in TBP

Temp (°C)	H_2O (M)	Ref.
0	3.92	[HAR64]
25	3.59	[HAR64]
	3.57	[ROD78]
40	3.34	[HAR64]
50	3.23	[HAR64]
60	3.07	[HAR64]

Aqueous-phase salting is a viable way to increase the distribution coefficient of an extraction. Salting is the addition of the salt of the anion such as LiBr to the acid form of the anion such as HBr. The value of salting was first noticed during the development of solvent extraction procedures designed to recover various elements from nuclear waste. Salting raised the distribution coefficients of some elements that could normally not be recovered. This increase in K_d was attributed to reduced competition between the

extractable species and the acid for TBP and to the continued formation of the extractable species [SCA57], [BES57], [HES57].

Previous experiments [CZE94] have been performed to study the extraction of tetravalent Rf into TBP from various concentrations of HCl. The behavior was compared to that of the lighter tetravalent group 4 or pseudogroup 4 tracers, Zr, Hf, Th, and Pu. The results are discussed and compared with results from this present study in Section 4.4 and 4.5.

In the current study, the extraction properties of bromide complexes of Rf from HBr solutions into TBP have been studied and compared with the same lighter tetravalent tracers and with Ti. All of the Ti studies were done by Bilewicz [BIL94]. Since bromide is a larger and softer (more polarizable) anion than chloride, the stability of Rf-bromide complexes is expected to differ from the stability of Rf-chloride complexes, and an experimental study of the two systems was undertaken.

4.3 Experimental Procedures

The tracers used to model Rf behavior were the group 4 homologs, Ti (stable), ^{95}Zr and ^{95}Hf, and the pseudogroup 4 homolog, ^{229}Th. ^{239}Pu^{4+} was also studied but its chemical behavior is expected to be quite different from the group 4 elements because of the partially filled 5f shell. Benzene was chosen as the diluent because it was used for the Rf-chloride studies [CZE94]. The benzene was of spectrophotometric grade and purchased from Fisher Scientific. The TBP (99+% pure) was purchased from Aldrich Chemical Company and used as received. The HBr was assayed at 47-49% and purchased from EM Science.

A titration was carried out to determine the actual concentration of the stock HBr. A few drops of a phenolphthalein / ethanol solution were added to the stock HBr. The

titration was carried out with 1 M NaOH. The concentration of the stock HBr was determined to be 9.0 M. Higher bromide concentrations were studied by salting with LiBr. However, the addition of a new component, in this case Li^+, added an additional degree of freedom, and increased the complexity of the system. Therefore, it was no longer possible to keep all but one variable constant. Nevertheless, the experiments were performed to compare the chemical behavior of Rf with its homologs under similar conditions.

The temperature was kept roughly constant throughout all experiments because of the impact a change in temperature has on the solubility of the aqueous and organic phases with respect to each other (Tables 4.2, 4.4, 4.5). The degree of solubility of water in TBP (Table 4.5) prompted a short experiment to measure the solubility of HBr in TBP. The various concentrations of HBr were titrated to identify their concentrations after two pre-equilibrations with TBP. After the first pre-equilibration with TBP in benzene, the concentration of HBr dropped by roughly 5% over the concentrations of HBr studied. There was no measurable drop in HBr concentration after the second pre-equilibration. Therefore, HBr was pre-equilibrated once with the organic phase before each experiment.

Previous studies [CZE94C] have shown that extractions from chloride solution into triisooctylamine (TIOA) are very sensitive to any HF present in the aqueous phase. An experiment was conducted to measure the effect of HF concentration on the distribution coefficient for tracers Zr and Hf in the TBP/HBr system. The results in Table 4.6 show that HF appreciably lowered the K_d of both tracers.

Table 4.6   Comparison of K_d of ^{95}Zr and ^{172}Hf With and Without HF

Org phase	Aq phase	K_d (^{172}Hf)	K_d (^{95}Zr)
0.35M TBP in benzene	8M HBr/0.02 M HF	0.095	0.074
0.35 M TBP in benzene	8M HBr/no HF	0.20	0.80

To insure that no fluoride contamination was present in the tracers, each tracer was mixed with a few drops of concentrated H_2SO_4, placed in a porcelain crucible, and heated to 300°C. Heating causes the SO_4^{2-} to displace all halides including F^-. The sulfate can then easily be displaced by the halide by adding the halide to the tracer and evaporating once. The borate from $NaBO_3$ is also good at displacing halides, but the Na salts are left over after evaporation, requiring an ion exchange column separation to remove the salt.

It was found during the experiments that a significant amount of Hf (more than 50% in some cases) sticks to teflon and various other organic and metallic surfaces, but that a negligible amount sticks to polypropylene and platinum. Therefore, polypropylene cones were used in the tracer experiments and platinum foils in the rutherfordium experiments. Polypropylene pipet tips were used for all experiments.

500 μL each of the aqueous and organic phases were placed in 5 mL polypropylene centrifuge cones. After the initial pre-equilibration, the phases were mixed for one minute, centrifuged for 30 seconds, separated, and counted with a germanium or alpha spectrometer system as described in Section 2.4.

The Ti was determined by Bilewicz et al. [BIL94] by atomic absorption spectroscopy using a Pye Unicam SP-9. The Ti solutions were prepared by dissolution of TiO_2 in HBr solutions with a Ti concentration less than 50 μg/ml. Final Ti concentrations were measured only in the aqueous phase. The Ti concentrations in the

organic phase were calculated by taking the difference in the concentration before and after the extraction.

For the Rf experiments, ^{261}Rf and other activities were transported from the target system to the collection site, collected on platinum foils, removed from the foil with 15 μL of aqueous phase (see legend in Figure 4.7 for aqueous phase concentrations), and added to 30 μL of organic phase (0.35 M TBP in benzene) in a 1 mL centrifuge cone. The phases were ultrasonically mixed for 5 seconds and centrifuged for 5 seconds. The organic phase was transferred to a tantalum foil and heated on a hot plate to dryness, leaving the activity on the foil. The foil was then placed on a PIPS detector to measure the alpha decay. The procedure took about 60 seconds to complete.

4.4 Results of Tracer and Rutherfordium Extractions

Initial experiments were performed to determine the concentration of TBP at which the extraction of tetravalent ^{95}Zr was greatest (Figure 4.1). The results of Nb are less important for these experiments because Nb is pentavalent, but the Nb results are included here for possible future comparisons with the pentavalent transactinide hahnium. The aqueous phase was 8.4 M HBr and the organic phase was various [TBP] in benzene. Figure 4.1 shows a maximum K_d (Zr) of 1.84 at 0.25 M TBP. The K_d falls off beyond 0.25 M TBP because of aggregation of the TBP, which inhibits the extraction of tetravalent zirconium. The K_d (Nb) remains roughly constant throughout the extraction range.

The next experiment examined the effect of varying the [H$^+$] while keeping [Br$^-$] constant (Figure 4.2). The aqueous phase was 8.5 M Br$^-$ at various [H$^+$], and the organic phase was 0.25 M TBP in benzene. LiBr was used to keep the [Br$^-$] constant while allowing the [H$^+$] to vary. The K_d for Zr increases steadily as the [H$^+$] increases, and is

similar to Figure 4.3 [CZE94] from the chloride studies on Zr where the TBP was kept constant at 1M, the [Cl⁻] was kept constant at 6 M, and the [H⁺] was varied. In that study, LiCl was used to keep the [Cl⁻] constant while allowing the [H⁺] to vary.

The effect on the extraction of Zr into 0.25 M TBP in benzene while varying the [Br⁻] and keeping [H⁺] constant at 4.9 M was also studied (Figure 4.4). LiBr was used to adjust the [Br⁻]. The K_d for Zr increased more slowly as the [Br⁻] increased than it did as a function of increasing [Cl⁻] using LiCl. Figure 4.5 [CZE94] shows the results of the chloride studies with Zr where TBP was kept constant at 1M, [H⁺] was kept constant at 6 M, and the [Cl⁻] was varied using LiCl.

Unfortunately, the data in Figures 4.2 and 4.4 could not be compared with Rf extraction results at similar concentrations because the K_d of Rf was too small to measure at the concentrations studied. The K_d of Rf was only measurable when LiBr was added to boost the [Br⁻] past the level of concentrated HBr, making it impossible to vary one parameter such as the [Br⁻] without affecting any of the other parameters such as the [H⁺].

To insure that the extraction system was working properly, the next experiment was performed to verify that log K_d varies linearly with log [TBP] at TBP concentrations low enough to prevent aggregation. A relatively straight line from tetravalent Zr would insure that random errors were minimal during the course of the extraction. Furthermore, the solvation number of Zr could be determined by calculating the slope of the straight line:

Taking the log of Equation 4.3:

Equation 4.4
$$\log K_d = \log K_1 + n \log [A_{aq}^-] + x \log [TBP_{org}]$$
$$|\quad y\quad |=|\qquad b\qquad |+|\quad mx\quad |$$

71

The anion [A$^-$], metal [M^{n+}], and external conditions such as temperature are kept constant so that Equation 4.4 becomes:

Equation 4.5
$$\frac{\delta \log K_d}{\delta \log[TBP_{org}]} = n$$

The solvation number of TBP is simply the slope n. This method is applicable so long as the metal is present only in trace concentrations, the concentration of TBP does not exceed a few percent to prevent aggregation, and acid concentration and temperature remain constant [HES58]. Figure 4.6 shows a plot of log K_d vs log [TBP]. The aqueous phase is 8.55 M HBr and the organic phase is variable [TBP] in benzene. The line is fairly straight indicating minimal random errors in the chemistry, and the slope, n, for the Zr plot calculated by linear regression is 0.78 ± 0.21. Thus the most likely extractable form of Zr is ZrBr$_4$•1TBP. This result is different from the chloride system where solvation numbers of ZrCl$_4$ complexes are 2 or 3. The different solvation number of 1 for the ZrBr$_4$ complex might be due to bromide being a larger ligand than chloride. The K_d of Nb stayed fairly constant throughout the extraction range. Since it was found that a higher Zr K_d results from an extraction with 0.35 M TBP than 0.25 M TBP, all subsequent experiments were performed with 0.35 M TBP in benzene.

In the next series of experiments, the K_d values of various tracers and Rf were measured at various [Br$^-$] above the level of concentrated HBr by adding LiBr. Because of this, it was not possible to vary one parameter such as the Br$^-$ concentration without affecting any of the other parameters such as the [H$^+$]. Still, this study was performed so a comparison could be made between the chemical behavior of the homolog tracers and that of Rf.

The results of this study are shown in Figure 4.7 where % extracted is plotted vs. [Br$^-$]. Equation 4.6 relates K_d to % extraction:

Equation 4.6
$$K_d \approx \frac{\%\text{Extracted} / 2}{1 - \%\text{Extracted}}$$

The concentrations of the salt and acid are shown in a table in Figure 4.7.

The amount of ^{95}Zr and ^{261}Rf extracted was above 88% throughout the range of concentrations studied whenever LiBr was added. The Rf point for the extraction condition where [HBr] = 9.0 M and no LiBr was added is also shown. Pseudo group 4 homolog ^{229}Th and group 5 element ^{95}Nb extracted between 70% and 90%. The amount of ^{239}Pu extracted gradually increased from about 25% to 70% throughout the range studied. The large difference in chemical behavior of ^{239}Pu^{4+} can be attributed to its f-electrons which makes it largely chemically unrelated to the other tracers studied in this experiment. Rf thus behaved most similarly to its group 4 homolog Zr. Incidentally, even though the most common oxidation state of Pu is 4+, other oxidation states are possible. Therefore, to insure that Pu was in a tetravalent state, a sample of Pu was first fumed with HNO$_3$ to oxidize it to a hexavalent state, then NaNO$_2$ was added to reduce it to the tetravalent state. In the chemical systems studied, Pu remained in the tetravalent state without having to control redox potentials.

At concentrations of 9.0 M HBr or less, LiBr was not added, and consequently, ^{229}Th and ^{261}Rf did not extract. When the aqueous phase consisted of LiBr alone, none of the tracers extracted. Only the presence of LiBr with HBr caused ^{229}Th and ^{261}Rf to extract. This is due to the combined effects of an increase in bromide concentration due to the addition of LiBr, the introduction of the Li$^+$ cation so that extractable species such as LiRfBr$_5$ are formed, and the advantage of reduced competition between the extractable species and the HBr acid for TBP.

Next, the extraction of the group 4 elements into 0.35 M TBP in benzene was studied as a function of [HBr]. The extraction of ^{95}Zr, ^{95}Nb, ^{172}Hf, and ^{261}Rf was investigated over a range of HBr concentrations from 7.75 M to 9.0 M. The extraction of

Ti was investigated by Bilewicz from 7.75 to 12 M HBr [BIL94]. Unfortunately, 12 M HBr was not available except for the Ti studies. Otherwise, the more commonly available constant-boiling azeotrope 9 M HBr was used. Figure 4.8 gives a plot of % extracted vs. [HBr] and shows that [95]Zr and [172]Hf extraction yields increase sharply with increasing [HBr] over narrow ranges. Zr started to extract at a lower [HBr] than Hf indicating that the tendency for Zr to form neutral bromide complexes is stronger than for Hf. Ti extracted only at 9.1 M HBr and higher. Rf did not extract over the entire range of HBr concentrations studied and only extracted with the addition of the salting agent LiBr. Therefore, Rf formed weaker complexes with bromide than either Zr or Hf, but the strength of the Rf-bromide complex relative to Ti-bromide remains unknown. Based on these results, the extraction trend in these tetravalent group 4 elements decreases in the order Zr>Hf>Rf?Ti. Since only neutral complexes extract, the extracted complex is most likely $MBr_xH_{x-4} \cdot yTBP$, where x is 4, 5, or 6 and y is the TBP solvation number. Further studies will be required to learn whether Rf or Ti comes next in the order of extraction. The Nb distribution coefficients remained high at all concentrations studied. An experiment performed with trivalent [152]Eu with 7.75 and 9.0 M HBr showed that it did not extract at all.

The chloride system was then compared to the bromide system. Figure 4.9 shows the effect of varying the concentration of HCl on the extraction of various tracers and on [261]Rf. The data for [261]Rf are from Czerwinski et al. [CZE94], and the others are from Bilewicz [BIL94]. In a related experiment done by Czerwinski et al. [CZE94], the % extraction values for Hf were much lower than the present values Bilewicz obtained for Hf. The Hf results from the Czerwinski et al. experiment were based on online data taken at the cyclotron, and the activity was collected onto teflon discs. As previously mentioned, it was found that Hf sorbs onto teflon which accounts for the lower extraction values.

Figure 4.9 is plotted as % extracted vs. [HCl]. The organic phase was 0.35 M TBP in benzene. The statistical errors were very small for the Rf homologs because high activity (>100 μCi) was used, and the statistical error for Ti was less than 5%. However, the statistical errors for Rf were large because of the few events observed.

Once again, Zr and Hf extraction yields increased sharply with increasing [HCl] over the range from about 5.5 M to 7.5 M. However, in the HBr system, the concentrations ranged from 7.75 M to 9.0 M HBr. This would seem to indicate that bromide is a weaker complexing ligand than chloride, as expected, since bromide is a softer, more polarizable ligand than chloride. This makes chloride a better match for the hard metal cations with which it bonds. Similar results were observed with Ti whose % extraction was consistently higher in the HCl system. Overall, the results indicate that the extraction trend for the tetravalent group 4 elements decreases in the order Zr>Hf>Rf>Ti, similar to the extraction trend observed for the bromide system. Based on the similarity between the two halide systems, Rf could be expected to start extracting between 9 and 10 M HBr.

4.5 Discussion

One effect responsible for the extraction trends seen in Figures 4.8 and 4.9 is the affinity of the metal cation for the halide. If the affinity for the halide is high enough that the metal cation bonds with at least four halides, then a neutral complex of the form $MHl_xH_{x-4} \cdot yTBP$ where x is 4, 5, or 6, M=metal, and Hl=halide will form and extract. Zr and Hf had a higher affinity for the halide than Ti and Rf in both Figures 4.8 and 4.9.

It is possible that the metal cation's affinity for the halide is high yet the complex does not extract. In such cases, the complexes could be anionic and take the form MHl_5^-, MHl_6^{2-}, or $HMHl_6^-$ where Hl represents chloride or bromide. This anionic effect was

not observed in Figures 4.8 and 4.9, since the amount of halide present was the same concentration as the H^+. However, Czerwinski [CZE94] shows that the effect was observed when a higher concentration of chloride over hydrogen ion was present in solution. Figure 4.10 shows that for Zr, Hf, and Rf, the $[H^+]$ was varied between 8 M and 12 M and the $[Cl^-]$ was kept constant at 12 M using LiCl [CZE94]. The data for Ti(stable) are from Bilewicz [BIL94] and the others are from Czerwinski et al. [CZE94]. For Ti, the $[Cl^-]$ was kept constant at 8.5 M and the $[H^+]$ was adjusted using $HClO_4$ [BIL94]. At lower $[H^+]$, Rf and Ti were not as well extracted as Zr and Hf because Rf and Ti formed anionic complexes. As $[H^+]$ increased, H^+ made the anionic Rf and Ti complexes neutral and thus extractable.

Another effect contributing to the increase in Rf extraction shown in Figure 4.10 and to the extraction trends observed in Figures 4.8 and 4.9 is the degree to which the metal cation will hydrolyze, which can explain why Rf and Ti extracted similarly yet have very different ionic radii. Hydrolyzed species such as $M(OH)_3Br \cdot xTBP$ usually will not extract into the organic phase because of the strong hydrogen bonding interaction between OH^- and H_2O. The lower % extraction for Rf and Ti at the lower $[H^+]$ in Figure 4.10 implies that Ti and Rf hydrolyzed more easily than either Zr or Hf. As the tendency for Ti and Rf to hydrolyze decreased with increasing $[H^+]$, they were both more able to form the extractable $MCl_4 \cdot xTBP$ complexes; thus, their % extraction increased. Meanwhile, since Zr and Hf hydrolyzed to a much lesser degree than Ti and Rf at the lower H^+ concentrations, their % extraction stayed high throughout the range of concentrations studied. The results confirm the hydrolysis results observed in the previous chapter that showed Rf hydrolyzed more easily than Zr and Hf.
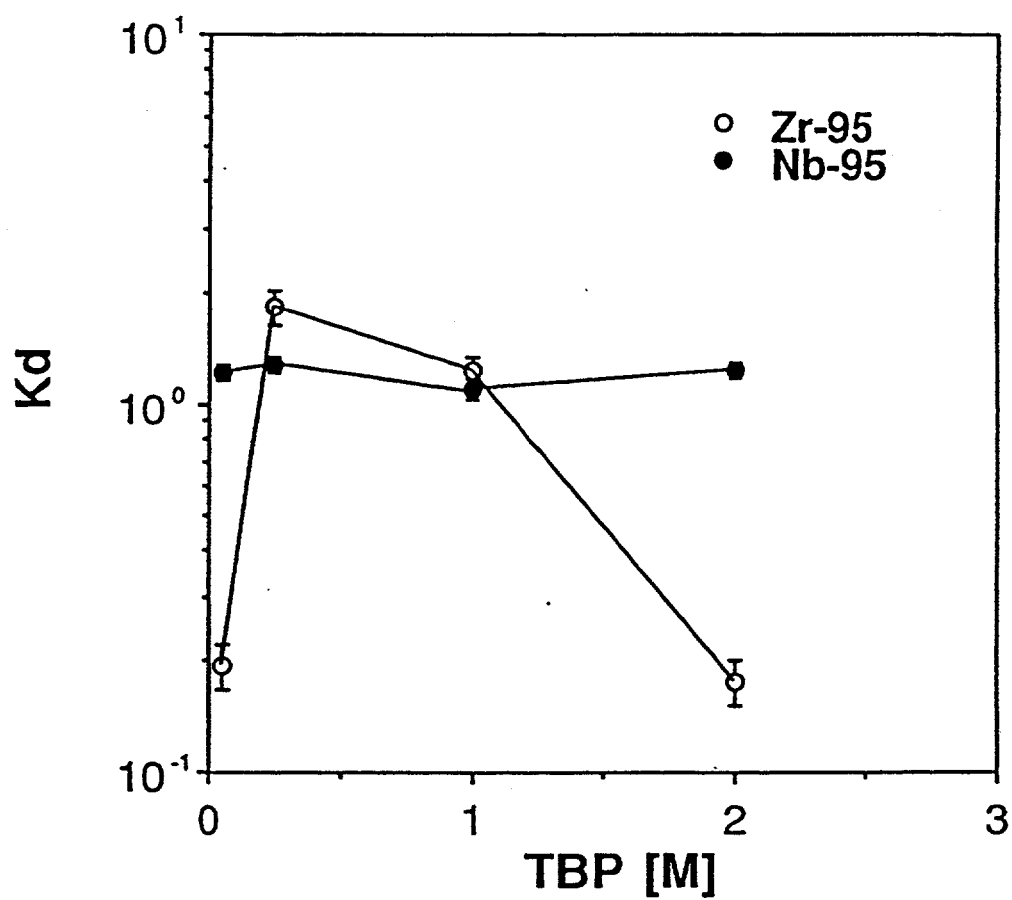
Figure 4.1 Distribution coefficients for extraction of ^{95}Zr and ^{95}Nb from 8.47 M
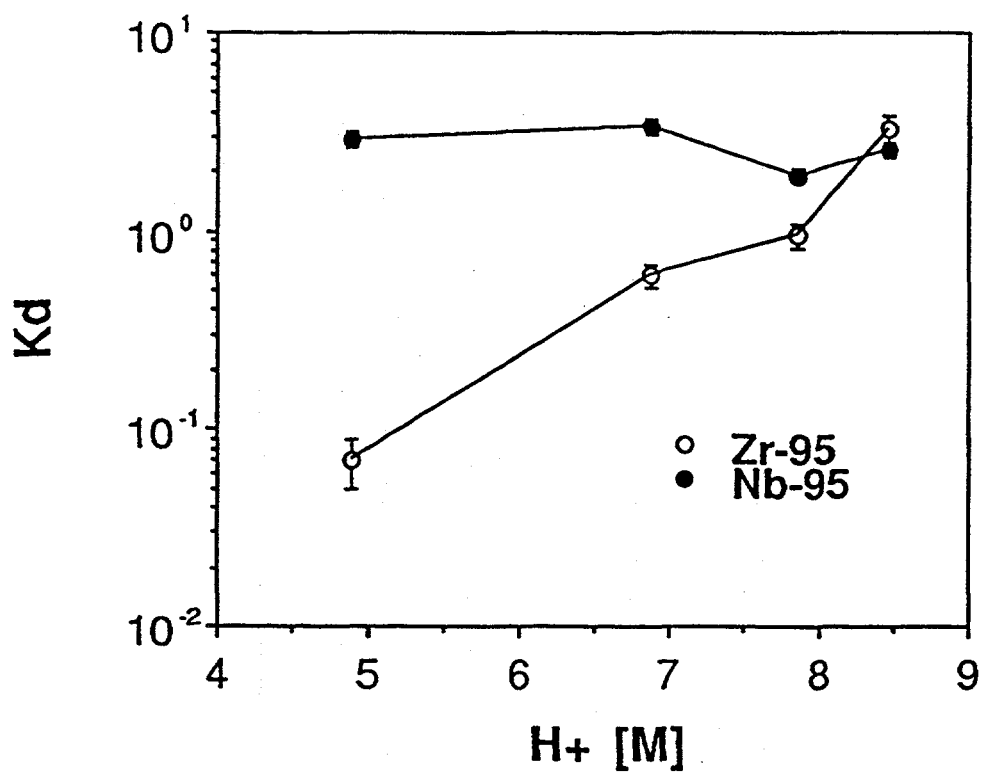HBr as a function of [TBP] in benzene.

Figure 4.2 Distribution coefficients for extraction of ^{95}Zr and ^{95}Nb into 0.25 M TBP in benzene as a function of [H$^+$] with [Br$^-$] held constant at 8.5 M.

Figure 4.3 Distribution coefficients for extraction of ^{95}Zr and ^{95}Nb into 1 M TBP in benzene as a function of [H$^+$] with [Cl$^-$] held constant at 6 M.

Figure 4.4 Distribution coefficients for extraction of ^{95}Zr and ^{95}Nb into 0.25 M TBP in benzene as a function of [Br$^-$] with [H$^+$] held constant at 4.9 M.
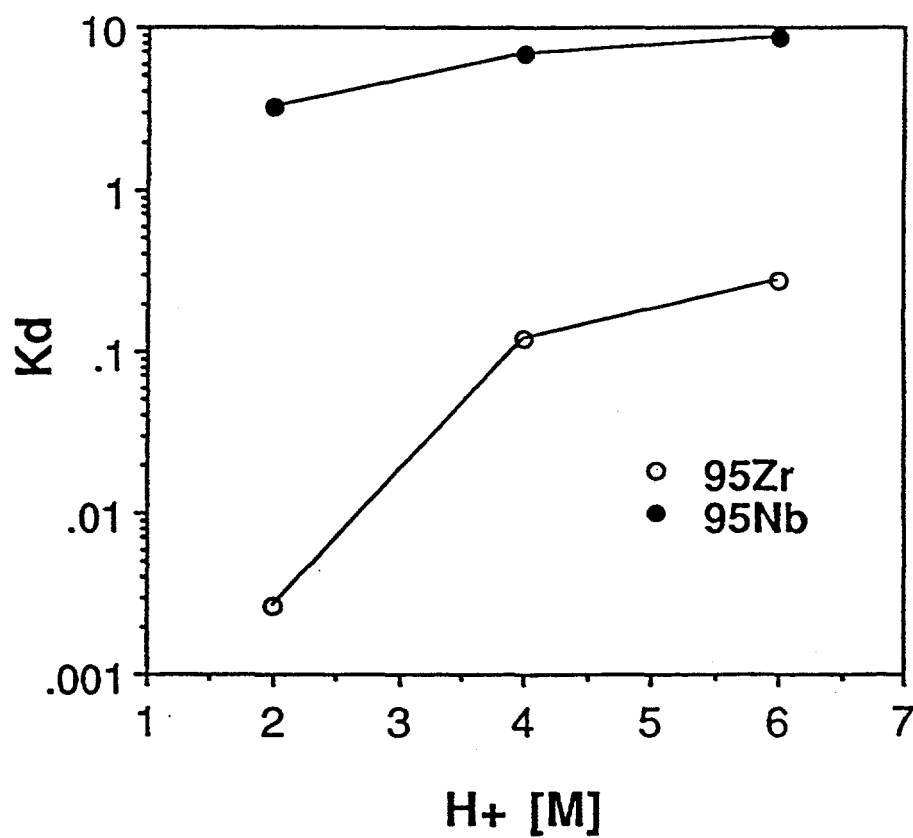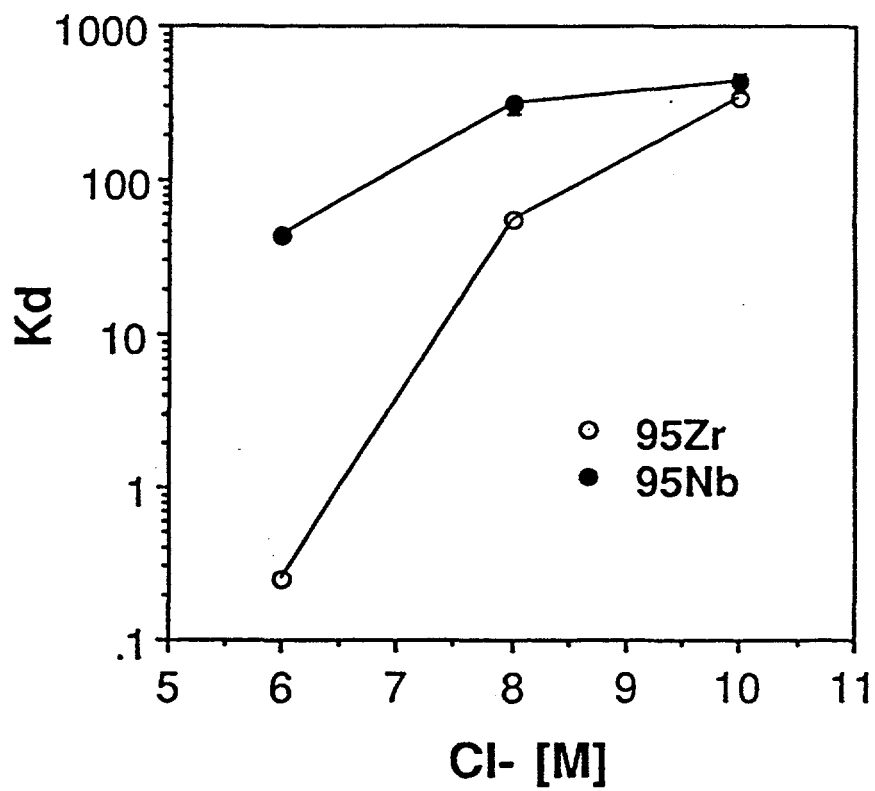
Figure 4.5 Distribution coefficients for extraction of ^{95}Zr and ^{95}Nb into 1 M TBP in benzene as a function of [Cl$^-$] with [H$^+$] held constant at 6 M.
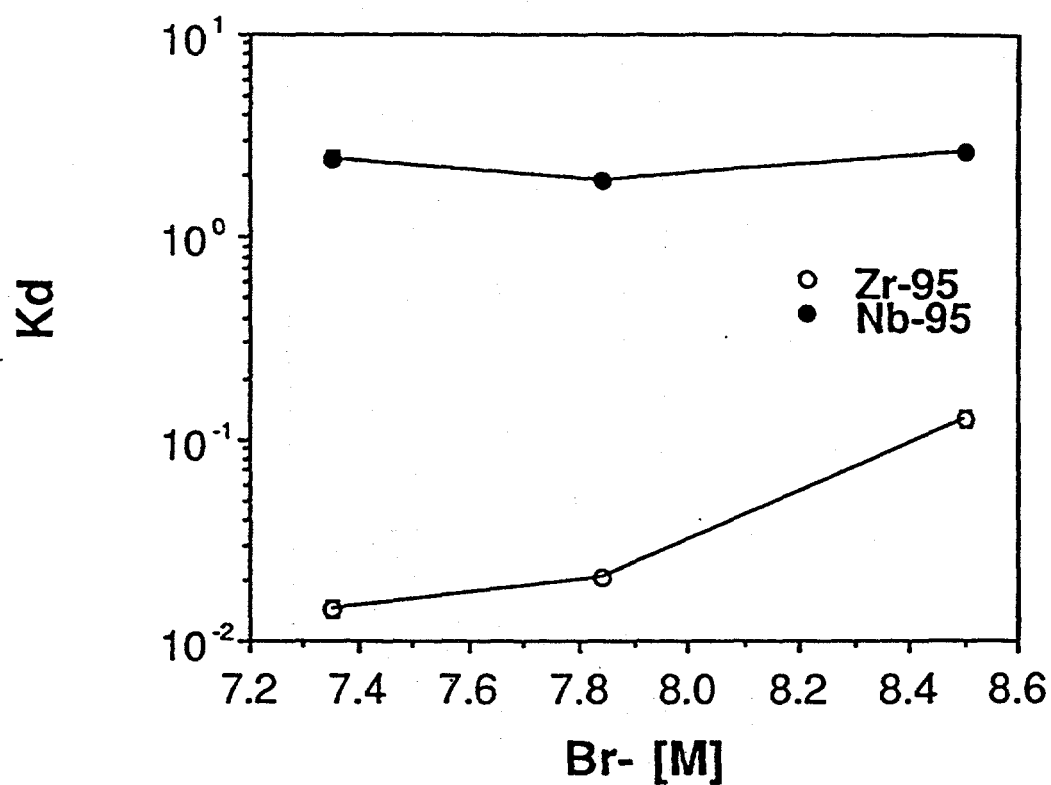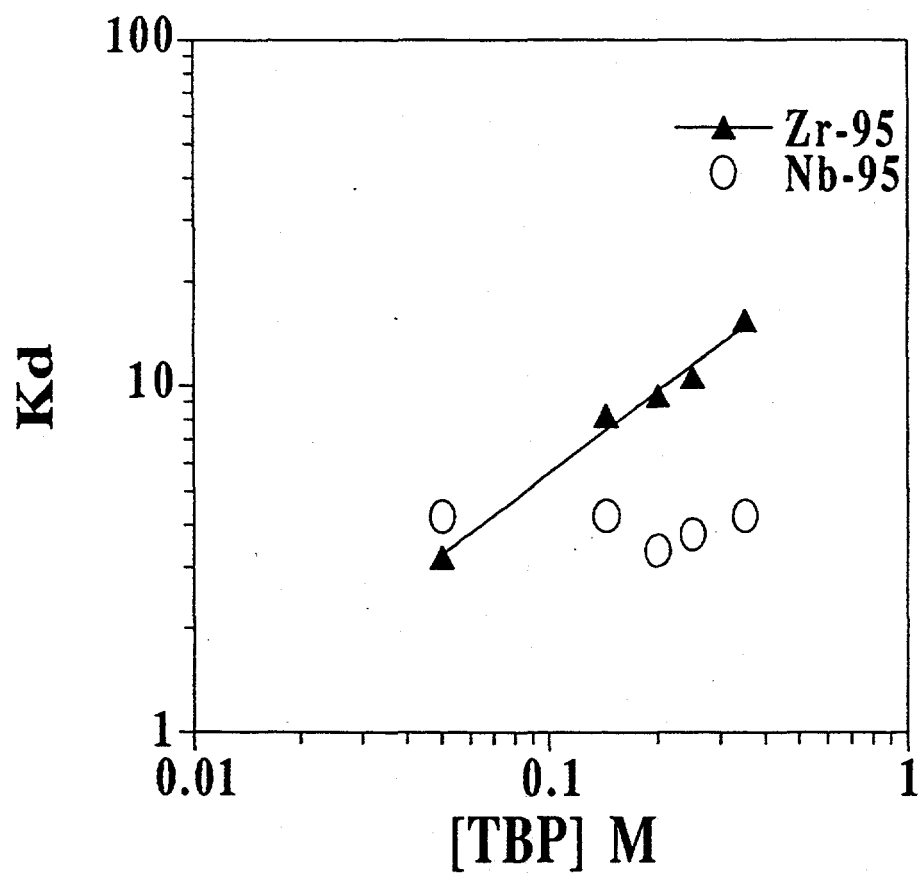
Figure 4.6 Distribution coefficients for extraction of ^{95}Zr and ^{95}Nb from 8.55 M HBr as a function of [TBP] in benzene. The slope of the Zr plot, calculated by linear regression, was 0.78 ± 0.21.
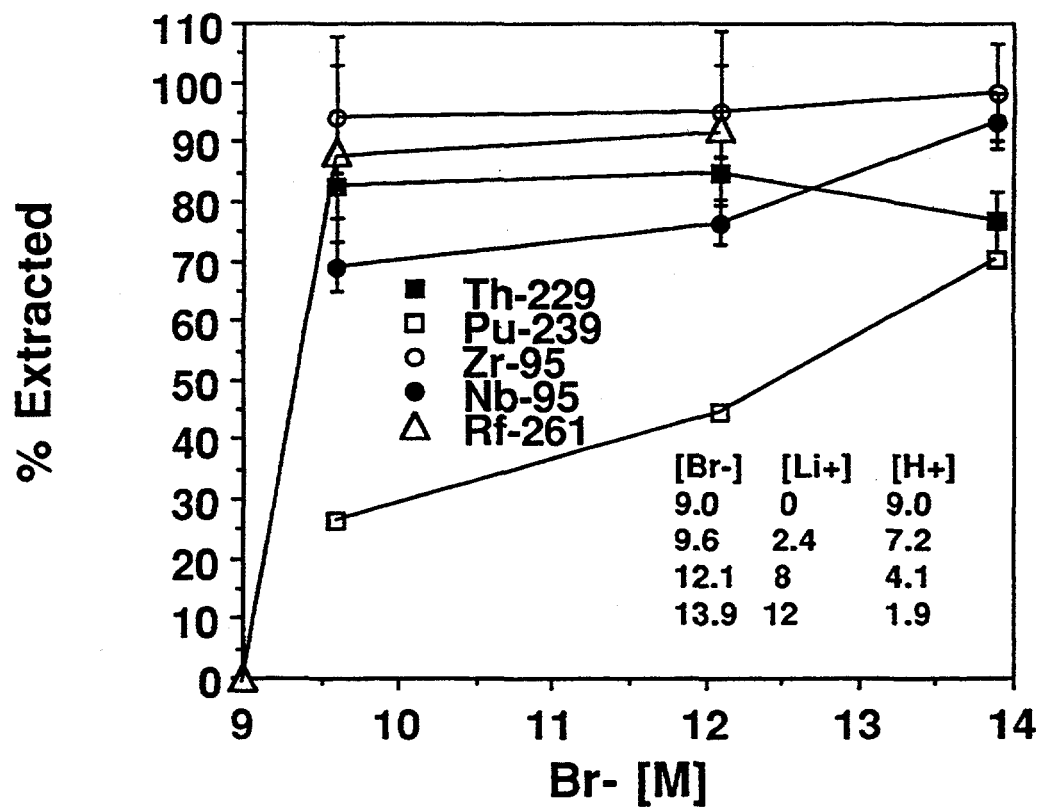
Figure 4.7 % Extraction of ^{95}Zr, ^{95}Nb, ^{229}Th, ^{239}Pu, and ^{261}Rf into 0.35 M TBP in benzene as a function of [Br$^-$], [Li$^+$], and [H$^+$]. The concentrations of Br$^-$, Li$^+$, and H$^+$ are shown in the legend.
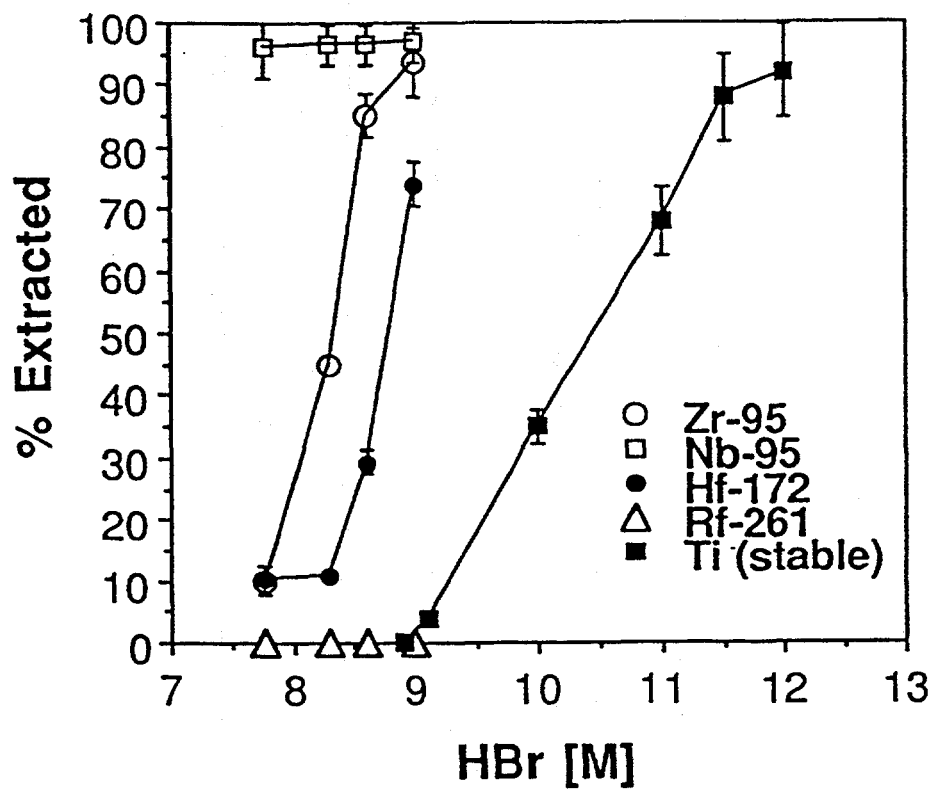
Figure 4.8 % Extraction of Ti (stable), ^{95}Zr, ^{95}Nb, ^{172}Hf and ^{261}Rf into 0.35 M TBP in benzene as a function of [HBr]. The data for Ti (stable) are from [BIL94].
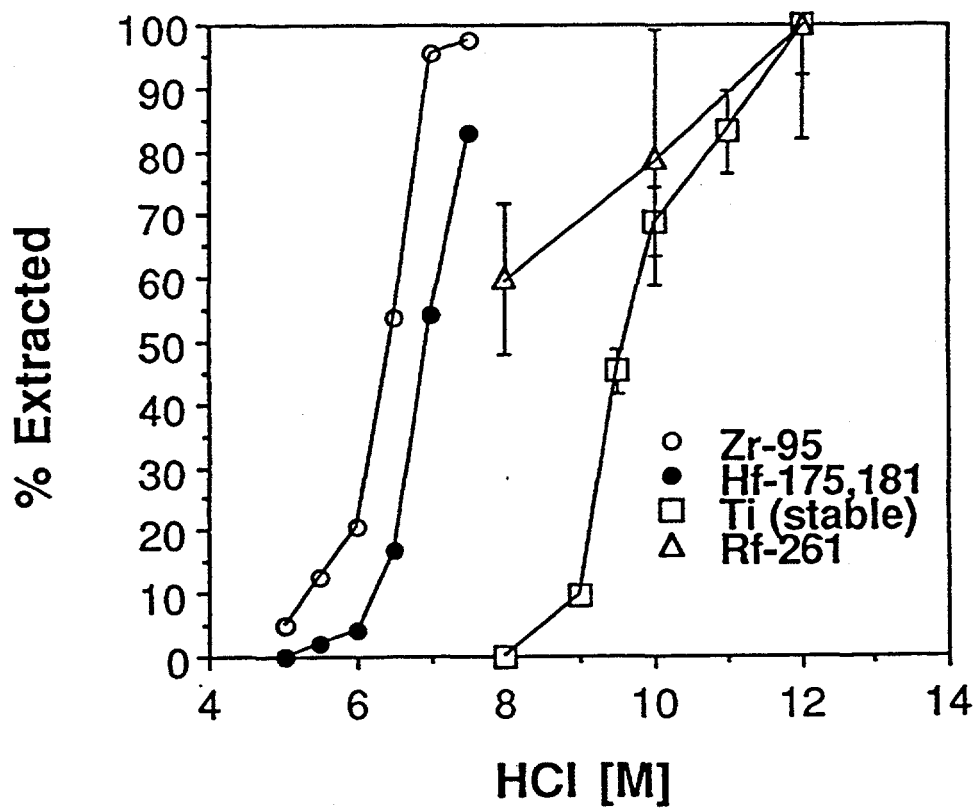
Figure 4.9   % Extraction of Ti (stable), ^{95}Zr, ^{175,181}Hf and ^{261}Rf into 0.35 M TBP in benzene as a function of [HCl]. The data for ^{261}Rf are from [CZE94], and the others are from [BIL94].

Figure 4.10 % Extraction of ^{95}Zr, ^{169}Hf and ^{261}Rf into 1 M TBP in benzene as a
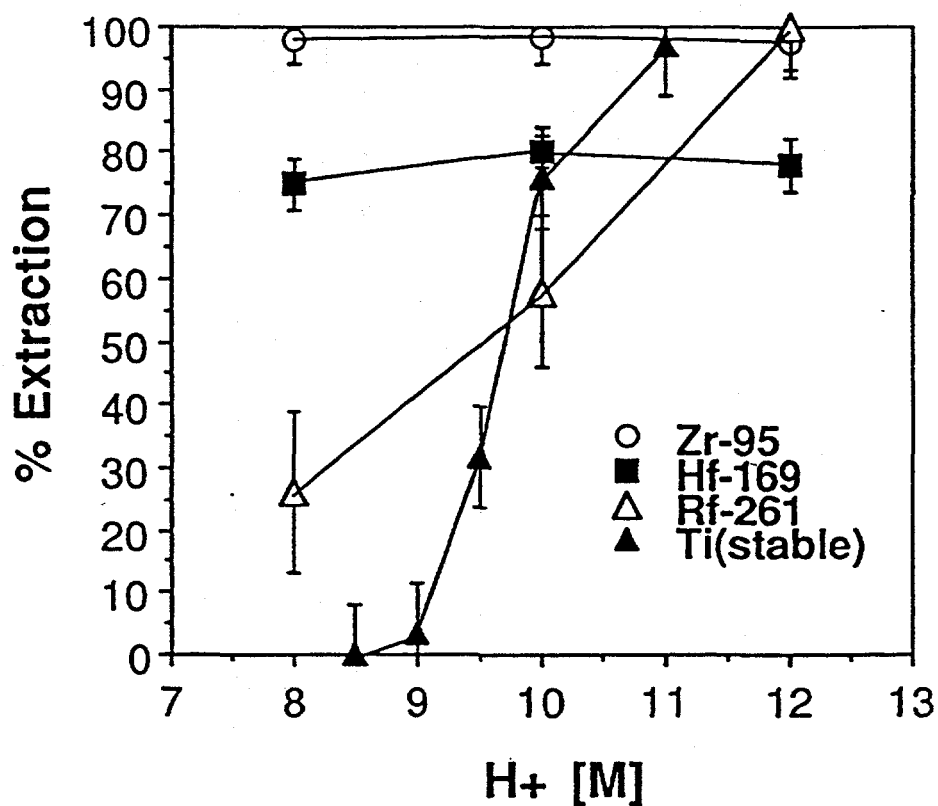function of [H$^+$] with [Cl$^-$] held constant at 12 M. % Extraction for Ti (stable) into
0.35 M TBP in benzene as a function of [H$^+$] with [Cl$^-$] held constant at 8.5 M.
The data for Ti(stable) are from [BIL94] and the others are from [CZE94].

Chapter 5

Extractions of Complexes with Same Coordination Number into Triisooctylamine

5.1 Introduction

The idea that the coordination number of Rf could be influenced by relativistic effects was discussed in Chapter 3. The results from that chapter showed that elements with different coordination numbers had different extraction behaviors because the coordination number of the element affected the tendency for the element to hydrolyze.

In this chapter, a short study employing the technique of solvent extraction was performed to provide an example of how complexes with the same coordination number (CN=6) extract. Other factors that affect extraction behavior such as ionic radius could then be examined.

The extractions were performed using the trialkylamine ligand triisooctylamine (TIOA). TIOA is a good extractant because of its strong complexing power for anions, its low solubility in the aqueous phase, its stability in the presence of high acid concentrations, its compatibility with a host of organic diluents, and its rapid separation from the aqueous phase [MAR69]. TIOA takes the molecular form $(C_8H_{17})_3N$ and extracts by forming ion pairs as follows:

Equation 5.1 $\qquad (C_8H_{17})_3N + H^+ + A^- \rightarrow (C_8H_{17})_3NH^+A^-$
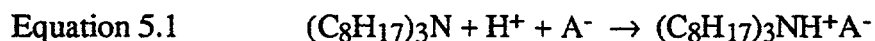
where A⁻ is an anionic metal complex. Since this reaction normally takes place in acidic solutions [MAR69], and since it has been observed that Ti, Zr and Hf have a coordination number of 6 with HF in the system studied [WIL87], various concentrations of HF were used in the aqueous phase for this extraction system. A solution of mixed xylenes purchased from Fisher Scientific (A.C.S. grade, 99% purity) was chosen as the organic diluent because previous results [BIL94] showed that it worked well with TIOA.

5.2 Extraction of Ti, Zr, and Hf

5.2.1 Procedure

The extraction of Ti, Zr, and Hf were first compared in a series of experiments in which their fluoride complexes were extracted into a solution of 0.25 M TIOA in o,m,p-xylene. The procedure was similar to the one in Chapter 4 (see Section 4.3) except that all aqueous phases were preequilibrated twice with the organic phase.

The results for Ti were determined by atomic absorption spectroscopy using a Pye Unicam SP-9 by A. Bilewicz [BIL94]. The Ti solutions were prepared by dissolution of TiO_2 in the concentration of HF to be studied with a Ti concentration less than 50 μg/ml. Final Ti concentrations were measured only in the aqueous phase. The Ti concentrations in the organic phase were calculated by taking the difference before and after the extraction.

5.2.2 Activity Loss

Since activity loss is a problem when evaporating at high temperatures using TIOA, studies were carried out with Zr to establish an optimal hot plate temperature setting that would evaporate off the organic phase in a timely manner yet minimize the amount of activity lost. Table 5.1 shows the results of activity loss using 30 μL organic phases. From these results, a hot plate setting of 600 Watts was shown to be an optimal setting.

Table 5.1 % ^{95}Zr Activity Lost from TIOA at Various Hot Plate Temperatures

Hot Plate (Watts)	Evaporation Time (sec)	Activity Lost (%)
475	22 s	12%
600	13 s	16%
700	9 s	22%

5.2.3 Results

The results in Figure 5.1 came from Bilewicz [BIL94] and showed that Zr and Hf extracted very similarly to each other and quite differently from Ti. The extraction decreases with increasing [HF] because of the increased competition between F$^-$ ions and MeF$_6^{2-}$ complexes for TIOA.

Since the results in Figure 5.1 were obtained at the Institute of Nuclear Chemistry in Warsaw, Poland, the experiments were repeated here at Lawrence Berkeley Laboratory to insure reproducibility. The results are shown in Figure 5.2. The experiments were

performed twice for each HF concentration for both ^{95}Zr and ^{175,181}Hf. Each point represents the average of the two results for each tracer, and the error bar for each point reflects the spread in error from the two results as follows:

Equation 5.2 $\quad \sqrt{\sigma_1^2 + \sigma_2^2}$

The Ti results could not be repeated since the technique of atomic absorption spectroscopy was not available at the time. Still, the Zr and Hf values were fairly close to the Warsaw values, and the predicted number of detectable events from ^{261}Rf (based on its cross section, detector geometry, gas-jet yield, chemical yields, and experiment run-time) that would be observed during a cyclotron run was statistically large enough so that the margin of error would be small and the spread observed between Ti and Zr/Hf could be resolved if required. This requirement would be necessary if the Rf results fell somewhere close to either Ti or Zr/Hf. Since the points from Rf would have somewhat large error bars due to the statistics of being produced an atom-at-a-time, it would be necessary to resolve whether Rf was behaving more like Ti or more like Zr/Hf.

5.3 Extraction of Rf

5.3.1 Procedure

Based on Figures 5.1 and 5.2, Rf was first studied at 0.5 M HF to establish a 100% extraction point against which other concentrations could be compared. 4, 6, and 8 M HF concentrations were also studied since these points gave the largest % extraction difference between the extraction of Ti and the extraction of Zr and Hf.

The solvent extraction procedure for Rf was similar to the one used to study Zr and Hf, but HF reacts slowly with glass to form fluorosilicates. Therefore, it can lower the effective concentration of fluoride in solution. Plastic was used for the whole experiment except during the separation of the phases, where glass spitzers were used. The glass spitzers did not affect the chemistry, since they were used to pull the organic phase after the phases were mixed and centrifuged. Also, HF was dilute enough so its rate of reaction with the spitzers was slow during the exposure times of only seconds. Therefore, the reaction of the glass spitzers with HF was negligible.

The activity was collected on platinum foil, picked up with 15 μL of aqueous phase (various [HF]) and placed into a polypropylene 5 mL centrifuge cone containing 30 μL of organic phase (0.25 M TIOA in xylene). The phases were mixed for 10 seconds and centrifuged for 5 seconds, then the organic phase was picked up with a glass spitzer, placed on a tantalum or nickel foil which was placed on a hot plate, evaporated, cooled under a jet of air, then the foil was counted on a PIPS alpha detector. Based on the results of Zr activity loss caused by evaporating with TIOA as discussed in Section 5.2.2, a hot plate setting of 600 Watts was used in the cyclotron experiments.

5.3.2 Results

A total of 1561 ^{261}Rf extraction experiments was performed. The organic phase was placed on tantalum foil during the first two runs at 0.5 M HF and for part of the third run at 4 M HF. Nickel foil was used thereafter. Table 5.2 lists the results of the runs where Ta foil was used, and Table 5.3 lists the results of the runs where Ni foil was used. Both tables list the number of experiments per run, the number of alpha singles and correlated pairs observed, and the HF concentration. Table 5.3 also lists the number of Po singles. The number of Rf singles in this table are the number of Po singles subtracted

from the number of total events. As can be seen from the data, most of the singles events in Table 5.3 were due to Po. During the post-run analysis, 8.375 MeV alphas from ^{213}Po were observed on the Ni foils because they had somehow become contaminated with ^{229}Th prior to the experiment. Therefore, the ^{213}Po alphas from the ^{229}Th decay chain had to be subtracted from the number of singles observed from ^{261}Rf, since the alpha energies of ^{213}Po (8.375 MeV) and ^{261}Rf (8.29 MeV) were close. The number of ^{213}Po alphas that were present on the Ni foils were determined based on its known energy and half-life.

Table 5.2 ^{261}Rf Solvent Extraction from various [HF] Solutions into 0.25 M TIOA in Xylene using Ta foil

Run #	[HF]	Singles	Pairs	# Experiments
1301	0.5 M	2	4	20
1302	0.5 M	100	8	330
1303	4 M	15	0	157

Table 5.3 ^{261}Rf Solvent Extraction from various [HF] Solutions into 0.25 M TIOA in Xylene using Ni Foil

Run #	[HF]	Po Singles	Rf Singles	Pairs	# Experiments
1303a	4 M	8	0	0	128
1304	0.5 M	6	1	0	95
1305	4 M	13	0	0	223
1306	8 M	7	1	0	125
1307	0.5 M	4	6	0	60
1308	6 M	15	0	0	250
1309	0.5 M	2	2	2	33
1310	8 M	8	0	0	140

The results in Tables 5.2 and 5.3 show that Rf extracted at 0.5 M HF during runs 1301, 1302, and 1309 but did not extract during any of the other runs. The correct conclusion is that Rf extracted only at 0.5 M HF.
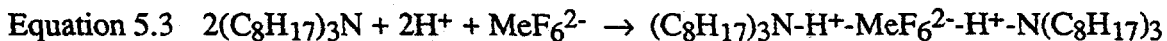
Still, it is troublesome that the number of single events observed decreased and that no pairs were observed when Ni foil was used except for run 1309. A comparison of the results from Ni and Ta foil at 0.5 M HF showed that a total of 102 singles from 350 experiments were observed when using Ta but only 9 singles out of 188 experiments were observed when using Ni. It can, therefore, be said that the Ni foil caused the activity to evaporate away along with the organic phase while on the hot plate. Evidently, the chemical properties of Ni caused it to heat to higher temperatures resulting in a larger loss of activity. In addition, the Ni foils were thinner than the Ta foils; therefore, the Ni foils heated faster than the Ta foils. Yield checks that were performed periodically throughout the experiment to insure that ^{254}Fm was being produced and transported properly showed no evident production or transport problems.

Despite the loss of activity from using Ni foil, Rf conclusively did not extract at 4 M, since run 1303 (157 experiments), performed with Ta foil at 4 M HF, showed no α–α correlated pairs. Unfortunately, no data for extractions with higher HF concentrations using Ta foil are available. However, the use of Ta foil at higher HF concentrations would probably not have resulted in Rf extracting anyway based on the results from Figure 5.1.

5.4 Discussion

Overall, the results show that the extraction trend for the group 4 elements decreases in the order Ti>Zr≈Hf>Rf. The extraction trend is the opposite of the trend of radii which decreases in the order Rf>Zr≈Hf>Ti (see Table 5.4).

93

Two factors determine the extraction trend. First, ion-pair formation favors smaller complexes such as TiF_6^{2-} and forms ion pairs as follows:

Equation 5.3 $\quad 2(C_8H_{17})_3N + 2H^+ + MeF_6^{2-} \rightarrow (C_8H_{17})_3N\text{-}H^+\text{-}MeF_6^{2-}\text{-}H^+\text{-}N(C_8H_{17})_3$

Therefore, for smaller complexes, H^+ forms a stronger bridge between the nitrogen in TIOA and the fluoride in the metal complex, so the ability to form ion pairs increases in the order $RfF_6^{2-} < ZrF_6^{2-} \approx HfF_6^{2-} < TiF_6^{2-}$. This order says that TiF_6^{2-} is most likely to form an ion pair and, therefore, extract into the organic phase.

The second factor that determines the extraction trend is the hydration effect. Smaller complexes bind more tightly to water molecules. Therefore, the hydration order is also $RfF_6^{2-} < ZrF_6^{2-} \approx HfF_6^{2-} < TiF_6^{2-}$. This order says that TiF_6^{2-} will most likely stay in the aqueous phase.

These two factors compete with each other such that when the interaction in water (hydration) is stronger than ion pair formation with the organic phase, the order of extraction is Ti<Zr≈Hf<Rf. On the other hand, when the ion pair formation with the organic phase is stronger (as in the case of TIOA), the extraction order is Rf<Hf≈Zr<Ti as observed in this study.

The ionic radius values for tetravalent Ti, Zr, and Hf with CN=6 were found in the literature [SHA76] and were determined by crystallographic techniques. Some estimates for the ionic radius of tetravalent Rf with CN=6 were also found in the literature. One study estimated 89 pm [GLE89] based on experimental data. Another study estimated 80 pm [JOH90] based on MCDF calculations. In any event, it is clear that the trend in ionic radii is the reverse of the extraction trend.

Table 5.4 Ionic Radii for the Group 4 Elements

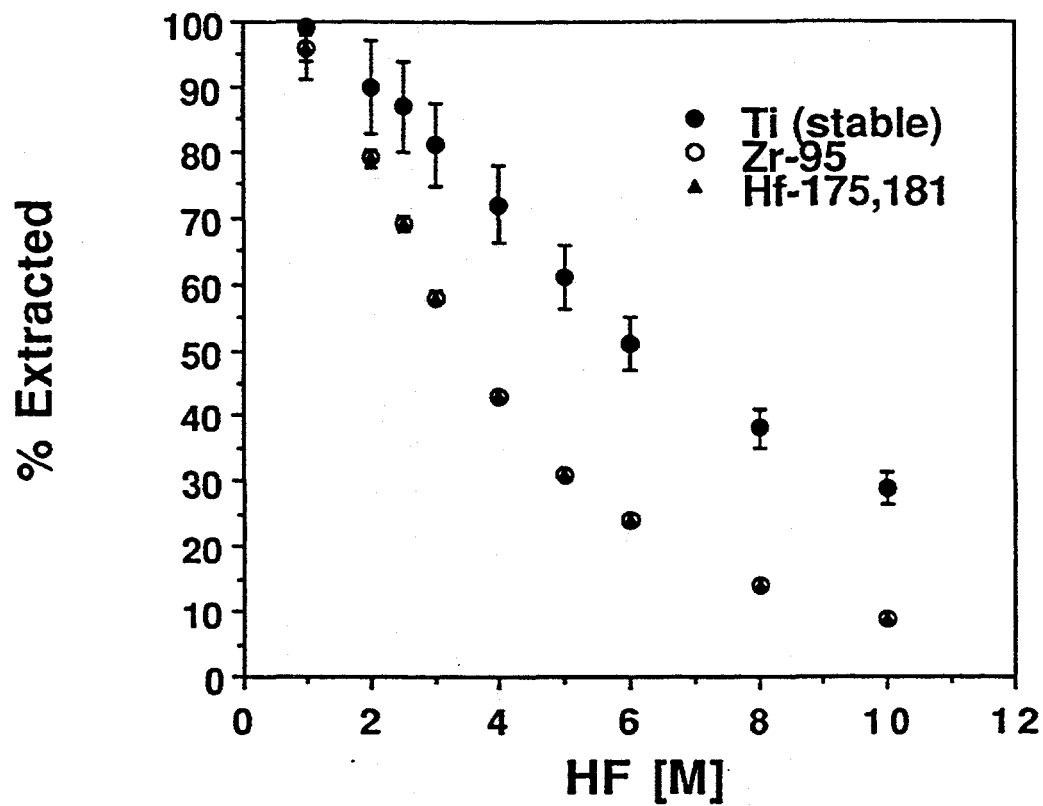| Element	Ionic Radius (Å)	References
Ti	0.605	[SHA76]
Zr	0.72	[SHA76]
Hf	0.71	[SHA76]
Rf	0.89	[GLE89]
Rf	0.80	[JOH90]

Figure 5.1 Extraction of Ti (stable), ^{95}Zr, and ^{175,181}Hf into 0.25 M TIOA in xylene
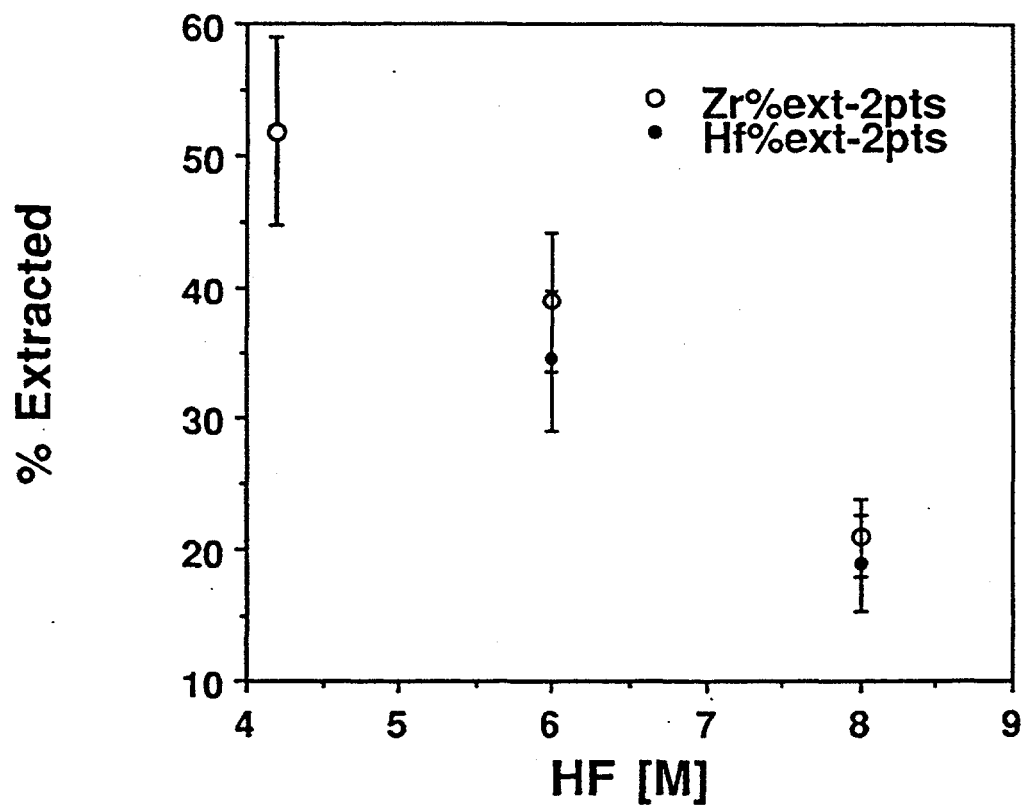as a function of [HF].
The data are from [BIL94].

Figure 5.2 Extraction of [95]Zr and [172]Hf into 0.25 M TIOA in xylene as a function of [HF]. The statistically weighted average of the two determinations is plotted and the errors denote the spread in the data.

Chapter 6

Search for ^{263}Rf

6.1 Introduction

The recent discovery [LOU93] of long-lived neutron-rich isotopes of element 106 and its implications about a deformed shell [SOB93] at N=162, Z=108 have sparked new interest in decay studies of neutron-rich transactinide isotopes. Neutron-rich isotopes have lower alpha and electron-capture (EC) decay Q values. The Geiger-Nuttall rule states that as the Q_α decreases, the half-life of the isotope increases exponentially. Presently, the longest-lived known isotope of Rf is 78-s ^{261}Rf. The discovery of a neutron-rich, longer-lived isotope of Rf would greatly facilitate studies of the chemical properties of Rf.

In one attempt by Czerwinski et al. [CZE92A], [CZE92B] to make ^{263}Rf, the ^{248}Cm(^{18}O,3n) reaction was used and extractions from chloride solution into thenoyltrifluoroacetone (TTA) were performed. A total of 7 spontaneous fission (SF) events were observed which were interpreted as preliminary evidence for the production of ^{263}Rf with a SF half-life near 500-s and a production cross section of 140 pb.

6.2 New Experiments with Thenoyltrifluoroacetone

6.2.1 Procedure

The previous TTA experiment employed a sound solvent extraction technique that used 0.5 M thenoyltrifluoroacetone (TTA) to extract Rf from 0.05 M HCl. Therefore, the same technique was used during this attempt to produce ^{263}Rf. However, a different procedure was used to take advantage of ^{263}Rf half-life estimates for alpha and fission decay. The ^{248}Cm (^{22}Ne, α3n) reaction was used with a beam energy of 116 MeV on target and a potential cross section of 120 pb was estimated using the JORPL [ALO74] tables. Folding in the gas jet yield, chemical yield, and detector efficiencies, the detection rate for a cross section of 120 pb would be 0.6 events per hour.

Because of lower Q values for α and EC decay, the partial half-lives of ^{263}Rf were expected to be longer than for the lighter isotopes of Rf. The predicted EC half-life was 1.5h (Q_{EC} = 1.33, log (ft) = 6.0), and the predicted α half-life was several hours (Q_α = 7.82). If the SF hindrance factor associated with the 159th neutron in Rf is between 10^3 and 10^5, the SF half-life would be 20s to 2000s and the overall half-life would be dominated by SF decay.

Based on the above ^{263}Rf half-life estimates for fission and alpha decay, two procedures were designed to a) look for the possibility of shorter-lived (<3600 sec) ^{263}Rf fissions and b) to look for longer-lived (>3600 sec) ^{263}Rf fissions and both short- and long-lived ^{263}Rf alphas.

To search for shorter-lived ^{263}Rf fissions, the activity was collected for ten minutes, picked up with 10 μL of 0.05 M HCl, mixed with 0.5 M TTA and centrifuged. The organic phase was removed, evaporated on a glass cover slip, and counted with a PIPS detector for fissions and alphas.

To search for longer-lived ^{263}Rf fissions and both short and long lived ^{263}Rf alphas, a special collection procedure was used. The activity was collected for five minutes, picked up with 10 uL of 0.05 M HCl, mixed with 0.5 M TTA, and centrifuged. The organic phases from the separations performed on the 5-minute collections were combined over a one hour period while the aqueous layer was removed after each experiment, evaporated on a glass cover slip, and alpha counted. Detection of ^{259}No alphas in the aqueous phase would imply ^{263}Rf production. The combined organic phases were added to an equal volume of 12M HCl to back extract ^{259}No^{2+}, the alpha-decay daughter of ^{263}Rf^{4+}.

This procedure of batching the organic phase for one hour, then back extracting, was repeated two more times. Following that, the organic phase was evaporated on a glass cover slip and counted for long-lived ^{263}Rf fissions and alphas. The entire procedure took 3 hours and was repeated six times.

6.2.2 Results

No evidence was observed for alphas from ^{259}No (E_α= 7.5 MeV) or ^{263}Rf. The sensitivity for detecting fissions was hampered by the relatively large amounts of ^{256}Fm also produced in the ^{22}Ne + ^{248}Cm reaction. Based on the production cross section ratios for ^{254}Fm and ^{256}Fm [LEE82] and the amount of ^{254}Fm observed after chemical separation during the experiment, 22.6 fissions from ^{256}Fm were expected to be observed. Therefore, a statistically significant number of fissions from ^{263}Rf relative to the 22.6 fissions expected from ^{256}Fm would have had to have been detected to get a positive result.

Since only 16 fissions were detected during the experiment, none of these could be attributed to ^{263}Rf. Figure 6.1 shows the production cross section limit vs. half-life for

^{263}Rf. Gas-jet yield, detector geometry, chemical yield, irradation time, separation time between end of irradiation and beginning of count, and the total count time were included in the cross section limit calculation. If the half-life of ^{263}Rf is 500^{+300}_{-200} seconds as previously predicted, then the upper limit on its production cross section would be 0.2 nb. This is close to the predicted cross section of 0.14 nb.

6.3 Experiments with ARCA

6.3.1 Procedure

Another attempt to identify ^{263}Rf was made during the LBL-German-Swiss collaboration at the LBL 88-Inch Cyclotron to study the chemical and nuclear properties of Rf and Ha in the fall of 1993. The ^{249}Bk(^{18}O,4n) reaction was used with a beam energy of 114-MeV to produce ^{263}Ha [KRA92] with an ^{18}O^{5+} energy of 93 MeV on the target. Chemical separations were carried out to study the decay properties of 27-s ^{263}Ha and search for evidence of ^{263}Rf produced by electron-capture decay in ^{263}Ha.

Activities from the ^{18}O + ^{249}Bk reaction were transported by the helium gas-jet to the Automated Rapid Chemistry Apparatus (ARCA) [SCH89] where computer controlled separations were repeatedly performed, on a one-minute time scale, producing Rf and Ha samples for α- and SF-pulse height analysis. The separation involved eluting Ha from cation exchange resin columns with 0.05M α-hydroxyisobutyrate (α-HIB) and then Rf with 0.5 M α-HIB. These one-minute separations were repeated five times to elute and collect Ha while keeping Rf on the column, then Rf was removed using 0.5 M α-HIB. All of these fractions had an extremely high degree of purity from the trivalent actinides such as Fm, allowing a search for SF decay at detection rates as low as one event per hour.

6.3.2 Results

The summed alpha spectrum from this experiment is shown in Figure 6.2. A total of 80 alphas and 22 fissions was observed over the course of 155 of the five minute cycles. Approximately 8.8 of these 22 ± 4.7 fissions were attributed to ^{256}Fm decay, leaving 13.2 ± 3.6 SFs due to the decay of ^{263}Rf. The 8.8 fissions are based on the known production cross section ratios for ^{254}Fm and ^{256}Fm [LEE82] and the amount of ^{254}Fm observed during the experiment after chemical separation. These ^{263}Rf fissions had a half-life of $600 \, ^{+300}_{-200}$ seconds, close to the 500 sec fission half-life observed in a previous study [CZE92A].

Based on the 10-nb ^{263}Ha production cross section [KRA92], these 13.2 SF events corresponded to a ^{263}Ha EC branch of ~5%. The resulting effective ^{263}Rf production rate was about a factor of 4 larger than that expected or observed [CZE92A] in either the ^{248}Cm(^{22}Ne,α3n) or ^{248}Cm(^{18}O,3n) reactions.

Alpha half-life predictions for ^{263}Rf were made using mass models from Satpathy [SAT88] and Möller [MOL88] and the alpha decay systematics of Hatsukawa et al. [HAT90], [HAT90A]. If the alpha energy of ^{263}Rf is between 7.74 and 8.0 MeV, the alpha half-life would be between 800 and 8000 seconds. Within this energy range, two events were observed at 7.9 MeV (Figure 6.2). The two events represent an alpha branch of 26% based on the 15.2 event total (13.2 fissions and 2 alphas) and accounting for a factor of 2 in the detection efficiencies between alphas and fissions. This alpha branch is reasonable based on the Hatsukawa systematics which predict a half-life of roughly 1500 seconds based on the 7.9 MeV decay energy.

If the alpha energy of ^{263}Rf is between 7.65 and 7.74 MeV, then any alphas from ^{263}Rf would be masked by alphas from 164-μs ^{214}Po. If the alpha energy is less than 7.65 MeV, then the predicted alpha half-life for ^{263}Rf would be greater than 10,000 sec, and thus too long to have been observed.

6.3.3 Attempted Confirmation Experiment

The tentative results from the previous experiment prompted a confirmation experiment. The same reaction was used to produce ^{263}Ha, and the same beam, energy, and target chamber setup were used, except that the ^{249}Bk target thickness was 390 μg/cm^2. However, the separation was performed manually, and a larger column with different resin was used. Further procedural changes from the ARCA experiment were made to take advantage of the observed 500-600 sec ^{263}Rf half-life. The complete procedural details are in Section 2.6.

6.3.3.1 Procedure Development - Tracers

Various tracers were used to optimize experimental conditions. Tetravalent ^{95}Zr and pentavalent ^{95}Nb were used to model the behaviors of tetravalent ^{263}Rf and pentavalent ^{263}Ha, respectively. Trivalent ^{152}Eu and ^{249}Cf were used to study actinide behavior. Figure 6.3 shows the positions of Zr and Nb from elutions with α-HIB using AG50 x 12 cation exchange resin. More than 80% of the ^{95}Nb eluted within the first six drops. ^{95}Zr started to elute at the 10th drop with more than 80% eluting by the 14th drop. These results were barely adequate, therefore, a new column was prepared with AG50 x 4 cation exchange resin to see if the separation could be improved. Figure 6.4 shows the improved results with most of the ^{95}Nb eluting within the first five drops and most of the ^{95}Zr eluting within four drops. 0.5 M α-HiB was not added until after the 12th drop to show if any straggling from ^{95}Nb was present which had previously been a problem with the AG50 x 12 cation exchange resin. The separation experiment was repeated several times with AG50 x 4 resin by various group members to insure the reproducibility of these results.

103

Due to time considerations, the resin in a column was used several times during the cyclotron run before being changed. To insure that the $^{152}Eu^{3+}$ tracer would not elute after several repeat separations, additional 0.5 M α-HiB was added onto the column after the ^{95}Zr was eluted and four batches of 25 drops each and a fifth batch of 100 drops was collected and counted. Counting periods of at least 6 hours were required because of the small amount of tracer that had eluted. The Li-drifted germanium detector used to analyze gamma emitting ^{152}Eu had background counts from the environment such as from cosmic rays, therefore, it was difficult to resolve the seemingly nonexistent ^{152}Eu peaks from the rest of the spectrum. To solve this problem, alpha emitting ^{249}Cf was eluted in a similar procedure and a separation factor of better than 3000:1 was achieved between tetravalent/pentavalent and trivalent tracers.

6.3.3.2 Procedure Development - Rf

The experimental procedure used at the cyclotron was similar and the column, resin, and solutions used during this experiment were identical to those used with the tracers studies. The activity was transported via the KCl/gas-jet and collected on a teflon disc for a total of 12 minutes. The teflon was repositioned after 6 minutes to prevent the growing mound of KCl from growing too high which would cause the top of the mound to flake off.

Halfway through the experiment, the collection time was raised to 20 minutes because a) the SF's in the 5+ fraction were compatible with the expected yield of ^{256}Fm and b) the SF's in the 4+ fraction seemed long compared to the 1 hour counting interval. The activity was picked up with 10 µl of unbuffered 0.075 M α-HiB, and loaded onto a column already pretreated with 0.075 M α-HiB. An additional 10 µl of 0.075 M α-HiB was used to pick up any remaining activity from the teflon disc. The activity was pushed

through using N_2 gas to just the top of the level of the resin. The flow rate was at least 5 seconds/drop. Additional 0.075 M α-HiB was added and $^{263}Ha^{5+}$ was eluted. Since the FCV was two drops, the first two drops were discarded. Drops 3-6 contained the 5+ ^{263}Ha fraction and were collected on a tantalum foil. The foil was placed onto a hot plate during the collection so evaporation could take place. This prevented overflow as subsequent drops were collected. The foil was then flamed and placed on one of five designated passivated ion-implanted planar silicon (PIPS) alpha detectors. Any remaining 0.075M α-HiB was pushed through to just the top of the level of the resin.

Unbuffered 0.5M α-HiB was then added and $^{263}Rf^{4+}$ was eluted. Again, the first two drops (drops 7-8) were discarded. Drops 9-14 were handled the same way as drops 3-6. The separation and elution was repeated five times with the same resin. Between experiments, the resin was pretreated with a few FCVs of unbuffered 0.075 M α-HiB.

The gas-jet efficiency was measured periodically during the experiment by collecting the activity from the gas-jet for five minutes, picking it up with 0.5 M α-HiB solution, and placing it on a Ta foil. The solution was then evaporated to dryness and the Ta foil was flamed. The production rate of the $^{252-255}Fm$ transfer products was determined by alpha spectroscopic analysis.

In the unlikely event that some activity from the 4+ fraction may have been left on the column after a series of experiments, the column was stripped after five experiments with 0.5 M α-HiB (pH = 4.3). The first 8 drops were collected on Ta foil, evaporated, flamed, and placed on a designated PIPS detector (detector 11). Any activity coming off the stripped column could then be taken into account during the post-run analysis.

To normalize the yield checks, a gold catcher foil was placed directly behind the ^{249}Bk target. All of the products recoiling from the target were caught in the gold catcher foil. The target was bombarded for 34 minutes, then the catcher foil was removed and dissolved in aqua regia. A new AG1 x 8 anion exchange column was prepared and an FCV of 9 drops was measured with 12M HCl. The dissolved gold and a 20λ aliquot (28

cpm after correcting for geometry) of ^{241}Am were loaded onto the column. The ^{241}Am was used to track the chemical yield of the actinides. The activity was eluted with 12M HCl while Au was retained on the resin. 30 drops were collected then transferred and evaporated on platinum foil then the foil was placed on a PIPS detector. The gas-jet transport efficiency was measured by comparing the production rates by the gold catcher foil method with the production rates after transport through the He/KCl gas-jet. In this experiment, the transport efficiency was around 60%.

An interesting observation was made during the course of the experiment. During direct catch yield checks (not to be confused with gold catcher foil yield checks), instead of simply collecting on Ta foil directly then flaming, the activity was collected on teflon, picked up with 0.075 M α-HiB, transferred to a Ta foil, the solution was evaporated, and the Ta foil was flamed. This was done to maintain constancy in experimental conditions. A substantial loss in yield was noticed. The activity was not lost on the teflon or pipet transfer tips. Rather, the α-HiB reacted with the KCl salt as follows:

$$\alpha\text{-HiB} + KCl \rightarrow HCl + K^+(\alpha\text{-HIB})^-$$

The activity was expected to remain on the Ta surface. However, since both HCl and K(α-HIB) are volatile, their sublimation apparently carried away the activity. This did not affect the chemical results because the activity was never evaporated in α-HiB solution during the separation experiments.

6.3.3.3 Results

Based on a 10 nb cross section for ^{263}Ha and a 5% EC branch from the previous experiment, 98 ^{263}Rf fission events were expected, assuming a 100% SF branch for

^{263}Rf. A total of 11 fissions were observed over the course of 238 experiments. Because of suspected background contamination from previous experiments, five PIPS detectors were counted for a period of 10 days after the experiment was completed to check for any background contamination. The background was measured at 0.5 fissions/detector/day. Hence, the 11 fissions observed were consistent with the detector background and could not be attributed to SF from ^{263}Rf.

Assuming that a statistically significant number of fissions from ^{263}Rf relative to the 11 observed fissions had to be observed in order to make a positive identification, a 0.5% EC branch from ^{263}Ha could have been detected. This result is inconsistent with the previous experiment that indicated a 5% EC branch from ^{263}Ha.

Several explanations could account for not observing the ^{263}Ha EC branch. Perhaps ^{263}Rf has a smaller SF branch and a larger alpha branch than expected. However, no alphas with half-lives out to 12000 seconds were observed that could be attributed to the decay of ^{263}Rf. It is possible that the alphas could have been masked by ^{214}Po (E_α= 7.687 MeV). But only two alpha events from the ^{263}Rf alpha daughter ^{259}No (E_α ^{259}No = 7.5 MeV) were observed (Figure 6.5). It is therefore unlikely that a significant alpha branch in ^{263}Rf exists.

Another possibility is that the masked ^{263}Rf alphas decayed to ^{259}No, which then EC decayed to ^{259}Md ($t_{1/2}$=103m) (Figure 6.6). However, the primary decay mode in ^{259}Md is SF so this decay chain is unlikely. It is also possible that ^{263}Rf EC decayed to the unknown isotope ^{263}Lr, in which case, the decay of ^{263}Lr might have gone unnoticed.

Since it was found in later experiments that Hf adsorbs onto teflon, another explanation is that ^{263}Rf adsorbed onto the teflon discs that were used to collect the activity from the gas-jet during this experiment.

In the ARCA experiment where a positive identification of ^{263}Rf was made, the apparatus which was used also was made of teflon. However, the activity which came into contact with teflon was mostly ^{263}Ha. It was then sorbed on a column where it EC

decayed to ^{263}Rf which could then be eluted. Therefore, Rf would not have come into contact with teflon.
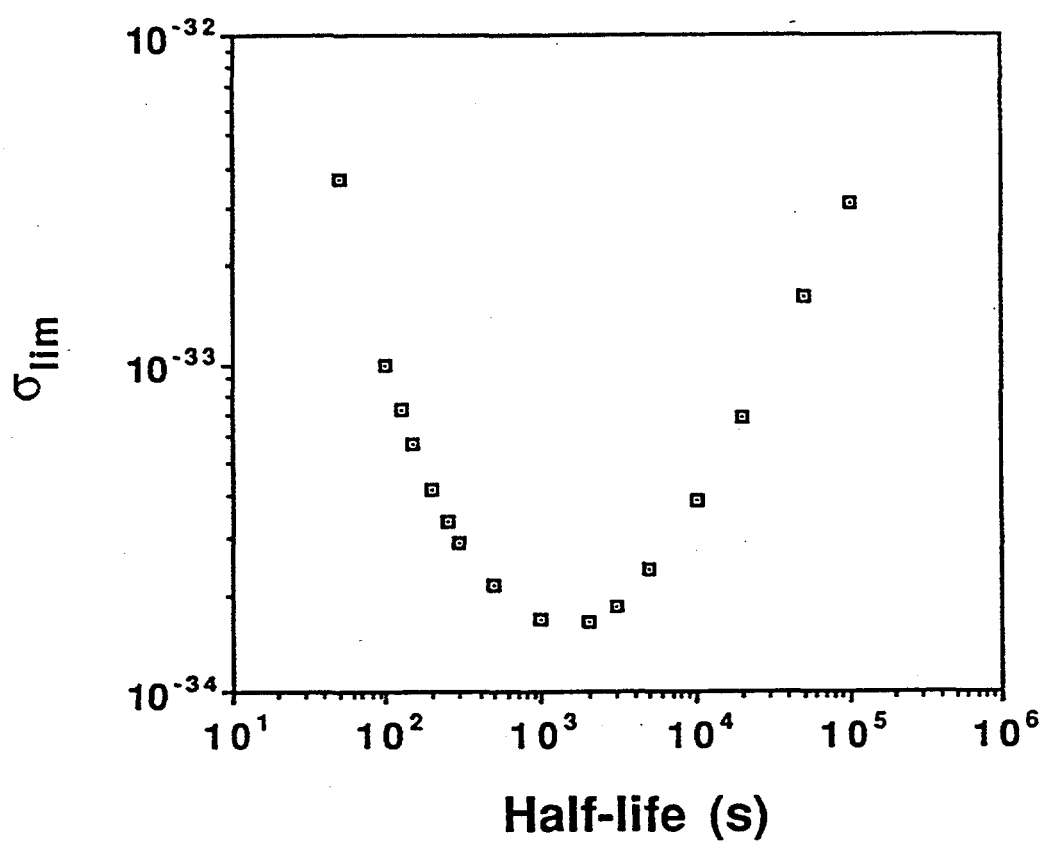
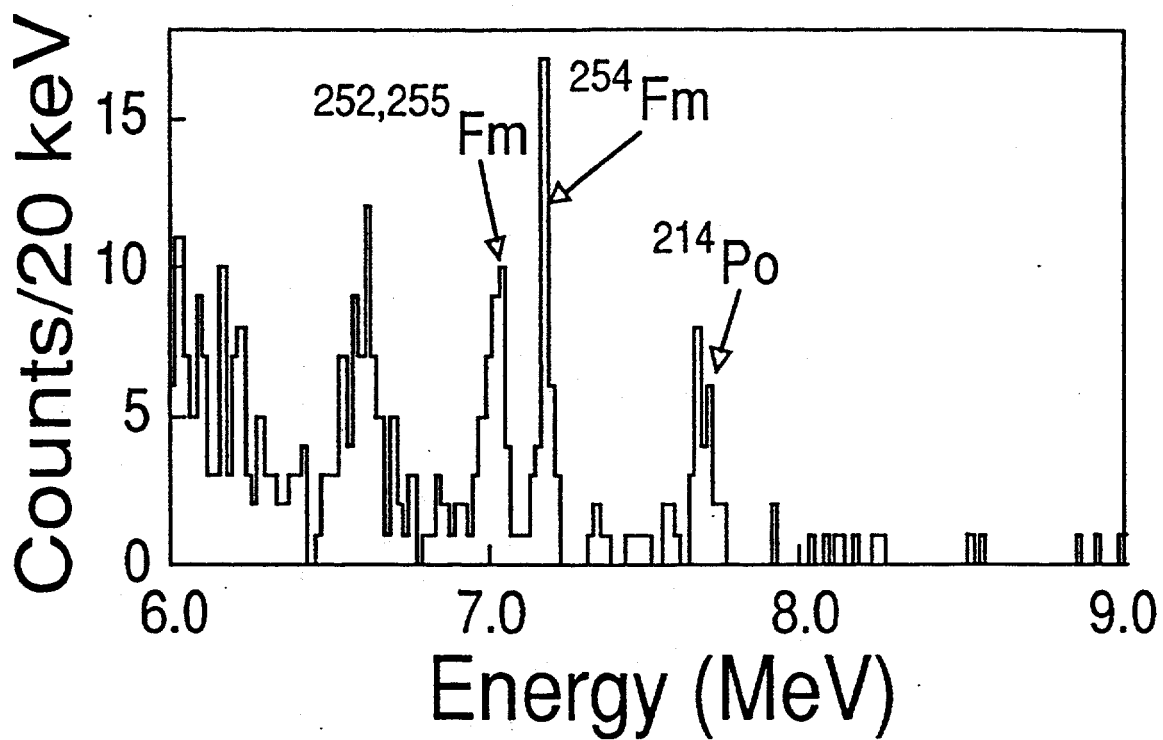Figure 6.1 ^{263}Rf production cross section limit plotted vs. its half-life.

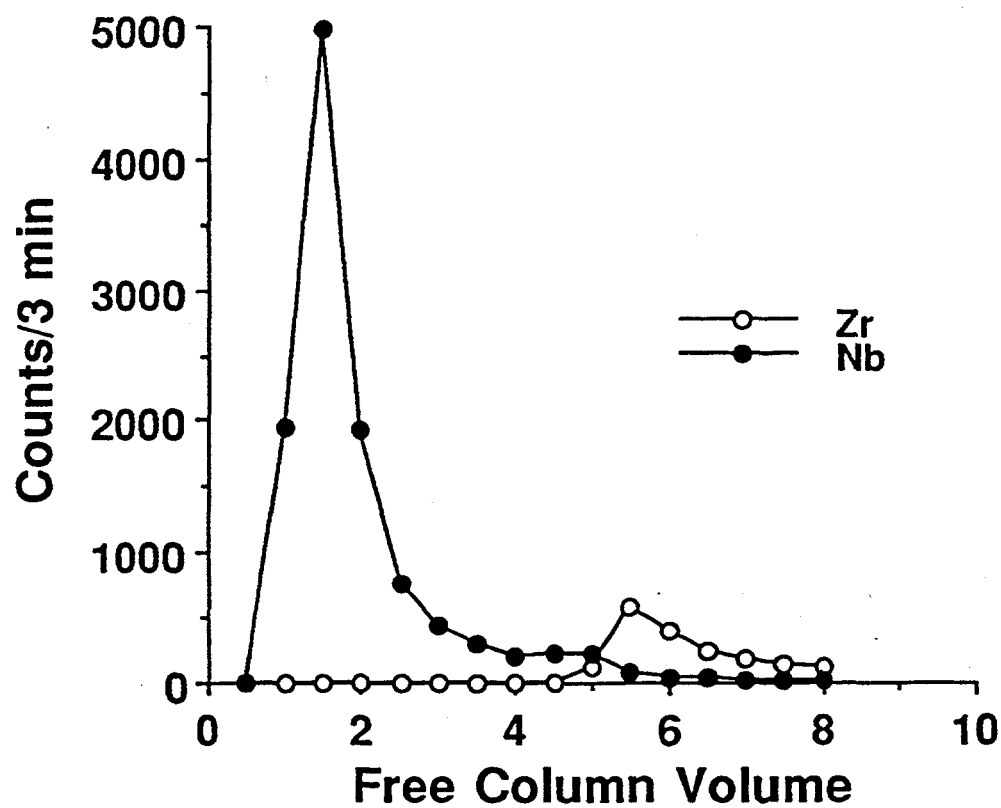Figure 6.2   Summed α-particle spectrum from 155 ^{263}Rf separations.

Figure 6.3 Elution of $^{95}Nb^{5+}$ and $^{95}Zr^{4+}$ from AG50 x 12 cation exchange resin column with 0.075 M and 0.5 M α-HiB, respectively. Flow rate was 10 sec/FCV.

Figure 6.4 Elution of $^{95}Nb^{5+}$ and $^{95}Zr^{4+}$ from AG50 x 4 cation exchange resin column with 0.075 M and 0.5 M α-HiB, respectively. Flow rate was 10 sec/FCV.
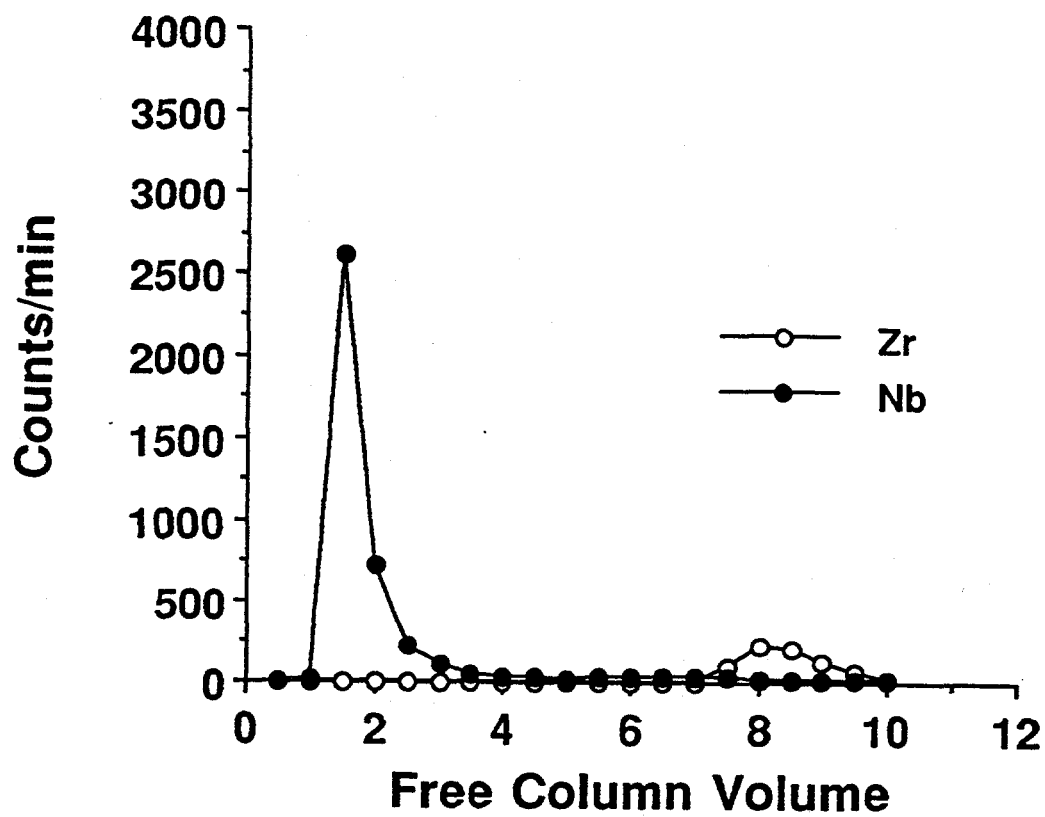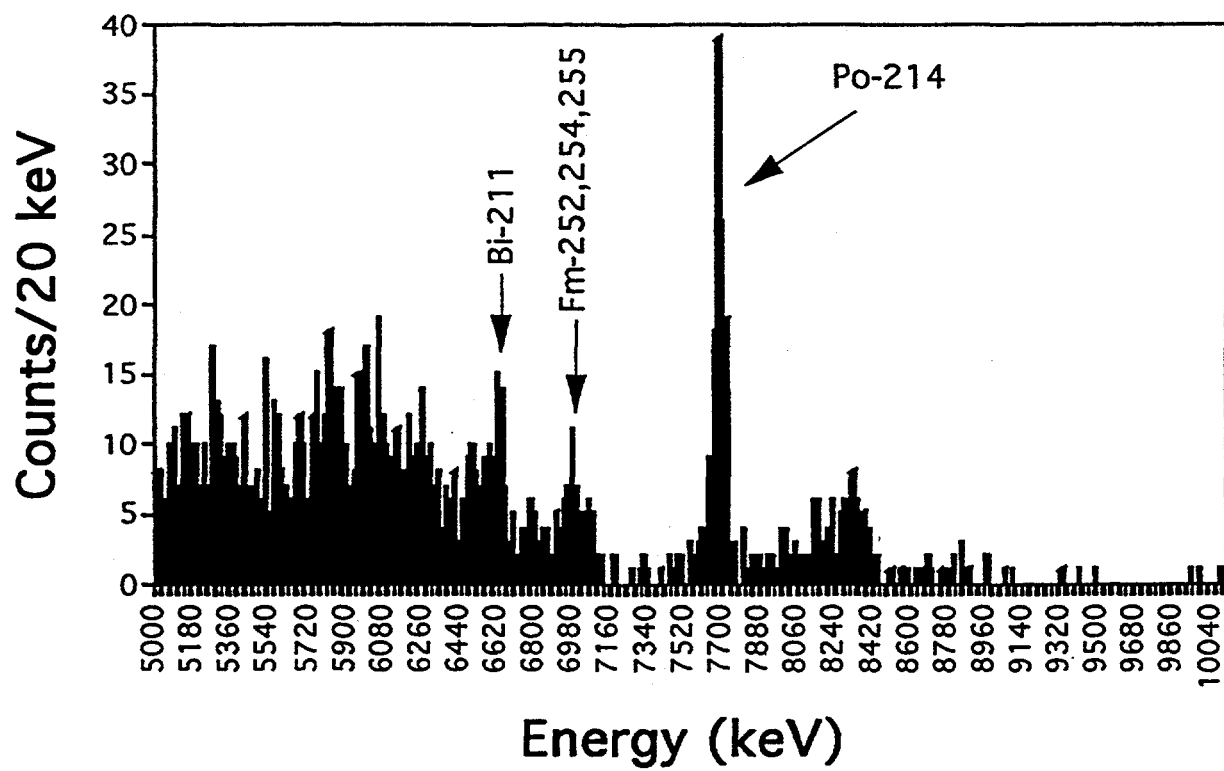
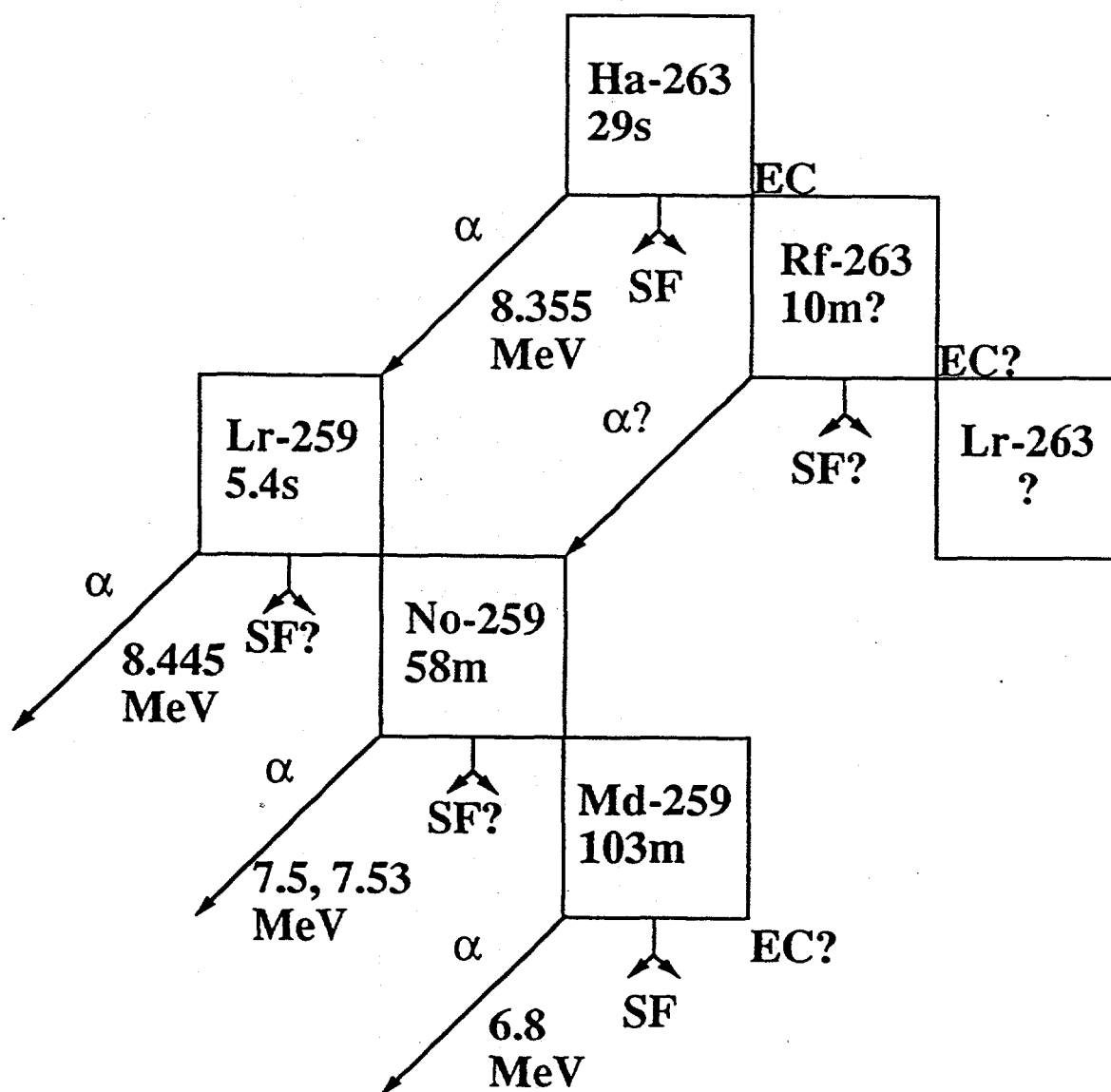Figure 6.5 Summed α-particle spectrum from 238 Rf-263 experiments.

Figure 6.6 ^{263}Ha Decay Chain.

Chapter 7

Conclusions

7.1 Surface Sorption Chemistry

The cobalt(II)ferrocyanide surface was shown to be a viable way to study the hydrolysis of the group 4 elements. The hydrolysis trend in the group 4 elements and pseudogroup 4 element Th was shown to decrease in the order Rf>Zr≈Hf>Th. The tendency for Rf to more easily hydrolyze than its lighter group 4 homologs is attributed to relativistic effects which destabilize the $6d_{5/2}$ shell and stabilize the $7p_{1/2}$ shell. Consequently, it was predicted that Rf would be prone to having a coordination number of 6 in most aqueous solutions. This lower-than-expected coordination number results in a higher charge density on the Rf cation, decreasing the distance of the Rf-O bond, and therefore, weakening the O-H bond.

7.2 Solvent Extraction Studies with Tributylphosphate

The hydrolysis trend observed in the surface sorption studies was confirmed in the solvent extraction studies with TBP. The extraction trends observed in the HCl and HBr systems which decreased in the order Zr>Hf>Rf>Ti for HCl and Zr>Hf>Rf?Ti (it is believed that Rf comes before Ti but not certain) for HBr showed that a) the trends were

115

similar for both HCl and HBr, b) the affinity of the metal cation for the halide was greater for Zr and Hf than for Rf and Ti, and c) Rf and Ti did not extract as well because they tended to hydrolyze more easily than Zr and Hf. The greater tendency for Rf and Ti to hydrolyze was shown in the extraction system where [Cl⁻] was kept constant and [H⁺] was varied between 8 and 12 M. As [H⁺] increased, the extraction of Rf and Ti increased because a) they were hydrolyzing less and b) more of the anionic complexes that had formed such as $RfCl_5^-$ were made neutral by the addition of a proton.

7.3 Solvent Extraction Studies with Triisooctylamine

This solvent extraction experiment with TIOA which is known to extract anionic species was used to show how factors other than coordination number affect complexation chemistry. In this case, extractions performed from HF solutions into TIOA showed that the extraction trend for the group 4 elements (Ti>Zr≈Hf>Rf) decreased in the reverse order of the trend of the ionic radii (Rf>Zr≈Hf>Ti).

The observed extraction trend was because the interaction of the metal complex in water (hydration) was weaker than the strength of the ion pair bond formed between the metal complex and TIOA (see Section 5.4 for a detailed discussion).

7.4 Search for ^{263}Rf

Production of ^{263}Rf was attempted via the ^{248}Cm (^{22}Ne, α3n) and ^{249}Bk(^{18}O,4n) reactions. The technique of solvent extraction was used to separate any ^{263}Rf by extracting from 0.05 M HCl into 0.5 M TTA. No alpha events were observed from either ^{259}No or ^{263}Rf. A total of 16 fissions were observed but were all attributed to ^{256}Fm.

From this experiment, the upper limit on the production cross section of ^{263}Rf is 0.2 nb in the ^{248}Cm (^{22}Ne, α3n) reaction at 116-MeV if its half-life is 500 sec as suggested by Czerwinski et al. [CZE92A].

Next, attempts with ARCA were made to detect ^{263}Rf produced by EC decay of ^{263}Ha produced in the ^{249}Bk(^{18}O,4n) reaction at 114-MeV. 22 $\pm$ 4.7 fissions were observed out of which 8.8 were attributed to ^{256}Fm decay and 13.2 to ^{263}Rf. The fissions attributed to ^{263}Rf had a half-life of 600 $^{+300}_{-200}$ seconds, close to its previously predicted half-life, and corresponded to a ^{263}Ha EC branch of $\approx$5% based on the 10-nb production cross section for ^{263}Ha [KRA92].

A confirmation experiment was then attempted using the same reaction as that used in the ARCA experiments and a similar chemical technique and procedure to that of the ARCA experiment. A total of 11 fissions were observed during the course of the experiment but were attributed to background contamination of the detectors in which the samples were counted. Based on these 11 fission events, a 0.5% EC branch from ^{263}Ha could have been detected. The 5% EC branch from ^{263}Ha was not observed possibly because any ^{263}Rf that was produced probably remained sorbed on the teflon disks (see Section 6.3.3.3) that were used to collect the activity from the gas-jet and thus not extracted.

7.5 Future Work

Solvent extraction studies of Rf from HBr into TBP should be further explored with higher concentrations of HBr. At the time the current study was performed, only the constant-boiling azeotrope, 9 M HBr, was available. However, it may be possible to obtain 12 M HBr, and since Rf is expected to extract at 12 M HBr, such studies would show whether Rf or Ti appears next after Hf in the extraction trend Zr>Hf>Rf?Ti.

Production of ^{263}Rf should be attempted to confirm the ARCA results but without the use of teflon. Platinum surfaces have been found not to sorb tetravalent elements and could therefore be used in a subsequent experiment. Since ^{263}Rf is predicted to have a much longer half-life than the current longest-lived isotope of Rf, 78-s ^{261}Rf, production of ^{263}Rf would allow more time for a chemical procedure to be performed, and thus facilitate new studies into the chemical properties of Rf.

Future success in studying the chemical properties of still heavier transactinides depends largely on the development of faster chemical separation systems. More conventional methods such as solvent extraction and ion exchange column chromatography would not be feasible for studying isotopes with half-lives much shorter than a minute. Even surface sorption which takes less time to perform than solvent extraction would not be applicable. Gas phase chromatography, on the other hand, is one method that could be refined so that it could be used to study isotopes with half-lives on the order of a few seconds. The system is primarily limited by the transport time of the activities to the detector.

In addition to refining current chemical separation systems, longer lived isotopes of a particular element could be produced. The recent discovery of longer-lived isotopes ^{265}Sg and ^{266}Sg (half-lives estimated between 2 and 30 seconds) and the prediction of enhanced stability around Z=108 and N=162 [SOB93A] have renewed hopes that longer-lived isotopes of the transactinides will continue to be discovered. The recent discovery of elements 110 and 111 have served to underscore this prediction, and the discovery of longer-lived isotopes would permit chemical studies. As of this writing, a collaborative experiment between LBL and GSI is underway to chemically study the recently discovered seaborgium isotopes.

References

[ABD90]   A. Abdul-Hadi, M. Hussonnois, Z. Szeglowski, B. Weiss, O. Constantinescu, G. Ardisson, C.R. Acad. Sci. Paris, 311, 1399 (1990).

[ALC56]   K.Alcock, S.S.Grimley, T.V.Healy, J.Kennedy, H.A.C.McKay, Trans. Faraday Soc., 52, 39 (1956).

[ALO74]   J. Alonso, Gmelin Handbuch der Anorganischen Chemie, 7b, 28 (1974).

[ANT77]   W.P. Antonovich, E.M. Newskaja, E.I. Shelihina, Russ. J. Inorg. Chem., 22, 363 (1977).

[AUM74]   D.C. Aumann, G. Müllen, Nucl. Instr. Meth., 75, 115 (1974).

[BAE76]   C.F. Baes, R.E. Mesmer, The Hydrolysis of Cations, Wiley, New York, 152-191 (1976).

[BAG75]   P.S. Bagus, Y.S. Lee, K.S. Pitzer, Chem. Phys. Lett., 33, 408 (1975).

[BEL75]   E.A.Belousov, L.Y.Zakharova, Russ. J. Phys. Chem, 49, 1695 (1975).

[BES57]   C.Best, H.A.C.McKay, P.Woodgate, J. Inorg. Nucl. Chem., 4, 315 (1957).

[BIL84]   A. Bilewicz, J. Narbutt, Isotopenpraxis, 20, 141 (1984).

[BIL94]   A. Bilewicz, Institute of Nuclear Chemistry and Technology, Warsaw, Poland, private communication (1994).

[BUR50]   L.L.Burger, U.S. Atomic Energy Commission Report HW-19065, General Electric Co., Richland, WA (1950).

[BUR51]   L.L.Burger, R.C.Forsman, U.S. Atomic Energy Commission Report HW-20936, General Electric Co., Richland, WA (1951).

[CHA87]   R.M. Chasteler, R.A. Henderson, D.M. Lee, K.E. Gregorich, M.J. Nurmia, R.B. Welch, D.C. Hoffman, Phys. Rev. C, 36, 5 (1987).

[CHR71]   N.E. Christensen, B.O. Seraphin, Phys. Rev. B, 4, 3321 (1971).

[COL78]   C.F.Coleman, R.E.Leuze, J. Tenn. Acad. Sci., 53, 102 (1978).

[CON52]   R.E. Connick, Z.Z. Hugus, Jr., J. Am. Chem. Soc., 74, 6012 (1952).

[CZE94]   K.R.Czerwinski, C.D. Kacher, K.E. Gregorich, T.M. Hamilton, N.J. Hannink, B. Kadkhodayan, S.A. Kreek, D.M. Lee, M.J. Nurmia, A. Türler, G.T. Seaborg, D.C. Hoffman, Radiochimica Acta, 64, 29 (1994).

[CZE92A]   K.R. Czerwinski, et al., LBL Nucl. Sci. Div. 1991 Ann. Rept., LBL-31855 p.54 (1992).

[CZE92B]   K.R. Czerwinski, Ph.D. Thesis, LBL-32233, 104 (1992).

[CZE94C]   K.R.Czerwinski, K.E. Gregorich, N.J. Hannink, C.D. Kacher, B. Kadkhodayan, S.A. Kreek, D.M. Lee, M.J. Nurmia, A. Türler, G.T. Seaborg, D.C. Hoffman, Radiochimica Acta, 64, 23 (1994).

[DES73]   J.P. Desclaux, Atomic Nucl. Data Tables, 12, 312 (1973).

[DES80]   J.P. Desclaux, B. Fricke, J. Phys. (Paris), 41, 943 (1980).

[EVA72]   J.E. Evans, R.W. Lougheed, M.S. Coops, R.W. Hoff, E.K. Hulet, Nucl. Instr. Meth., 102, 389 (1972).

[FRI75]   B. Fricke, in Structure and Bonding, Eds. J.D. Dunitz, et al., Springer-Verlag, Berlin-Heidelberg-New York, 21, 90-142 (1975).

[GHI70]   A. Ghiorso, M. Nurmia, K. Eskola, P. Eskola, Phys. Lett., 32B, 95 (1970).

[GHI71]   A. Ghiorso, M. Nurmia, K. Eskola, P. Eskola, Phys. Rev., C4, 1850 (1971).

[GLE89]   V.A. Glebov, L. Kasztura, V.S. Nefedov, B.L. Zhuikov, Radiochim. Acta, 46, 117 (1989).

[GOB92]   M.K. Gober, J.V. Kratz, H.P. Zimmermann, M. Schädel, W. Brüchle, E. Schimpf, K.E. Gregorich, A. Türler, N.J. Hannink, K.R. Czerwinski, B. Kadkhodayan, D.M. Lee, M.J. Nurmia, D.C. Hoffman, H. Gäggeler, D. Jost, J. Kovacs, U.W. Scherer, A. Weber, Radiochimica Acta, 57, 77 (1992).

[GRE88]   K.E. Gregorich, R.A. Henderson, D.M. Lee, M.J. Nurmia, R.M. Chasteler, H.L. Hall, D.A. Bennett, C.M. Gannett, R.B. Chadwick, J.D. Leyba, D.C. Hoffman, G. Herrmann, Radiochimica Acta, 43, 223 (1988).

[GRE]   K.E. Gregorich, private communication.

[GRE90]   K.E. Gregorich, LBL-29306, Nucl. Instr. Meth. A 302, 135 (1991).

[HAA93]   P.A. Haas, Sep. Sci. & Tech., 28 (17-18), 2479 (1993).

[HAR59]   C.D.Harrington, A.E.Ruehle, Uranium Production Technology, van Nostrand, Princeton, N.J. (1959).

[HAR64]   C.J.Hardy, D.Fairhurst, H.A.C.McKay, A.M.Wilson, Trans. Faraday Soc., 60, 1626 (1964).

[HAR79]   W.R. Harris, K.N. Raymond, J. Am. Chem. Soc., 101, 6534 (1979).

[HAR81]   W.R. Harris, K.N. Raymond, F.L. Weitl, J. Am. Chem. Soc., 103, 2667 (1981).

[HAT90]   Y. Hatsukawa, PhD Thesis, Tokyo Metropolitan University (1990).

[HAT90A]   Y. Hatsukawa, H. Nakahara, D.C. Hoffman, Phys. Rev. C, 42, 674 (1990).

[HEN90]   R.A. Henderson, PhD Thesis, LBL-29568 (1990).

[HES57]   E.Hesford, H.A.C.McKay, D.Scargill, J. Inorg. Nucl. Chem., 4, 321 (1957).

[HES58]   E.Hesford, H.A.C.McKay, Trans. Faraday Soc., 54, 573 (1958).

[HIG59]   C.E.Higgins, W.H.Baldwin, B.A.Soldano, J. Phys. Chem., 63, 115 (1959).

[HOF]   D.C. Hoffman, private communication.

[HOF80]   D.C. Hoffman, D.M. Lee, A. Ghiorso, M. Nurmia, K. Aleklett, Phys.
            Rev. C, 22, 1581 (1980).

[HUL80]   E.K. Hulet, R.W. Lougheed, J.F. Wild, J.H. Landrum, J.M. Nitschke, A.
            Ghiorso, J. Inorg. Nucl. Chem., 42, 79 (1980).

[JOH90]   E. Johnson, B. Fricke, O.L. Keller, Jr., C.W. Nestor, Jr., T.C. Tucker, J.
            Chem. Phys., 93 (1990).

[KAD93]   B. Kadkhodayan, PhD Thesis, LBL-33961, 22-23 (1993).

[KAD93A]   B. Kadkhodayan, PhD Thesis, LBL-33961, 106 (1993).

[KAT86]   J.J.Katz, G.T.Seaborg, L.R.Morss, The Chemistry of the Actinide
            Elements: Volume 1, Chapman and Hall, New York, 525-534 (1986).

[KEL84]   O.L. Keller, Jr., Radiochim. Acta, 37, 169 (1983).

[KLE90]   J. Kleinberg (ed.), Collected Radiochemical and Geochemical Procedures,
            5th edition, LA-1721, p. I194-I196, (1990).

[KRA92]   J.V. Kratz, M.K. Gober, M.K. Zimmerman, H.P. Schädel, W. Brüchle,
            E. Schimpf, K.E. Gregorich, A. Türler, N. Hannink, K.R. Czerwinski, B.
            Kadkhodayan, D.M. Lee, M.J. Nurmia, D.C. Hoffman, H. Gäggeler, D.
            Jost, U.W. Scherer, and A. Weber, Phys. Rev. C., 45, 1064 (1992).

[LAN49]   W.G. Lanham, T.C. Runion, U.S. Atomic Energy Commission Rep.
            ORNL-479, Oak Ridge National Laboratory, Oak Ridge, Tenn. (1949).

[LEE82]   D. Lee, et al, Phys. Rev. C, 25, 1, 289 (1982).

[LER87]   R.G. Leres, RAGS - An "Off-the-Shelf" Hardware and System Software
            Small Data Acquisition Computer, LBL-24808 (1987).

[LIE67]   K.H. Lieser, J. Bastian, A.B.J. Hecker, W. Wild, J. Inorg. Nucl. Chem.,
            29, 815 (1967).

[LOU93]   R. Lougheed et al., Proc. Actinides '93, Santa Fe, NM 1993.

[MAE61]   W.J. Maeck, G.L. Booman, M.E. Kussy, J.E. Rein, Analytical Chem.,
            33, 1775 (1961).

[MAR69]   Y. Marcus and A.S. Kertes, Ion Exchange and Solvent Extraction of Metal
            Complexes, Wiley-Interscience, New York, 741 (1969).

[MAR69A]   Y. Marcus and A.S. Kertes, Ion Exchange and Solvent Extraction of Metal
            Complexes, Wiley-Interscience, New York, 62 (1969).

[MCK75]   H.A.C.McKay, D.Scargill, A.G.Wain, Gmelins Handbuch der
            Anorganischen Chemie, Transurane A1, II, Springer-Verlag, Berlin, 308
            (1975).

[MCK77]   H.A.C.McKay, M.G.Sowerby, M.Bustraan, J.Monitzaan, A.van Dalen,
            B.Verkerk, The Separation and Recycling of Actinides, European Atomic
            Energy Community Rep. EUR-5801e, Brussels (1977).

[MOL88]   P. Möller, J.R. Nix, Atom. Data Nucl. Data Tables, 39, 241 (1988).

[MOO83]   K.J. Moody, PhD Thesis, LBL-16249 (1983).

[MUL75]   G. Müllen, D.C. Aumann, Nucl. Instr. Meth., 128, 425 (1975).

[NAK69]   K. Nakamura, J. Inorg. Nucl. Chem., 31, 455 (1969).

[NAK70]   K. Nakamura, J. Inorg. Nucl. Chem., 32, 2265 (1970).

[NAR86]   J. Narbutt, J. Siwinski, B. Bartos, A. Bilewicz, J. Radioanal. Nucl.
            Chem., 101, 41 (1986).

[NAR88]   J. Narbutt, A. Bilewicz, B. Bartos, Chem. Anal., 33, 399 (1988).

[NAZ68]   B.N. Nazarienko, O.W. Mandzakadze, Russ. J. Inorg. Chem., 14, 1219
            (1968).

[NAZ68A]   B.N. Nazarienko, G.W. Fliantikova, Russ. J. Inorg. Chem., 13, 1855
            (1968).

[NAZ71]   B.N. Nazarienko, W.P. Antonovich, E.M. Newskaja, Russ. J. Inorg.
            Chem., 16, 2387 (1971). [English version p. 1273]

[NAZ71A]   B.N. Nazarienko, W.P. Antonovich, E.M. Newskaja, Russ. J. Inorg. Chem., 16, 1844 (1971).

[NAZ71B]   B.N. Nazarienko, W.P. Antonovich, E.M. Newskaja, Russ. J. Inorg. Chem., 16, 997 (1971).

[PIT79]   K.S. Pitzer, Accts of Chem. Res., 12, 271 (1979).

[PRO65]   W.E. Prout, E.E. Russel, H.J. Groh, J. Inorg. Nucl. Chem., 27, 473 (1965).

[QUR91]   M. Qureshi, K.G. Varshney, Inorganic Ion Exchangers in Chemical Analysis, CRC Press, 21 (1991).

[RAT91]   W.H. Rathbun, From Chaos To Order: The Microstar Data Acquisition and Analysis System, LBL-29734 (1991).

[RAT93]   W.H. Rathbun, K.E. Gregorich, M.F. Mohar, NSD Annual Report, LBL-35768, 82 (1993).

[REU83]   U. Reus, W. Westmeier, Nucl. Data Tables, 29, 193 (1983).

[ROD78]   J.W.Roddy, J. Inorg. Nucl. Chem., 40, 1787 (1978).

[SAE77]   K.E. Saeger, J. Rodies, J. Gold Bull., 10, 10 (1977).

[SAT88]   L. Satpathy, R.C. Nayak, Atom. Data Nucl. Data Tables, 39, 241 (1988).

[SCA57]   D.Scargill, K.Alcock, J.Fletcher, E.Hesford, H.A.C.McKay, J. Inorg. Nucl. Chem., 4, 304 (1957).

[SCH84]   W.W.Schulz, J.D.Navratil, A.E.Talbot, Science and Technology of Tributyl Phosphate Volume 1, CRC Press, Florida, 71 (1984).

[SCH88]   U.W. Scherer, J.V. Kratz, M. Schädel, W. Brüchle, K.E. Gregorich, R.A. Henderson, D.M. Lee, M. Nurmia, D.C. Hoffman, Inorganica Chimica Acta, 146, 249 (1988).

[SCH89]   M. Schädel, et al, GSI Preprint, GSI-89-38 (1989).

[SCH92]   M. Schädel, W. Brüchle, E. Schimpf, H.P. Zimmermann, M.K. Gober, J.V. Kratz, N. Trautmann, H. Gäggeler, D. Jost, J. Kovacs, U.W.

Scherer, A. Weber, K.E. Gregorich, A. Türler, N.J. Hannink, B. Kadkhodayan, D.M. Lee, M.J. Nurmia, D.C. Hoffman, Radiochimica Acta, 57, 85 (1992).

[SEA90]   G.T. Seaborg, W.D. Loveland, The Elements Beyond Uranium, John Wiley & Sons, 75 (1990).

[SEA90A]   G.T. Seaborg, W.D. Loveland, The Elements Beyond Uranium, John Wiley & Sons, 95 (1990).

[SHA76]   R.D. Shannon, Acta Crystal, A32(5), 751 (1976).

[SIL70]   R. Silva, J. Harris, M. Nurmia, K. Eskola, A. Ghiorso, Inorg. Nucl. Chem. Lett., 6, 871 (1970).

[SMI76]   R.M. Smith, A.E. Martell, Critical Stability Constants, Plenum Press, New York, Vol 4, 105 (1976).

[SOB93]   A. Sobiczewski, Phys. Particles Nuclei, 25, 295 (1993).

[SOB93A]   A. Sobiczewski, Proc. Actinides '93, Santa Fe, NM (1993).

[VES72]   V. Vesely, V. Pekarek, 19, 1245 (1972).

[WAL84]   F.W. Walker, D.G. Miller, F. Feiner (eds.), Chart of the Nuclides, 13th Edition, General Electric Co. (1984).

[WIL62]   A.M. Wilson, L. Churchill, K. Kikuk, Anal. Chem. 34, 203 (1962).

[WIL87]   G. Wilkinson, Comprehensive Coordination Chemistry, Vol. 3, Pergamon Press, Oxford, 363-441 (1987).

[YAN78]   C.Y. Yang, K.H. Johnson, J.A. Horsley, J. Chem. Phys., 68, 1001 (1978).

[ZHU90]   B.L. Zhuikov, V.A. Glebov, V.S. Nefedov, I. Zvara, Radioanal. and Nucl. Chem. Articles, 143, 103 (1990).

[ZVA74]   I. Zvara, B. Eichler, V.Z. Belov, T.S. Zvarova, Y.S. Korotkin, M. Hussonnois, Sov. Radiochem., 16, 709 (1974).

[ZVA76]   I. Zvara, V.Z. Belov, V.P. Domanov, M.R. Shalaevskii, Sov. Radiochem., 18, 328 (1976).